

**We thank Reviewer #1 for his or her useful comments on our manuscript. All comments have been thoroughly considered so as to improve the manuscript. Hereafter Reviewers' comments are written in *black italics*, our responses in bold black fonts and the changes in the manuscript in blue bold.**

*The manuscript consists of a case study of the vertical structure and optical properties of mineral dust observed during nine flights over the western Mediterranean from June 14th to July 4th 2013. The focus is on determining the refractive index, the spectral scattering coefficient, the particle number concentrations both sub-micronic and super-micronic and finally the Angstrom exponent. As the profiles provide vertically resolved information on these quantities, the respective roles of mineral dust and pollution aerosol in modulating these parameters can be analyzed and put into the context of a late spring, early summer period over the region. The authors describe well the methods used, the uncertainties of the instruments and the significance of the different profiles they collected.*

*R1.1. The terminology 'intermediate layer' and 'elevated layer' are confusing as one expects a lower layer. I propose to the author to change this terminology by defining a below-3km layer as one that encompasses the Marine Boundary Layer and the bottom of the free troposphere and the above-3km layer as the one that includes the free troposphere above 3km of the western Med.*

**« Intermediate dust layer » and « elevated dust layer » are replaced by « below-3km dust layer » and « above-3km dust layer », respectively, throughout the text.**

*R1.2. Here are two references really worthwhile citing as they constitute precursor work on the physical characteristics of dust over the Mediterranean and on the role of dust in heterogeneous chemistry respectively: Van Dingenen et al, 2005 and Bauer et al., 2004. In addition, it would be worth mentioning the work of Gian Paolo Gobbi and F. Barnaba who documented through LIDAR measurements the vertical structure of dust layers over the Mediterranean Sea with some very elevated extension above 10km.*

**These references are now added in the manuscript.**

*R1.3. The authors might not be aware of a debate among modelers on how absorbing dust really is. These measurements of the refractive index are very nice in that they could bring this debate towards a closure. Here are the 3 papers that to my knowledge incited to rethink the values of refractive indices that were originally published in the OPAC database:*

*Kaufman, Y. J., Tanré, D., Dubovik, D. O., Karnieli, A., and Remer, L. A.: Absorption of sunlight by dust as inferred from satellite and ground-based remote sensing, *Geophys. Res. Lett.*, 28, 1479–1482, 2001.*

*Moulin, C., Gordon, H. R., Banzon, V. F., and Evans, R. H.: Assessment of Saharan dust absorption in the visible from Sea- WiFS imagery, *J. Geophys. Res.*, 106(D16), 18 239–18 250, doi:10.1029/2000JD900812, 2001.*

*Balkanski, Y., Schulz, M., Claquin, T., and Guibert, S.: Reevaluation of Mineral aerosol radiative forcings suggests a better agreement with satellite and AERONET data, *Atmos. Chem. Phys.*, 7, 81-95, doi:10.5194/acp-7-81-2007, 2007.*

As the authors will see from looking at Figure 1, 2 and 4 from the paper Balkanski et al., 2007, dust is less absorbing than what most modeling groups are assuming, studies that are included in the discussions of latest IPCC report.

**Thank you for this relevant comment. We agree with Reviewer #1 that the dust absorption as represented by the imaginary part of the refractive index in models should be reassessed. This is especially true when comparing the values observed for dust from our in-situ measurements ( $n_i$  between 0.000 – 0.005) with that published in the OPAC database ( $n_i = 0.006$ ) that is widely used by the modelling and remote sensing communities. We add in the results and conclusion sections a comparison of our observations with the OPAC dataset.**

**Additional text P21632 L7: We compared our measurements on dust absorption properties with values published in the OPAC aerosol database that is widely used by modelling and remote sensing communities. The result of this comparison indicates an overestimation of dust absorption properties in the OPAC database. The  $n_i$  value achieved in the OPAC database ( $n_i=0.006$ ) is high compared to values observed for Saharan mineral dust in source region and over the Mediterranean during ADRIMED ( $n_i$  between 0.000–0.005). This finding is in line with previous studies showing disagreements in dust absorption between satellite retrievals and modelling studies that has been solved by decreasing the imaginary part of the dust refractive index (Kaufman et al, 2001; Moulin et al, 2001; Balkanski et al., 2007; Mian Chin et al., 2009).**

**Additional text P21636 L20: A straightforward comparison of our results with values published in the OPAC aerosol database, which is widely used by the remote sensing communities, suggests that the OPAC database overestimate dust absorption.**

*R1.4. The discussion page 21629 of the manuscript, assumes that only dust will influence the single scattering albedo (SSA), the authors should be much more careful when they state this. Although dust represents more than 80% of the total aerosol load, only a few percent of the mass of rBC or 15% of  $SO_4$  will change by 0.01 to 0.03 this SSA. They should reword this passage saying that if rBC is less than 1% of the total load, then they can do this inference, if not the SSA will decrease due to rBC and the value they measure/infer is a lower limit to the actual SSA of dust.*

**We do not understand the Reviewer's comment here since this paragraph aims at presenting the SSA for dust scenes in different air masses. The influence BC-laden air masses on the SSA of dust layers is presented.**

*Minor points:*

*R1.5. The assumptions for the computation of SSA in Table 5 that appears on the line "w0 (chemistry)" have not been well presented. If the authors took a simple weighted average, it is erroneous; it should be weighted by the product of the optical depth times the asymmetry factor of each aerosol component.*

**The equation used to calculate  $w_0$ (chemistry) is added in section 4.2.**

**Additional text: Calculations of  $w_0$  were performed as follows:**

$$\omega_0 = \frac{\sum_i (k_{ext,i} - k_{abs,i}) \cdot C_{m,i}}{\sum_i k_{ext,i} \cdot C_{m,i}} \quad (9)$$

R1.6. Page 21618: the authors make the assumption of the sphericity of dust particles but do not give the proper references to indicate that this assumption is reliable. Please indicate the work that have studied and quantified the effect of dust non-sphericity.

**Mineral dust particles are certainly irregular, not spherical particles. The a-sphericity affects the angular distribution of the scattered light, mostly in the backward region at scattering angles larger than 80% (Mishchenko, 2009). Neglecting the particle a-sphericity induce a large uncertainty in the retrieved aerosol optical thickness from the satellite reflectance measurements. However, Mischenko et al. (1995) showed that the sphere model could be a suitable approximation for nonspherical dust in radiative flux simulation, because the optical depth, the single scattering albedo and the asymmetry factor are similar in the two cases. Because we only investigate angular-integrated properties, and for sake of comparison with the large majority of field data published so far, in this paper we only perform calculations in the spherical approximation.**

**Additional text: In this study, we have decided to neglect the non-sphericity of mineral dust since the sphere model has been shown to produce negligible errors when computing radiative fluxes and flux related quantities, i.e. aerosol optical depth (AOD),  $\omega_0$  and  $g$  (Mishchenko et al., 1995). Because we only investigate angular-integrated properties and for sake of comparison with the large majority of field data published so far, in this paper we only perform calculations in the spherical approximation.**

R1.7. Page 21622; lines 21-22: Change “Relatively frequent dust episodes could be observed as it is typical for the season (Moulin et al., 1998).  $\hat{A}_z$  with ‘Moulin et al. (1998) have documented the frequency of dust episodes across the Mediteranean Sea, summer occurrences are quite frequent. ‘”

**This is corrected.**

R1.8. Page 21623, lines 10 to 13: please clarify the following sentence: “ Values obtained during ADRIMED are consistent with those obtained near dust source regions within 1.5 days after emission (Formenti et al., 2011b; Weinzierl et al., 2011; Ryder et al., 2013b), but, for a comparable transport time, higher than after long-range transport over the Atlantic ocean (Maring et al., 2003; Weinzierl et al., 2011).”

**The sentence has been rewritten.**

**Updated text: “During ADRIMED,  $D_{\text{eff},c}$  values obtained in dust layers having spent less than 1.5 days in the atmosphere are consistent with those obtained near dust source regions (Formenti et al, 2011b; Weinzierl et al., 2011). Conversely, dust layers having spent more than 1.5 days in the atmosphere present higher  $D_{\text{eff},c}$  than previously observed over the Atlantic ocean (Maring et al., 2003; Weinzierl et al., 2011).”**

R1.9. Page 21634 lines 16 to 20 : Change : “Dust particles originating from Algeria, Tunisia and Morocco were sampled in the western Mediterranean basin after being transported 1–5 days of transport.” To “Dust particles originating from Algeria, Tunisia and Morocco were sampled in the western Mediterranean basin after 1 to 5 days of transport from the source regions.”

**This is corrected.**

*R1.10. Page 21635 lines 3 and 4 Change : ‘ ‘ Mineral dust carried higher concentration of pollution particles at intermediate altitude (1–3 km a.s.l.)...’ to ‘ ‘ Measurements showed the presence of mineral dust together with higher concentration of pollution particles at intermediate altitude (1–3 km a.s.l.)...’*

**This is corrected.**

### **References:**

**Formenti, P., Schütz, L., Balkanski, Y., Desboeufs, K., Ebert, M., Kandler, K., Petzold, A., Scheuven, D., Weinbruch, S., and Zhang, D.: Recent progress in understanding physical and chemical properties of African and Asian mineral dust, *Atmos. Chem. Phys.*, **11**, 8231-8256, 10.5194/acp-11-8231-2011, 2011b.**

**Maring, H., Savoie, D. L., Izaguirre, M. A., Custals, L., and Reid, J. S.: Mineral dust aerosol size distribution change during atmospheric transport, *J. Geophys. Res.-Atmos.*, **108**, 10.1029/2002jd002536, 2003.**

**Mian Chin, Diehl, T., Dubovick, O., Eck, T. F, Holben, B. N, Sinyiuk, A., and Streets, D. G.: Light absorption by pollution, dust, and biomass burning aerosols: a global model study and evaluation with AERONET measurements, *Ann. Geophys.*, **27**, 3439-3464, doi:10.5194/angeo-27-3439-2009, 2009.**

**Mishchenko, M. I., Lacis, A. A., Carlson, B. E., and Travis, L. D. : Nonsphericity of dust-like tropospheric aerosols : implications for aerosol remote sensing and climate modelling, *Geophys. Res. Lett.*, **22(9)**, 1077-1080, 1995.**

**Mishchenko, M. I., Electromagnetic scattering by nonspherical particles: A tutorial review, *Journal of Quantitative Spectroscopy and Radiative Transfer*, **11**, 808-832, 10.1016/j.jqsrt.2008.12.005, 2009.**

**Weinzierl, B., Sauer, D., Esselborn, M., Petzold, A., Veira, A., Rose, M., Mund, S., Wirth, M., Ansmann, A., Tesche, M., Gross, S., and Freudenthaler, V.: Microphysical and optical properties of dust and tropical biomass burning aerosol layers in the Cape Verde region- an overview of the airborne in situ and lidar measurements during SAMUM-2, *Tellus B*, **63**, 589-618, 10.1111/j.1600-0889.2011.00566.x, 2011.**

We thank Reviewer #2 for his or her useful comments on our manuscript and appreciate the time and energy that must have been spent on this detailed review. All comments have been thoroughly considered so as to improve the manuscript. Hereafter Reviewers' comments are written in *black italics*, our responses in **bold black fonts** and the changes in the manuscript in **blue bold**.

*This is a clearly-written and presented article showing key results of dust size distribution and optical properties measured over the Mediterranean during the ChArMEx/ADRIMED aircraft field campaign. The results add to the body of data building up to document dust properties and how they may change with transport, which can contribute to model and satellite retrieval validation and improvement. In particular the authors present results showing the minimal impact of pollution on dust properties, and retention of coarse mode particles which they attribute to turbulence in the dust layer. I recommend that this article is published, subject to some minor corrections, mainly concerned with further information on inlet impacts on sampling and size distributions, and some additional clarifications and additions to the figures.*

Specific comments

R2.1. “Moderate light absorption” – which do you mean, moderate to light, moderate, or light? These are all different!

**“Moderate” referred to the ability of particles to absorb light.**

**Updated text: “Moderate absorption of light by the dust plumes was observed with values of aerosol single scattering albedo at 530 nm ranging from 0.90 to  $1.00 \pm 0.04$ .”**

R2.2. “assumed similar” would be better than “assimilated” here

**Thank you, this is corrected.**

R2.3. 21610 L5-7 – and global transport of dust in general as well?

**This is added in the text.**

**Updated text: “The results presented here add to the observational dataset necessary for evaluating the role of mineral dust on the regional climate and rainfall patterns in the western Mediterranean basin and understanding their atmospheric transport at global scale.”**

R2.4. Introduction – please give an overview of what is contained in each following section at the end of the introduction.

**We now provide an overview of the different sections in the introduction.**

**Additional text:** “Section 2 describes the aircraft strategy, the instrumentation and the method used to determine the aerosol size distribution, chemical composition and the associated optical properties. Section 3 presents the campaign meteorology, the dust vertical profiles and the results of the aerosol properties within the dust plumes. Section 4 explores the potential factors affecting the variability of the aerosol properties due to altitude and dust age. Section 5 concludes this article.”

R2.5. Figure 1: Is it possible to change the aspect ratio of the figure so the landmasses appear more in proportion? Currently it appears squashed east-west.

**The scale of the figure is changed.**

R2.6. Some flight tracks/colours are not visible. Do some flight tracks overly others? E.g. F35, F38? If so describe this in the caption.

**The colour codes of F35 and F38 are changed in order to better identify flight tracks in the figure.**

R2.7. 21613 On what basis were the non-dust flights removed from the analysis?

**Flights dedicated to the measurement of dust plumes were firstly planned using different dust plume forecast models, as explained in section 2.1. Sampling of mineral dust was then further confirmed by analysing satellite images and backward trajectories of the air masses, which are described in section 2.4. We add a sentence in section 2.1. to clarify it.**

**Additional text: “These flights were carefully selected to provide measurements of air masses from dust active sources based on the analysis of satellite images and backward trajectories, as described in section 2.4.”**

R2.8. L20-25 – what spatial distance is covered during a vertical profile?

**This information is added in the text.**

**Updated text: “The general flight strategy consisted of two main parts: first, profiles from 300 m up to 6 km above sea level (asl) were conducted by performing a spiral trajectory 10-20 km wide to sound the vertical structure of the atmosphere and identify interesting dust layers. “**

R2.9. Table 1 – I believe times should be in UTC for ACP papers.

**Time are already expressed in UTC in Table 1, there was a typesetting error.**

**Updated text: “Times are expressed in Coordinated Universal Time (UTC).”**

R2.10. Section 2.2.1 – It would be useful to define what the authors refer to by ‘nominal size’ here.

**The definition is added in the text.**

**Updated text: The SMPS system provided the number size distribution of the electrical mobility diameter from the 30 - 400 nm in 135 nominal size classes (i.e. size classes provided by the instrument and not corrected for the dynamic shape factor) over time scans lasting 120 seconds.**

R2.11. 21615 L10 – “possible errors in the FSSP sizing were assumed to be 30% of the particle diameter” – this sentence is confusing – do you mean errors in number concentration as a function of size? Please explain.

**No, we referred to the measurement uncertainty in diameter. This is clarified in the text.**

**Updated text: The FSSP has an uncertainty in diameter of about 30 % according to Baumgardner et al. (1992).**

R2.12. L14-15 – again, what do you mean precisely by ‘particle sizing?’

**This is clarified.**



**Updated text: According to the calibration of the GRIMM with standard, we assumed an uncertainty in diameter of 10%.**

R2.13. 21618 L16 -21619, L7 – This (i.e. excluding data) is an interesting approach to the problem of scattering response vs size. It would be interesting to mention whether including the omitted data made much difference to the resulting size distribution? I.e. perhaps this approach is overly cautious.

Figure A compares the particle size distributions measured by the FSSP on its full size range with that obtained by the GRIMM for different dust layers sampled during the campaign. Systematic differences in the size distributions measured by the instruments can be seen around 2  $\mu\text{m}$  most likely due to the fact that the light intensity response of the instruments is unique in this size range. Therefore we believe that datapoints obtained from the FSSP must be excluded from the analysis.

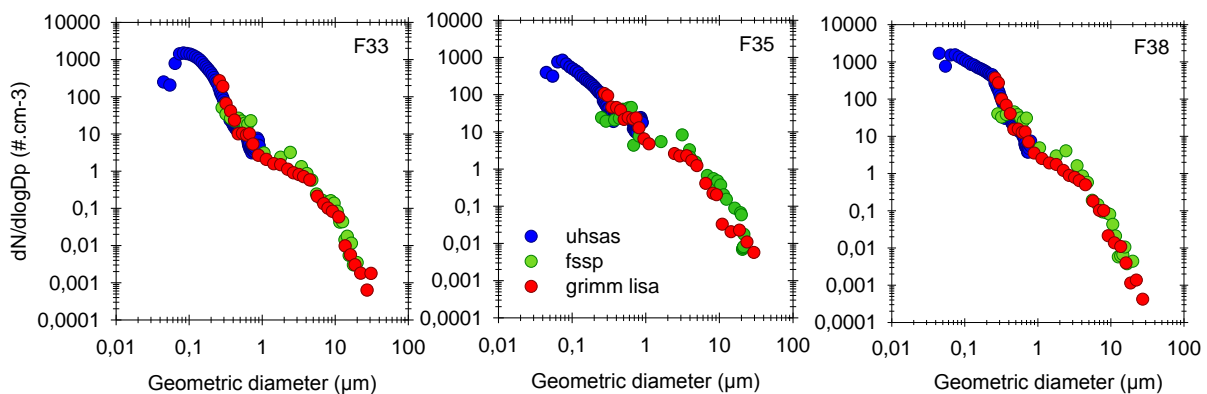


**Figure A. Comparison of the number size distributions measured by the UHSAS, FSSP and GRIMM within different dust layers during the campaign.**

**Additional text P21619 L5: During ADRIMED, systematic differences in the size distributions measured by the FSSP-300 and the GRIMM were observed around 2  $\mu\text{m}$ .**

R2.14. The authors may be interested in a method of including error bars in refractive-index corrected particle size based on the scattering-size response, which can be represented by freely available software described in Rosenberg et al. (2012) and also discussed in Ryder et al. (2015) and the associated ACPD discussion. This allows the data in the region omitted in this paper to be included, but with appropriate error bars.

As we mentioned above in R2.13., datapoints in the size range where the light intensity response of the instruments would be unique have been removed for data analysis. As a consequence, errors in size distributions are only due to the accuracy of the stepwise variation of the refractive index in the iterative procedure and the measurement uncertainties.

R2.15. Figure 3 – what do the horizontal error bars for FSSP represent? What are the sizing errors for the other instruments?

Horizontal errors bars display the bin sizing uncertainties of the FSSP. The sizing errors for the other instruments are given in section 2.2.1. They are smaller than the size of the symbols in Figure 3.

**Additional text: Horizontal errors bars display the bin sizing uncertainties of the instruments.**

*R2.16. 21620 L1-2 – why was  $d_{\text{eff}}$  calculated separately for coarse and fine fractions? It would make sense to provide one value for the entire size distribution, or at least to provide this value in the data analysis as well.*

**The separation of  $D_{\text{eff}}$  between the coarse and fine modes allows to discriminate if differences in aerosol size distributions within dust plumes are either due to differences in the size/concentration of pollution particles or to differences in the size of mineral dust.**

*R2.17. Section 2 – what is the instrumental error on the nephelometer and CAPS instrument?*

**The uncertainties on the nephelometer and CAPS measurements are added.**

**Additional text P21616 L26: Uncertainty in  $\sigma_{\text{scat}}$  measured with the nephelometer is estimated to be 5% (Muller et al., 2011a).**

**Additional text P21617 L5: Uncertainty in  $\sigma_{\text{ext}}$  measured with the CAPS is estimated to be 3% (Massoli et al., 2010).**

*R2.18. 21620 L18-21 – what were the errors between calculated & measured scattering and extinction of the final values? How many cases were there?*

**The errors between calculated and measured  $\sigma_{\text{scat}}$  and  $\sigma_{\text{ext}}$  were 5% and 3%, respectively. This is already stated in section 2.3.: “The calculated values of  $\sigma_{\text{scat}}$ (530 nm) and  $\sigma_{\text{ext}}$ (530 nm) were compared to that measured by the nephelometer and the CAPS, and values having the closest agreement within the measurement error bars were chosen as the best estimate.”.**

*R2.19. 21621 L1-3 – what is the reference for these cut-offs? If no previous published work is available on these values, data & evidence should be provided here for them.*

**Information on the modelling and experimental tests performed to characterize sampling inlets are added in the manuscript.**

**Additional text: The in-aircraft aerosol instruments sampled through isokinetic and isoaxial aerosol inlets. The nephelometer and GRIMM were set up behind the AVIRAD inlet, while the CAPS, SMPS and SP2 were set up behind the Community Aerosol Inlet (CAI). Particle loss can occur both as a result of the inlet aspiration efficiency and the transport losses in the pipework between the inlet and the instruments. The cut-off diameter, at which the passing efficiency of the inlet equals 50%, was determined by a set of wind-tunnel experiments (unpublished data). The passing efficiency was determined as the ratio of the particle number concentration measured by GRIMM optical counters behind the sampling lines of the AVIRAD and CAI inlets to the particle number concentration measured in the main flow of the wing tunnel where the air speed was 93 m s<sup>-1</sup> as the cruise speed of the ATR-42. Monodisperse polystyrene latex spheres of 0.6, 1.2, 4.6, 7.9 and 11  $\mu\text{m}$  diameter (Duke Scientifics, Thermo Sci.) and polystyrene divinylbenzene spheres of diameter varying between 1 and 35  $\mu\text{m}$  in diameter (also purchased from Duke Scientifics) were first diluted and then put in a reservoir connected to a peristaltic pump. The pump tubing was connected to a pneumatic spinning disk (SPIDI) in order to spray a large amount of droplets from the solution, some droplets having a particle incorporated. An air mover was mounted beneath the SPIDI and thus the droplets were rapidly evaporated. The particle size-dependent passing efficiency of**



the AVIRAD and CAI sampling inlets shown in Figure S2 indicates that the cut-off diameter value, expressed as optical equivalent, is 12  $\mu\text{m}$  for the AVIRAD inlet and 5  $\mu\text{m}$  for the CAI.

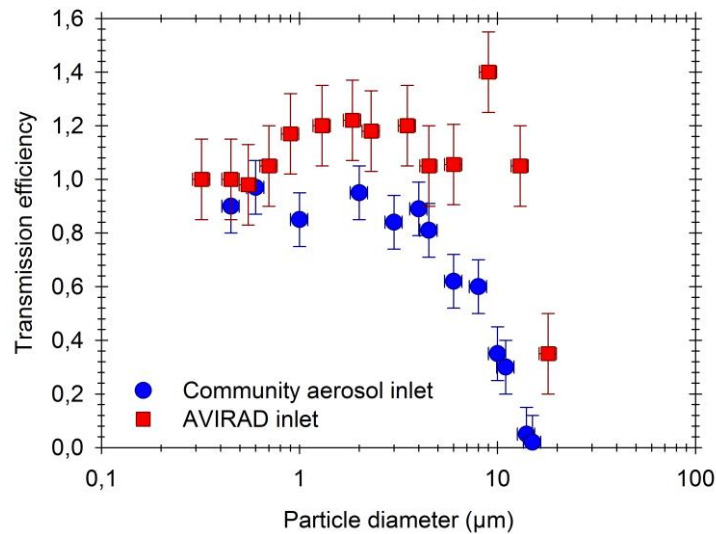


**Figure S2. Particle size-dependent passing efficiency of the AVIRAD and CAI sampling inlets.**

R2.20. L6-9 – some of these errors, particularly the 0.04 on the single scattering albedo (SSA), are relatively large. The authors say they are within the range covered by the measurement uncertainties, but do not state their values. Therefore the authors should provide values for measurement uncertainty of scattering and extinction coefficients, and on SSA as a result.

**Measurement uncertainties of scattering and extinction coefficients are added in the text. Please look at our response to comment R2.17 above.**

R2.21. Section 2, inlets

More discussion of this point is required. Firstly the GRIMM is measuring a size distribution behind the AVIRAD inlet with a 12 micron cut-off, yet the authors present a size distribution from this inlet up to a nominal size of 32 microns, and what looks like a corrected size of around this value in Fig 3b. If the cut-off value of the inlet is accurate, then the size distribution beyond 12 microns should not be used. Secondly the nephelometer also measures behind the AVIRAD instrument, cutting off at 12 microns, while the CAPS measures extinction behind the community inlet cutting off at 5 microns. This difference should be stated explicitly. How do the authors deal with this discrepancy, e.g. in calculating SSA and in comparing to the mie calculations from the size distributions? A short description of this is provided but it needs more explanation & description of their method.

**GRIMM size distributions above the nominal diameter of 12  $\mu\text{m}$  are removed from data analysis to simplify the methodology section.**

**The fact that the instruments sampled through two different inlets is now clearly stated in the manuscript (please look at R2.19 for further information). We provide additional explanation of the method used to estimate the errors associated with the calculated optical parameters due to the inlets passing efficiencies.**

**Additional text P21620 L22: To assess the impact of the inlets sampling efficiency on the measured optical properties, Mie scattering calculations were performed to estimate  $n_r$ ,**

$n_i$ ,  $\omega_0$ ,  $g$  and  $k_{ext}$  using either the full size distribution or the size distribution measured behind the aircraft inlets. For  $\omega_0$ ,  $g$  and  $k_{ext}$ , we considered a fixed refractive index of  $1.52-0.003i$ , reflective of the values observed for Saharan dust in source region (Schladitz et al., 2009; Formenti et al., 2011a; Ryder et al., 2013a). The discrepancies between  $\omega_0$ ,  $g$  and  $k_{ext}$ , including or not larger particle sizes were used to estimate the errors associated to the inlets sampling efficiency. For  $n_r$  and  $n_i$ , we estimated the difference between  $\tilde{n}$  derived from the iterative procedure described above (i.e. Fig. 2) using the full size distribution as input parameter and that obtained from the size distribution measured behind the aircraft inlets. The absolute errors associated with  $\omega_0$ ,  $g$  and  $k_{ext}$  due to the passing efficiencies of the inlets were in the range covered by the measurements uncertainties of both optical parameters and size distributions, which were estimated to be 0.02, 0.002, 0.04, 0.05 and 0.08, respectively.

R2.22. 21662 L1-12 – could the dust masses also be tracked via the SEVIRI imagery, and were they in agreement with the age and source locations from HYSPLIT?

**Dust source regions and transport pathways identified from HYSPLIT were confirmed by SEVIRI observations, as well as by the quantification of Si/Al and Fe/Ca ratios. Information on the method and the uncertainties in identifying dust source regions and age are already given in sections 2.4. and 3.4, respectively.**

R2.23. 21622 L19 – 700hPa is more mid-atmosphere than ‘upper’ atmosphere.

**This is corrected.**

R2.24. Figure 1 – the squares give the impression that the source regions were very definite and refined. In reality this is probably quite unlikely given the uncertainty in hysplit back trajectories. Please give some measure of spatial uncertainty for each of the sources. Several tools such as ensembles and matrices are now available on HYSPLIT to provide such information easily.

**A discussion on the uncertainties of our identification of dust source region is already given in section 3.4.**

R2.25. Figure S4 – it is extremely difficult to make out the wind barbs from these plots. Please improve the readability of the figure – I suggest plotting fewer wind barbs.

**Figures S4 and S5 have been replotted with fewer wind barbs to improve their readability.**

R2.26. 21624 L10 – what method was used to calculate the value of  $Z_b$ ? Was it done by eye? Likewise for  $Z_s$ . What do you use  $Z_s$  to infer? Looking at the profiles in Fig S6, it would often appear that  $Z_b$  should be at a lower altitude on some occasions – e.g. around 300m in F32 rather than 1km. Likewise, the reason for the altitude of the  $z_s$  line is not clear, for example in F30 and F31 there is little change in wind direction at the line. Please provide information on how  $Z_b$  and  $Z_s$  were chosen. This has been done previously in a systematic way, for example, in E.Jung et al., 2013, JGR, *oi:10.1002/jgrd.50352*, where layers are referred to as ‘marine boundary layer,’ ‘intermediate layer,’ and ‘Saharan air layer.’

**Thank you for this comment. Figures 5 and S6 have been corrected accordingly.**

**The method used to identify  $Z_b$  and  $Z_s$  is provided in P21624 L13: “The top height of the boundary layer was identified as the height at which the temperature profile showed the highest discontinuity and the water vapor mixing ratio decreased the most rapidly. The**

shear level was determined from the sudden increase in wind speed and change in wind direction. »

R2.27. Fig S6 – both the blue lines appear similar in colour (different shades of dark blue). Please change the colour. Potential temperature axis is not readable due to too many numbers on the x-axis.

**The colour code and the scale of the potential temperature axis are changed.**

R2.28. 21625 L4 – F31 does not appear to be a single homogeneous layer.

**Both total number concentration and Angstrom exponent stayed rather constant with the altitude in F31. There was also no clear evidence from wind speed and direction of the presence of two distinct elevated layers.**

R2.29. L10 – McConnell et al. (2008) angstrom values were  $>0$  over the source region (figs 5a and c)

**Yes, McConnell angstrom values were  $>0$  but they were also  $<0.5$ . They did not reach the value of 0.9 that we obtained during F38.**

R2.30. Fig 6 – One would assume that the locations of the profiles in Fig 5 correspond to the stars in fig 1. I.e. expect the F32 profile to be at Minorca. The F38 track is not visible on Fig 1. Why then do the end points of the trajectories in Fig 6 not correspond to the profile locations? **The F38 profile was located at Lampedusa (i.e. Table 1) that corresponds well to the localisation of the end point of the trajectory in Figure 6. The colour code of flights tracks in Fig. 1 is modified to make them more visible.**

R2.31. Figure 7 – have the categories shown here been created purely based on the altitude of measurement, or do they relate to the placing of lines  $z_b$  and  $Z_s$  in Fig 5 in any way?

**The classifications were derived from the altitude of measurement. This is already written in the caption of the figure: “Size distributions are classified as a function of the altitude of the layer: elevated dust layer above 3 km a.s.l. (red), intermediate dust layer between 1.5–3 km a.s.l. (blue) and the boundary layer below 1 km (green).”**

R2.32. 21627 L4 – ‘indiscriminate of’?

**Thank you, this is corrected.**

R2.33. L4-6 – it is surprising that the intermediate dust shows a greater coarse mode than the elevated dust – based on Fig 5 it seems that there were more coarse particles in the elevated layer. It would be useful to show Fig 7 a and b normalized by total number and volume respectively, so that the relative differences in size distribution can be seen. Then fig 7c could be shown as a separate figure, enlarged for clarity – it is quite difficult to see some of the detail and different lines here.

**It can be seen in Figure 9 that the differences in the coarse mode between the two elevated dust layers stayed within the measurement error bars, so the variation is most likely not significant. The relative differences in size distributions are already discussed in section 4.1. and can be seen from the vertical variation of  $D_{\text{eff}}$  shown in Figure 9.**

R2.34. L22 – what do you mean by ‘good’?

This is clarified in the text.

**Additional text:** The spread of volume size distributions obtained during ADRIMED overlaps with those measured during other airborne campaigns close to dust source regions (AMMA, FENNEC and SAMUM-1) in the coarse mode size range (Figure 7c).

R2.35. L23 – Please clarify what is meant by  $D_{eff,c}$  here – is this  $d_{eff}$  of particles  $d > 1$  micron, or  $d_{eff}$  of mode 4 in table 3?

The definition of  $D_{eff,c}$  is now reminded in this section.

**Updated text:** “Effective diameters of the coarse mode  $D_{eff,c}$  (i.e. estimated in the size 1-32  $\mu\text{m}$  as defined in eq. 7) ranged from 3.8 to 14.2  $\mu\text{m}$  during ADRIMED”

R2.36. L27 – ‘uncounted’ – do you mean, ‘fewer particles larger than 10  $\mu\text{m}$  were counted’?

Yes, thank you.

R2.37. Figure 8 – presumably one SLR equates to one data point. How do you deal with data from the vertical profiles? Are they averaged over an altitude range depending on the vertical structure? What do the error bars represent?

The altitude used to plot the data points is already given in the caption: “The altitude indicated for vertical profiles refers to the middle of the layer”.

A description of the error bars has been added in the caption.

**Additional text:** Horizontal error bars display the uncertainties of the parameters. Vertical error bars indicate the altitude range used to calculate each data point.

R2.38. Figure 8 – adding in horizontal lines at 1.5 and 3km to represent and differentiate the different dust altitude categories shown in Fig 7 would be useful. It would also be useful to add in some measure of size as an extra plot – e.g. ratio of  $N_{coarse}$  to  $N_{fine}$ , or  $d_{eff,coarse}/d_{eff,fine}$ .

Horizontal lines are added in Figure 8 to differentiate the elevated and intermediate dust layers. We have the impression, however, that representing the vertical distribution of either  $N_c/N_f$  or  $D_{eff,c}/d_{eff,f}$  would not help to improve our understanding of the evolution of dust size distribution since we would not be able to discriminate if variations are due to differences in the size/concentration of pollution particles or to differences in the size /concentration of mineral dust.

R2.39. 21629 L9 – ‘these layers’ – do you mean the higher altitude layers?

Yes, this is clarified.

**Updated text:** As  $\tilde{n}$  was found to be constant with the altitude (i.e. Figure 8a-b), these variations in  $g$  and  $k_{ext}$  were probably due to the variability in particles size distributions, which is consistent with the larger fraction of fine particles found in the higher altitude dust layers.

R2.40. L1-14 – the variation of optical properties with height is worthy of a bit more discussion. It appears that  $n_r$  and  $n_i$  are independent of altitude, there is some evidence for a decrease in SSA beneath 3km, and beneath 3km  $g$  decreases while  $k_{ext}$  increases. The latter ( $g$  and  $k_{ext}$ ) are consistent with an increase in the proportion of accumulation mode particles relative to the coarse particles – which is why it would be useful to add a size metric to this figure.

Even if the vertical variability of the optical parameters were most likely related to differences in dust size distributions, we do not believe that this result deserves further

discussion. Differences in  $g$ ,  $k_{\text{ext}}$  and  $D_{\text{eff},c}$  between the intermediate and elevated dust layers were low and statistically not significant regarding corresponding error bars. Therefore we would prefer not to expand this discussion in the paper.

The discussion on the vertical variation of optical parameters mentioned by Reviewer #2 is already provided in the paper: “Only slightly low values of  $g$  (from  $\sim 0.7$  to  $\sim 0.8$ ) and  $k_{\text{ext}}$  (from  $\sim 0.3$  to  $\sim 0.7 \text{ m g}^{-1}$ ) were observed for some dust layers below 3 km a.s.l. As  $\tilde{n}$  was found to be constant with the altitude (i.e. Fig. 8a and b), these variations in  $g$  and  $k_{\text{ext}}$  were probably due to the variability in particles size distributions, which is consistent with the larger fraction of fine particles found in these dust layers (i.e. Fig. 7a).”

Moreover, the vertical distribution of the size distribution can already be seen in Figures 7 and 9.

*R2.41. 21630 L2-5 – There is not strong evidence here that the transport conditions affect the optical properties of the dust layer – in fact based on Fig 8 and the discussion in the preceding paragraphs of the paper, I would argue the opposite. The results presented here would suggest that transport altitude/air mass encounters affects the resulting vertical structure, but I would be doubtful if more than that can be claimed. Additionally, nothing is known about the dust size distribution or optical properties at uplift, which may have been different in each case.*

**Our conclusions on dust optical properties referred to observations conducted from remote-sensing techniques and presented below in the paragraph. To avoid any confusion, the end of the paragraph is modified to better support the conclusions drawn from our observations.**

**Updated text: Overall, these contrasting results highlight the major role of the transport conditions (height, air mass encountered) of the dust plumes in governing the mixing processes of mineral dust with other aerosol species.**

*R2.42. 21630 L17- do you mean ‘upper 3km’? If not please define what sort of size you mean when referring to ‘pollution particles.’ Again, it may be helpful to the reader here to include some measure of number concentration in the figure (e.g. ratio of  $N_{\text{coarse}}/N_{\text{fine}}$ , or sub-divide the fine mode into ratio of number concentrations).*

**No, “lower 3 km” is right. It can be seen in the higher proportion of fine mode particles in the lower 3 km altitude. Please look at our responses of R2.16 and R2.33 concerning  $D_{\text{eff},c}/D_{\text{eff},f}$ .**

*R2.43. L25-26 – ‘ $D_{\text{eff},c}$  of the dust plume did not show any systematic dependence on altitude’ – on the contrary there does seem to be a small shift to smaller values of  $d_{\text{eff}}$  above 3km. What are the mean & standard deviation values of  $d_{\text{eff}}$  in these 2 altitude ranges, and can you provide evidence that there is no systematic change?*

**Please look at our response to R2.41.**

*R2.44. Figure 10 – please include  $d_{\text{eff}}$  for the coarse mode in this figure or supply 2 plots to include it. Due to the limited settling velocity of fine mode particles,  $d_{\text{eff},f}$  would not be expected to change much on the timescales shown, whereas  $d_{\text{eff},\text{coarse}}$  might be expected to change significantly.*

**The time evolution of  $D_{\text{eff},c}$  is presented in Figure 11 to investigate the effect of sedimentation processes on the proportion of large particles in dust size distributions. The aim of Figure 10 is to explore the role of the transport time of the dust plumes on their**

mixing rate with pollution particles. Despite the export of pollution particles within dust layers up to 3 km altitude,  $D_{\text{eff,c}}$  did not vary substantially with altitude (Figure 9b) due to the external mixing of mineral dust with pollution. So we do not believe that it would be relevant to show the time evolution of  $D_{\text{eff,c}}$  for the intermediate and elevated dust layers in this section.

*R2.45. 21632 L26 – a value of 0.64 for  $k_{\text{ext}}$  seems at the high end compared to values shown in Fig 8e. How do the authors reconcile the choice of this value? What are the uncertainties on the SSA values calculated from the chemical composition?*

**The  $k_{\text{ext}}$  value of 0.64 recommended by OPAC is indeed among the highest values obtained during ADRIMED. Dust absorption depends on the dust mineralogical composition and hence can vary with dust source region. The OPAC parametrization consists of a heterogeneous mixture of quartz and clay minerals originating from different sources. As a result the default OPAC's type mineral dust could slightly differ from dust sampled during ADRIMED and this could result in some differences in  $k_{\text{ext}}$  values of dust at emission. Without proper measurements of dust properties at uplift, we can only speculate on that issue and we decided to assume an average  $k_{\text{ext}}$  value of dust at emission as provided in OPAC dataset. It is also worth noting that this average value remain within the range of values retrieved during ADRIMED.**

To estimate the uncertainties on the SSA calculated from the chemical composition would require to know the uncertainties on  $k_{\text{ext}}$ . As mentioned above, without measurements of dust plume at uplift, we decided to use an average  $k_{\text{ext}}$  value from OPAC. Unfortunately the uncertainty of this parameter is not provided. However SSA obtained from chemical composition ranged from 0.93-0.97 which falls within the range of values obtained from optical measurements ( $0.92\text{--}0.99 \pm 0.04$ ). Our calculation is thus conclusive without knowing SSA uncertainties.

*R2.46. Can the chemical data provide any information on composition as a function of size? For example, generally the authors assume that dust is present at all particle sizes and subsequent conclusions (e.g. Fig 10 is discussed as dust, albeit being fine mode). What evidence is there that dust is present in all size ranges? Likewise, can the chemical data be used to support the conclusion that more pollution was present in intermediate compared to elevated dust layers?*

**Analysis of size segregated sampling by electron microscopy is planned to address more specifically this point, whereas the chemical analysis available at this stage are size-integrative. However, there is clear evidence from the aerosol size distribution (i.e. Figure 7) of the presence of fine dust particles within the dust layers ( section 3.3) in agreement with earlier work in proximity of source regions (Chou et al., 2008; McConnell et al., 2008; Kandler et al., 2009). Indeed a peak in the accumulation mode similar as that observed in dust source region and not present in the MBL (Figure 7) suggests the presence of dust particles in the fine mode.**

*R2.47. Figure 11 – Please clarify how effective diameter is provided for each dataset in the figure. For example, the Fennec data represent effective diameter for the full size distribution. It is likely the case for the other campaigns. Therefore it would be better to show the ADRIMED data as  $d_{\text{eff}}$  for the full size distribution in order to compare like with like. Additionally it should be noted that the other campaign data points are averages of many individual cases, while the*



*ADRIMED data points each represent 1 SLR (?) (or profile?). This is appropriate due to the focus of this paper on the ADRIMED measurements, but the authors should also provide one mean data point for the campaign with error bars so that it can be easily represented in future studies/publications. This is useful and important data and it should be provided in a way that allows it to be taken forward easily.*

**Since the aim of Figure 11 is to investigate the evolution of large dust particles with time, we would prefer to present  $D_{\text{eff}}$  for the coarse mode only.  $D_{\text{eff}}$  for the coarse mode has been calculated from the number size distribution and using equation (7) for ADRIMED, AMMA, SAMUM 1,2 and PRIDE datapoints. For Fennec, we mistakenly used  $D_{\text{eff}}$  provided in Figure 11 of Ryder et al. (2013) that referred actually to the full size distribution. Figure 11 is now corrected accordingly. Moreover, a mean data point for the ADRIMED campaign is added in the figure.**

*R2.48. 21634 L10-14 – can the authors speculate on whether this is greater than expected up/downdraft values over the Atlantic, and whether this might also help explain (or not) why Fig 11 intriguingly suggests that larger particles are transported over the Mediterranean more effectively than over the Atlantic?*

**To the best of our knowledge, no study to date has explored possible differences in the thermal turbulence within layers circulating over the Atlantic and the Mediterranean basin. This research topic should clearly be investigated in the future to better understand the differences in the sedimentation of large Saharan dust particles during these two main transport pathways and to improve the representativeness of the temporal evolution of dust size distribution in models.**

*Final comments:*

*R2.49. What were the AODs of the sampled cases? What were the AODs in the polluted regions out of dust plumes? (I.e. how strong were levels of background pollution?) Since the pollution appears to have negligible effect on the dust properties, it would be useful to know whether this is because pollution levels were low in general in the area/time period, or conversely if loadings of pollution were moderate-high, and still not impacting the dust layer properties. I see this is discussed briefly in the conclusion but it would merit a mention in the results section as well.*

**A short paragraph on the representativeness of our results including AOD values is added in the text.**

**Additional text P21632 L7: The ADRIMED field campaign was characterized by moderate aerosol optical depth (AOD) with averaged values ranging between 0.1 – 0.6 at 440 nm as observed by AERONET/PHOTONS sun-photometers (see Figure 19 of Mallet et al., 2015). Outside of dust events, the AOD displayed values from 0.1 to 0.2 (440 nm), while it reached values up to 0.8 under dusty conditions. Although higher AOD values have already been observed in the Mediterranean region during intense pollution or biomass burning events (Pace et al., 2005; Alados-Arbodas et al., 2011), values obtained during ADRIMED are typical of those observed in summertime (Nabat et al., 2015). This observation is also supported by the mass concentration of the main anthropogenic compounds that reached typical values for the region, as discussed previously. Our result on the moderate absorption properties of the dust plumes is thus likely relevant to dust events in the western Mediterranean in the absence of intense pollution or biomass burning emissions and can be used for constraining modeling studies and satellite retrievals that make assumption on dust optical properties.**

## **References:**

- Alados-Arboledas, L., Müller, D., Guerrero-Rascado, J. L., Navas-Guzman, D. Pérez-Ramirez, D., and Olmo, F. J. : Optical and microphysical properties of fresh biomass burning aerosol retrieved by Raman lidar, and star-and sun-photometry, *Geophys. Res. Lett.*, **38**, L01807, doi:10.1029/2010GL45999.
- Baumgardner, D., Dye, J. E., Gandrud, B. W., and Knollenberg, R. G.: Interpretation of measurements made by forward scattering probe (FSSP-300) during the airborne arctic stratospheric expedition, *J. Geophys. Res.-Atmos.*, **97**, 8035-8046, 1992.
- Chou, C., Formenti, P., Maille, M., Ausset, P., Helas, G., Harrison, M., and Osborne, S.: Size distribution, shape, and composition of mineral dust aerosols collected during the African Monsoon Multidisciplinary Analysis Special Observation Period 0: Dust and Biomass-Burning Experiment field campaign in Niger, January 2006, *J. Geophys. Res.-Atmos.*, **113**, D00C10, 10.1029/2008JD009897, 2008.
- Formenti, P., Rajot, J. L., Desboeufs, K., Saïd, F., Grand, N., Chevaillier, S., and Schmechtig, C.: Airborne observations of mineral dust over western Africa in the summer Monsoon season: spatial and vertical variability of physico-chemical and optical properties, *Atmos. Chem. Phys.*, **11**, 6387-6410, 10.5194/acp-11-6387-2011, 2011a.
- Kandler, K., SchÜTz, L., Deutscher, C., Ebert, M., Hofmann, H., JÄCkel, S., Jaenicke, R., Knippertz, P., Lieke, K., Massling, A., Petzold, A., Schladitz, A., Weinzierl, B., Wiedensohler, A., Zorn, S., and Weinbruch, S.: Size distribution, mass concentration, chemical and mineralogical composition and derived optical parameters of the boundary layer aerosol at Tinfou, Morocco, during SAMUM 2006, *Tellus B*, **61**, 32-50, 10.1111/j.1600-0889.2008.00385.x, 2009.
- Mallet, M., Dulac, F., Formenti, P., Nabat, P., Sciare, J., Roberts, G., Pelon, J., Ancellet, G., Tanré, D., Parol, F., di Sarra, A., Alados, L., Arndt, J., Auriol, F., Blarel, L., Bourriane, T., Brogniez, G., Chazette, P., Chevaillier, S., Claeys, M., D'Anna, B., Denjean, C., Derimian, Y., Desboeufs, K., Di Iorio, T., Doussin, J. F., Durand, P., Féron, A., Freney, E., Gaimoz, C., Goloub, P., Gómez-Amo, J. L., Granados-Muñoz, M. J., Grand, N., Hamonou, E., Jankowiak, I., Jeannot, M., Léon, J. F., Maillé, M., Mailler, S., Meloni, D., Menut, L., Momboisse, G., Nicolas, J., Podvin, J., Pont, V., Rea, G., Renard, J. B., Roblou, L., Schepanski, K., Schwarzenboeck, A., Sellegri, K., Sicard, M., Solmon, F., Somot, S., Torres, B., Totems, J., Triquet, S., Verdier, N., Verwaerde, C., Wenger, J., and Zapf, P.: Overview of the Chemistry-Aerosol Mediterranean Experiment/Aerosol Direct Radiative Forcing on the Mediterranean Climate (ChArMEx/ADRIMED) summer 2013 campaign, *Atmos. Chem. Phys. Discuss.*, **15**, 19615-19727, 10.5194/acpd-15-19615-2015, 2015.
- Muller, T., Laborde, M., Kassell, G., and Wiedensohler, A.: Design and performance of a three-wavelength LED-based total scatter and backscatter integrating nephelometer, *Atmos. Meas. Tech.*, **4**, 1291-1303, doi:10.5194/amt-4-1291-2011, 2011a.
- Massoli, P., Keabian, P. L., Onasch, T. B., Hills, F. B., and Freedman, A., Aerosol light extinction measurements by Cavity Attenuated Phase Shift (CAPS) Spectroscopy: Laboratory validation and field deployment of a compact aerosol particle extinction monitor, *Aerosol Sci. Tech.*, **44**:6, 428-435, DOI:10.1080/02786821003716599, 2010.
- Nabat, P., Solmon, F., Mallet, M., Michou, M., Sevault, F., Driouech, F., Meloni, D., di Sarra, A., Di Biagio, C., Formenti, P., Sicard, M., Léon, J.-F., and Bouin, M. -N.: Dust aerosol radiative effects during summer 2012 simulated with a coupled regional aerosol-

atmosphere-ocean model over the Mediterranean, *Atmos. Chem. Phys.*, **15**, 3303-3326, doi:10.5194/acp-15-3303-2015, 2015.

Pace, G., Meloni, D., and di Sarra, A.: Forest fire aerosol over the Mediterranean basin during summer 2003, *J. Geophys. Res.*, **110**, D21202, doi:10.1029/2005JD005986, 2005.

Ryder, C. L., Highwood, E. J., Lai, T. M., Sodemann, H., and Marsham, J. H.: Impact of atmospheric transport on the evolution of microphysical and optical properties of Saharan dust, *Geophys. Res. Lett.*, **40**, 2433-2438, 10.1002/grl.50482, 2013a.

Schladitz, A., Muller, T., Kaaden, N., Massling, A., Kandler, K., Ebert, M., Weinbruch, S., Deutscher, C., and Wiedensohler, A.: In situ measurements of optical properties at Tinfou (Morocco) during the Saharan Mineral Dust Experiment SAMUM 2006, *Tellus B*, **61**, 64-78, 10.1111/j.1600-0889.2008.00397.x, 2009.



1       **Size distribution and optical properties of mineral dust**  
2       **aerosols transported in the western Mediterranean**

3  
4   C. Denjean<sup>1,2</sup>, F. Cassola<sup>3</sup>, A. Mazzino<sup>3</sup>, S. Triquet<sup>1</sup>, S. Chevaillier<sup>1</sup>, N. Grand<sup>1</sup>, T. Bourriane<sup>4</sup>,  
5   G. Momboisse<sup>4</sup>, K. Sellegri<sup>5</sup>, A. Schwarzenbock<sup>5</sup>, E. Freney<sup>5</sup>, M. Mallet<sup>6</sup> and P. Formenti<sup>1</sup>

6  
7   [1] Laboratoire Interuniversitaire des Systèmes Atmosphériques (LISA), UMR-CNRS 7583,  
8   Université Paris-Est-Créteil (UPEC) et Université Paris Diderot (UPD), Institut Pierre Simon  
9   Laplace (IPSL), Créteil, France

10   [2] Leibniz Institute for Tropospheric Research (TROPOS), Permoserstraße 15, 04318, Leipzig,  
11   Germany

12   [3] Department of Physics and INFN, Genoa, Italy

13   [4] Centre National de Recherches Météorologiques (CNRM), Météo-France, Toulouse, France

14   [5] Laboratoire de Météorologie Physique (LaMP), CNRS/Université Blaise Pascal, Clermont-  
15   Ferrand, France

16   [6] Laboratoire d'Aérodynamique (LA), Université de Toulouse, CNRS, Toulouse, France

17  
18   Correspondance to :

19   Cyrielle Denjean ([cyrielle.denjean@meteo.fr](mailto:cyrielle.denjean@meteo.fr)~~[denjean@tropos.de](mailto:denjean@tropos.de)~~), Paola Formenti  
20   ([paola.formenti@lisa.u-pec.fr](mailto:paola.formenti@lisa.u-pec.fr))

## 1 **Abstract**

2 This study presents *in situ* aircraft measurements of Saharan mineral dust transported over the  
3 western Mediterranean basin in June-July 2013 during the ChArME<sub>x</sub>/ADRIMED (the  
4 Chemistry-Aerosol Mediterranean Experiment / Aerosol Direct Radiative Impact on the  
5 regional climate in the MEDiterranean region) airborne campaign. Dust events differing in  
6 terms of source region (Algeria, Tunisia and Morocco), time of transport (1-5 days) and height  
7 of transport were sampled. Mineral dust were transported above the marine boundary layer,  
8 which conversely was dominated by pollution and marine aerosols. The dust vertical structure  
9 was extremely variable and characterized by either a single layer or a more complex and  
10 stratified structure with layers originating from different source regions. Mixing of mineral dust  
11 with pollution particles was observed depending on the height of transport of the dust layers.

12 Dust layers carried higher concentration of pollution particles below 3 km above sea level (asl.)  
13 at intermediate altitude (1-3 km) than above 3 km asl. at elevated altitude (>3 km), resulting in  
14 scattering Angstrom exponent up to 2. below 3 km asl. 2 within the intermediate altitude.

15 However, the optical properties of the dust plumes remained practically unchanged with respect  
16 to values previously measured over source regions, regardless of the altitude. Moderate  
17 absorption of light by the dust plumes ~~Moderate light absorption of the dust plumes~~ was  
18 observed with values of aerosol single scattering albedo at 530 nm ranging from 0.90 to 1.00 ±  
19 0.04. Concurrent calculations from the aerosol chemical composition revealed a negligible  
20 contribution of pollution particles to the absorption properties of the dust plumes that was due  
21 to a low contribution of refractory black carbon in regards to the fraction of dust and sulfate  
22 particles. This suggests that, even in the presence of moderate pollution, likely a persistent  
23 feature in the Mediterranean, the optical properties of the dust plumes could be assimilated to  
24 those of native dust in radiative transfer simulations, modeling studies and satellite retrievals  
25 over the Mediterranean. Measurements also showed that the coarse mode of mineral dust was  
26 conserved even after 5 days of transport in the Mediterranean, which contrasts with the  
27 gravitational depletion of large particles observed during the transport of dust plumes over the  
28 Atlantic. Simulations with the WRF mesoscale meteorological model highlighted a strong  
29 vertical turbulence within the dust layers that could prevent deposition of large particles during  
30 their atmospheric transport. This has important implications for the dust radiative effects due to  
31 surface dimming, atmospheric heating and cloud formation. The results presented here add to  
32 the observational dataset necessary for evaluating the role of mineral dust on the regional  
33 climate and rainfall patterns in the western Mediterranean basin.

34



1

2 **1. Introduction**

3 Mineral dust aerosols constitute a major fraction of airborne particulate matter (Huneeus et al.,  
4 2012) and their contribution to the Earth's climate system is of considerable significance. In  
5 particular, dust aerosols exert a significant effect on global radiative budget by scattering and  
6 absorbing longwave and shortwave radiation (IPCC, 2013), thereby impacting the vertical  
7 profile of temperature and atmospheric stability (Jing et al., 2008) and the precipitation rate  
8 (Rosenfeld et al., 2001; Andreae and Rosenfeld, 2008; Choobari et al., 2014).

9 The Sahara desert hosts the maximum dust emission and atmospheric dust loading in the world  
10 (Choobari et al., 2014). Strong winds and convection produced by intense surface heating can  
11 uplift mineral dust particles into the free troposphere, where they are advected over large  
12 distances at the continental and intercontinental scales (d'Almeida, 1986; Goudie and  
13 Middleton, 2001; Engelstaedter et al., 2006). Along the year, the transport pathway of Saharan  
14 dust is mainly controlled by low-pressure systems over the Atlantic or North Africa, high  
15 pressure over the Mediterranean region, or high pressure at upper level over Africa (Moulin et  
16 al., 1998; Querol et al., 2009; Salvador et al., 2014). A significant fraction of dust loaded from  
17 Africa sources are transported westward across the Atlantic Ocean as far as the Caribbean  
18 (Maring et al., 2003; Doherty et al., 2008), the United States (Perry et al., 1997; Prospero et al.,  
19 2002) and South America (Swap et al., 1992; Formenti et al., 2001; Ansmann et al., 2009).  
20 Large Saharan dust storms are also carried across the Mediterranean Sea to Europe (Moulin et  
21 al., 1998; Koren et al., 2003; Collaud Coen et al., 2004; Papayannis et al., 2008). During such  
22 outbreaks, mineral dust emerges as the largest PM<sub>10</sub> source at rural and urban sites in the  
23 Mediterranean basin (Pey et al., 2013; Salvador et al., 2014).

24 Considerable uncertainties in quantifying the climatic effect of mineral dust arise from a lack  
25 of knowledge of their properties and spatial and vertical distributions over many regions of the  
26 world. In particular, to estimate the magnitude of the dust radiative effect, an accurate  
27 description of both particle size distribution and optical properties and their link with the  
28 chemical composition is necessary (Sokolik and Toon, 1996; Tegen et al., 1996). The size  
29 distribution is a fundamental parameter to estimate the aerosol radiative effect and atmospheric  
30 lifetime, but its representation remains challenging due to the large size spectrum of mineral  
31 dust, from hundreds of nanometers to tenths of micrometers (Formenti et al., 2011a). In  
32 particular, an accurate description of the coarse mode particles is vital since the presence of  
33 large particles enhance the capacity of mineral dust in absorbing radiation at short and long

Code de champ modifié

Code de champ modifié

Code de champ modifié

Code de champ modifié

Code de champ modifié

Code de champ modifié

Code de champ modifié

1 wavelengths (McConnell et al., 2008; Otto et al., 2009; Sicard et al., 2014), modify the  
2 atmospheric heating rate (Ryder et al., 2013a) and affect cloud formation (Koehler et al., 2009).  
3 Once in the atmosphere, mineral dust can undergo various aging processes, such as  
4 heterogeneous reactions with gas-phase compounds (Sullivan and Weber, 2006; Ma et al.,  
5 2012), condensation of low-volatile species (Clarke et al., 2004; Sullivan and Prather, 2007),  
6 cloud processing (Levin et al., 1996; Trochkin et al., 2003) and coagulation (Fan et al., 1996;  
7 Zhou et al., 1996; Levin et al., 2005). Because of these processes, the physico-chemical  
8 properties (composition, mixing state, shape, and size distribution) of dust aerosols might  
9 evolve during transport, leading in turn to the evolution of the optical properties (Formenti et  
10 al., 2011a). A recent study of Kanitz et al. (2014) has shown significant differences in the optical  
11 properties of two Saharan dust plumes over the Atlantic Ocean, resulting from different aging  
12 processes affecting the dust. Henceforth, the radiative effect of mineral dust should depend on  
13 the travel distance and pathway, residence time over their source regions and air masses  
14 encountered (Garrett et al., 2003).

15 The Mediterranean basin provides ideal conditions to investigate the changes in Saharan dust  
16 properties as numerous concurrent anthropogenic and natural sources of aerosols are active over  
17 this region. Case studies of mixing of Saharan dust with industrial/urban, marine and biomass  
18 burning particles have been documented in the past (Koçak et al., 2012; Mantas et al., 2014),  
19 and could explain the large variability of the values of single scattering albedo  $\omega_0$  (0.83-0.92 at  
20 the wavelength of 440 nm) reported by various studies (Sicard et al., 2012; Mallet et al., 2013).  
21 In past years, intensive field campaigns including *in situ* airborne measurements have mostly  
22 focused on properties of mineral dust at emission (e.g., over the Saharan and the Sahelian source  
23 regions) and over the Atlantic Ocean, and their comparison to trace the temporal evolution  
24 during transport (Formenti et al., 2003, 2011b; Reid et al., 2003; McConnell et al., 2008;  
25 Osborne et al., 2008; Heintzenberg, 2009; Weinzierl et al., 2009, 2011; Haywood et al., 2011;  
26 Ryder et al., 2013a,b). On the contrary, observations in the Mediterranean region were mostly  
27 limited to remote sensing from the ground (e.g. Moulin et al., 1997; Hamonou et al., 1999;  
28 Meloni et al., 2006; Saha et al., 2008; Basart et al., 2009; Gómez-Amo et al., 2011; Perrone and  
29 Bergamo, 2011; Mallet et al., 2013; Pey et al., 2013; Marconi et al., 2014) or spaceborne (de  
30 Meij and Lelieveld, 2011; Gkikas et al., 2012).

31 To fill this gap, the Aerosol Direct Radiative Impact on the regional climate in the  
32 MEDiterranean region (ADRIMED) field campaign, part of the international cooperative  
33 research program ChArMEx (the Chemistry-Aerosol Mediterranean Experiment;  
34 <http://charmex.lscse.ipsl.fr>) took place with the main objectives of characterizing Saharan dust

Code de champ modifié

Code de champ modifié

Code de champ modifié

Code de champ modifié

1 plumes by coordinated aircraft and ground-based measurements (Mallet et al., 2015). In this  
2 paper, we present *in situ* aircraft measurements obtained in June-July 2013 over the  
3 Mediterranean basin. The objective is to determine possible changes of dust properties during  
4 long-range transport over the western Mediterranean basin and explore the potential reasons for  
5 changes. ~~Particle size distribution, chemical composition and the associated optical properties~~  
6 ~~are presented, and their variability due to altitude and dust age are discussed.~~  
7 Section 2 describes the aircraft strategy, the instrumentation and the method used to determine  
8 the aerosol size distribution, chemical composition and the associated optical properties.  
9 Section 3 presents the campaign meteorology, the dust vertical profiles and the results of the  
10 aerosol properties within the dust plumes. Section 4 explores the potential factors affecting the  
11 variability of the aerosol properties due to altitude and dust age. Section 5 concludes this article.

## 12 **2. Measurement and methodology**

### 13 **2.1. Aircraft strategy**

14 The ATR-42 aircraft of SAFIRE (French aircraft service for environmental research,  
15 <http://www.safire.fr>) based at Cagliari (39°15'N, 9°03'E, Italy) conducted 16 flights in the  
16 period 14 June - 04 July 2013. In this paper, we present results from the 9 flights dedicated to  
17 the observation of mineral dust plumes that occurred between 16 June and 03 July 2013. ~~These~~  
18 ~~flights were carefully selected to provide measurements of air masses from dust active sources~~  
19 ~~based on the analysis of satellite images and backward trajectories, as described in section 2.4.~~

20 The ATR-42 aircraft performed research flights in the area between 35° - 43° N and -4° - 13°  
21 E, covering the western Mediterranean region to probe the Saharan dust properties in a range  
22 of varying transport pathways and source regions. The flight tracks are shown in Figure 1 and  
23 a summary of flight information is provided in Table 1.

24 The airborne missions were planned using four different dust plume forecast models (MACC  
25 ALADIN-Dust, SKIRON and BSC-DREAM8b v2.0) and satellite images from the SEVIRI  
26 radiometer on the Meteosat Second Generation (MSG) satellite, all available in real time from  
27 the ChArMex Operating Center (<http://choc.sedoo.fr/>) during the campaign. The general  
28 weather forecast was made daily by the French school of Meteorology (ENM), at Météo-France  
29 in Toulouse.

30 The general flight strategy consisted of two main parts: first, profiles from 300 m up to 6 km  
31 above sea level (asl) were conducted ~~by performing a spiral trajectory 10-20 km wide~~ to sound  
32 the vertical structure of the atmosphere and identify interesting dust layers. Afterwards, the  
33 identified dust layers were probed by straight levelled runs (SLR), where the aircraft flew at  
34

Code de champ modifié

1 fixed altitudes, to provide information on dust spatial variability and properties. Horizontal  
2 flight legs in the dust layers lasted 20-40 min to allow aerosol collection on filters. At the typical  
3 aircraft cruise speed of 100 m s<sup>-1</sup>, samples had spatial resolution ranging from 121 to 242 km.  
4

## 5 **2.2. Instrumentation**

6 The ATR-42 basic instrumentation provides meteorological parameters including temperature,  
7 dew point temperature, pressure, turbulence, relative humidity, wind speed, direction, CO and  
8 O<sub>3</sub> concentrations (Saïd et al., 2010). Only instruments relevant to microphysical properties,  
9 chemical composition and optical properties of aerosols are detailed in Table 2.

Code de champ modifié

10

### 11 **2.2.1. Aerosol concentration and size distribution**

12 The total number concentration of particles larger than 5 nm in diameter was measured using a  
13 butanol-based condensation nucleus counter (CPC, TSI model 3075) corrected for  
14 coincidences.

15 The particle number size distribution was measured over the largest possible size spectrum by  
16 combining optical and electrical mobility techniques.

17 The number size distribution in the submicron range was measured with an in-cabin Scanning  
18 Mobility Particle Sizer (SMPS) and a wing-mounted Ultra High Sensitivity Aerosol  
19 Spectrometer (UHSAS, Droplet Measurement Technologies). The SMPS consisted of a  
20 Differential Mobility Analyzer (DMA, Villani et al., 2007) interfaced to a Condensation

Code de champ modifié

21 Particle Counter (CPC, TSI model 3010). A closed-loop recirculation was used for the sheath  
22 flow of the DMA. The SMPS system provided the number size distribution of the electrical  
23 mobility diameter from the 30 - 400 nm in 135 nominal size classes (i.e. size classes provided

24 by the instrument not corrected for the dynamic shape factor) over time scans lasting 120

25 seconds. Therefore, only data acquired during SLR are considered. Data were processed by  
26 taking into account the particle electrical charging probabilities, the CPC counting efficiencies,

27 the DMA transfer functions and the diffusion losses in the SMPS and CPC systems. The  
28 UHSAS is an optical-scattering laser-based aerosol spectrometer, providing the number size

29 distribution of the optical equivalent diameter from 0.04 to 1 µm in 99 nominal size classes at  
30 a time resolution of 1 second. The spectrometer integrates light scattering between 22 to 158°

31 at 1054 nm. Due to reduced counting efficiency at size larger than 0.9 µm, only data at lower  
32 sizes are considered in this paper. The uncertainties on the particle diameter were estimated to

33 be 5% and 10% for the SMPS and UHSAS, respectively (Wiedensohler et al., 2012; Cai et al.,  
34 2008).

Code de champ modifié

Code de champ modifié

1 The number size distribution in the supermicron range was measured by the combination of  
2 two different optical particle counters (OPC). A wing-mounted Forward Scattering  
3 Spectrometer Probe (FSSP, Particle Measuring System, Model 300) measured the optical size  
4 distribution in the nominal size range of 0.28 to 20  $\mu\text{m}$  (Baumgardner et al., 1992). Data were  
5 recorded in 30 size classes at 1 second interval. The FSSP-300 is based on the measurement of  
6 the light scattered between 3 and 12° at 632.8 nm. ~~The FSSP has an uncertainty in diameter of  
7 about 30 % according to Baumgardner et al. (1992). Possible errors in the FSSP 300 sizing  
8 were assumed to be 30 % of the particle diameter according to Baumgardner et al. (1992).~~ A  
9 GRIMM OPC (model sky-OPC 1.129) operated inside the cabin at a 6-second time resolution  
10 and measuring the optical size distributions between 0.3 and 32  $\mu\text{m}$  on 32 size classes in  
11 nominal diameter. ~~However, only data at nominal size below 12  $\mu\text{m}$  were considered here due  
12 to the passing efficiency of the aerosols inlets connected to the GRIMM (see section 2.3.2. for  
13 further information).~~ The instrument integrates light scattering between 30 and 150° at 655 nm.  
14 According to the calibration of the GRIMM with standard, we assumed ~~an uncertainty in  
15 diameter of 10%. 10% uncertainties in particle sizing.~~

Code de champ modifié

Code de champ modifié

16

## 17 2.2.2. Aerosol chemical composition

18 Bulk aerosol samples were collected on-board by filtration through two stainless-steel filter  
19 units mounted in parallel. Sampling was performed only during constant altitude sequences  
20 lasting more than 25 minutes in order to guarantee sufficient mass loading of the filter samples.  
21 After exposure, samples were stored and transported at -20°C to avoid later modification. Once  
22 in the laboratory, samples collected on 42-mm diameter polycarbonate membranes (nominal  
23 pore size 0.4  $\mu\text{m}$  Nuclepore, Whatman) were cut in halves that were analyzed to yield the  
24 elemental and ionic composition. Concentrations of elements from Na to Pb were measured by  
25 wavelength-dispersive X-ray fluorescence (WD-XRF) using a PW-2404 spectrometer  
26 (Panalytical). Details of the analytical protocols are provided by Formenti et al. (2008). The  
27 concentration of water-soluble ions were determined by Ion chromatography (IC) with a  
28 Metrohm IC 850 device equipped with an injection loop of 100  $\mu\text{l}$ . For anionic species, IC has  
29 been equipped with Metrosep A supp 16 (250/4.0mm) column associated with a metrosepA  
30 supp 16 guard pre-column heated at 65°C. For simultaneous separation of inorganic and short-  
31 chain organic anions, elution has been realized with eluant composed at 20% by ultrapure water  
32 and at 80% by a solution 7.5 mM  $\text{Na}_2\text{CO}_3$  and 0.75mM NaOH. The elution flow rate was 0.8  
33  $\text{mL min}^{-1}$ . For cationic species, IC has been equipped with a Metrosep C4 (250/4.0mm) column  
34 associated to a metrosep C4 guard column heated at 30°C. Elution has been realized with an

1 eluant composed with 0.7 mM of dipicolinic acid and 1.7 mM of nitric acid. The elution flow  
2 rate was 1 mL min<sup>-1</sup>.

3 The mass concentration of refractory black carbon particles (rBC) was measured using a single  
4 particle soot photometer (SP2, DMT). The SP2 uses a continuous intra-cavity Nd:YAG laser at  
5 the wavelength of 1064 nm to heat rBC-containing particles to their vaporization point. Single  
6 particle rBC mass was derived from the peak intensity of the thermal radiation emitted by the  
7 incandescent rBC detected by the SP2. This method allows the quantification with 100%  
8 efficiency of rBC mass in single particles with mass equivalent diameters between 80-500 nm  
9 (Moteki and Kondo, 2010). The total rBC mass loading was reported as the sum of all the  
10 detected single particle rBC masses. Prior to the measurement field campaign, the SP2 was  
11 calibrated using fullerene soot particles, which have been shown to give similar SP2 response  
12 as ambient rBC (Moteki and Kondo, 2010; Baumgardner et al., 2012; Laborde et al., 2012).

13

### 14 **2.2.3. Aerosol scattering and extinction coefficients**

15 The particle scattering coefficient ( $\sigma_{scat}$ ) was measured at three wavelengths (450, 550 and 700  
16 nm) with an integrating nephelometer (TSI, model 3563), which integrates light scattered by  
17 particles at scattering angle between the incident and scattered radiation between 7° and 170°.  
18 The instrument operated at a volumetric flow rate of 30 L min<sup>-1</sup> and the data were acquired at  
19 1-s time resolution. The instrument was calibrated with free-particle air and high-purity CO<sub>2</sub>  
20 prior to and after the campaign. Uncertainty in  $\sigma_{scat}$  measured with the nephelometer is  
21 estimated to be 5% (Muller et al., 2011a). Measured values were corrected for the angular  
22 truncature error in the nephelometer measurements at angles smaller than 7° and greater than  
23 170° as described in section 2.3.2.

24 The particle extinction coefficient ( $\sigma_{ext}$ ) was measured with a Cavity Attenuated Phase Shift  
25 particle light extinction monitor (CAPS-PMex, Aerodyne Research) operated at the wavelength  
26 of 530 nm. The instrument relies on measuring the average time spent by the light within the  
27 sample cell. The sampling volumetric flowrate was 0.85 L min<sup>-1</sup> and data were processed with  
28 a time resolution of 1 second. Uncertainty in  $\sigma_{ext}$  measured with the CAPS is estimated to be  
29 3% (Massoli et al., 2010).

30

### 31 **2.3. Aerosol data analysis**

32 Figure 2 depicts the iterative procedure used to retrieve the aerosol size distribution and optical  
33 parameters relevant to this paper. We focused our attention on aerosol parameters used in  
34 climate models for calculating the direct and semi-direct aerosol radiative effects:



1 - The complex refractive index  $\tilde{n}$  defined as  $n_r - in_i$ , where  $n_r$  and  $n_i$  are the real and imaginary  
2 part representing the particle scattering and absorption properties, respectively.

3 - The single scattering albedo  $\omega_0$  (unitless) representing the balance between the scattering and  
4 the absorbing properties and defined as:

$$\omega_0(\lambda) = \frac{\sigma_{scat}(\lambda)}{\sigma_{ext}(\lambda)} \quad (1)$$

5 where  $\sigma_{scat}$  is the aerosol scattering coefficient (expressed in  $Mm^{-1} = 10^{-6} m^{-1}$ ),  $\sigma_{ext}$  the aerosol  
6 extinction coefficient ( $Mm^{-1}$ ) and  $\lambda$  the wavelength (nm).

7 - The asymmetry parameter  $g$  (unitless) describing the angular distribution of the scattered  
8 radiation and defined as:

$$g(\lambda) = \frac{1}{2} \int_0^\pi \cos(\Theta) \sin(\Theta) P(\Theta, \lambda) d\Theta \quad (2)$$

9 where  $P(\Theta, \lambda)$  is the scattering phase function and  $\Theta$  is the scattering angle.

10 - The mass extinction efficiency  $k_{ext}$  ( $m^2 g^{-1}$ ) representing the total light extinction per unit mass  
11 concentration of aerosol and calculated as:

$$k_{ext}(\lambda) = \frac{\sigma_{ext}(\lambda)}{C_m} \quad (3)$$

12 where  $C_m$  is the aerosol mass concentration ( $\mu g m^{-3}$ ).

13 In this study, we have decided to neglect the non-sphericity of mineral dust since the sphere  
14 model has been shown to produce negligible errors when computing radiative fluxes and flux  
15 related quantities, i.e. aerosol optical depth (AOD),  $\omega_0$  and  $g$  (Mishchenko et al., 1995). Because  
16 we only investigate angular-integrated properties and for sake of comparison with the large  
17 majority of field data published so far, in this paper we only perform calculations in the  
18 spherical approximation.

19

### 20 **2.3.1. Assessment of aerosol size distribution**

21 The particle size distribution was derived from the SMPS, UHSAS, GRIMM and FSSP-300.

22 For size distributions measured by SMPS, the electrical mobility  $D_m$  and the geometric particle  
23 diameters  $D_g$  are related by the dynamic shape factor  $\mathcal{X}$  (DeCarlo et al., 2004):

$$D_g = \frac{D_m}{\mathcal{X}} \quad (4)$$

24 The dynamic shape factor  $\mathcal{X}$  depends on the shape of the particles (Hinds, 1999). Dust particles  
25 are predominantly non-spherical (Chou et al., 2008). In this study, we have decided to neglect  
26 the non-sphericity of mineral dust to maintain retrieval conditions similar to those of previous  
27 literature studies on dust in source region. Henceforth,  $\mathcal{X}$  was set to unity.

1 Optical sizing instruments (i.e. UHSAS, GRIMM, FSSP-300) measure the amount of light  
 2 scattered by a single particle and convert this into a geometric particle size. This conversion  
 3 depends on the complex refractive index of the aerosol, as well as on the optical geometry and  
 4 the laser wavelength of the instrument. The correction procedure used the Mie scattering theory  
 5 for homogeneous spheres with known complex refractive index (Bohren and Huffman, 1983).  
 6 As discussed by Reid et al. (2003), the conversion of scattered light into particle size can lead  
 7 to ambiguity in the sizing of the coarse mode diameters. If the light intensity response of the  
 8 optical sizing instruments is non-unique it can lead to oversizing of larger particles. This  
 9 happens mostly for forward scattering probes, such as the FSSP-300, as demonstrated in Figure  
 10 S1 showing a flattening in the scattering cross section curves integrated over the FSSP-300  
 11 scattering angle range (3-15°) between 2 and 10 µm diameter. For the GRIMM 1.129 scattering  
 12 angles (30-150°), the scattering cross section is unique with size, except between 1.5-2 µm  
 13 where an inflection point can be seen. [During ADRIMED, systematic differences in the size  
 14 distributions measured by the FSSP-300 and the GRIMM were observed around 2 µm.](#) Given  
 15 the response curves in Figure S1, data between 2-10 µm and 1.5-2 µm diameter from the FSSP-  
 16 300 and the GRIMM, respectively, were not considered in this paper.

17 Figure 3 presents an example of size distributions measured in a dust plume by the different  
 18 instruments. As will be discussed below, the value of  $\tilde{n} = 1.53 - 0.004i$  at 530 nm was the most  
 19 appropriate to reconstitute both scattering and extinction coefficient and therefore we present  
 20 results using this value in Figure 3. Overall, the comparison between different instruments  
 21 shows good consistency, giving credence to the measurements and the choice of refractive  
 22 index and dynamic shape factor.

23 The resulting number and volume size distributions were parameterized by fitting four log-  
 24 normal distributions, as:

$$\frac{dN}{d \log D_p} = \sum_{i=1}^4 \frac{N_{tot,i}}{\sqrt{2\pi} \cdot \log \sigma_i} \exp \left[ -\frac{(\log D_p - \log D_{p,g,i})^2}{2(\log \sigma_i)^2} \right] \quad (5)$$

$$\frac{dV}{d \log D_p} = \sum_{i=1}^4 \frac{N_{tot,i} \cdot \frac{\pi}{6} \cdot D_p^3}{\sqrt{2\pi} \cdot \log \sigma_i} \exp \left[ -\frac{(\log D_p - \log D_{p,g,i})^2}{2(\log \sigma_i)^2} \right] \quad (6)$$

25 each mode  $i$  being characterized by characterized by the integrated number concentration  $N_{tot,i}$ ,  
 26 the geometric median diameter  $D_{p,g,i}$  and the geometric standard deviation  $\sigma_i$  (i.e. Figure 3).

27 To provide a synthetic representation of the particle number size distributions, the effective  
 28 particle  $D_{eff}$  was calculated as :

$$D_{eff} = \frac{\int D_p^3 \frac{dN}{dD_p} dD_p}{\int D_p^2 \frac{dN}{dD_p} dD_p} \quad (7)$$

1  $D_{eff}$  has been estimated separately on the fine and coarse fractions in the size ranges 0.053-1  $\mu\text{m}$   
 2 (referred as  $D_{eff,f}$  thereafter) and 1-32  $\mu\text{m}$  (referred as  $D_{eff,c}$ ), respectively.

### 4 2.3.2. Assessment of aerosol optical properties

5 An iterative procedure was used to derive  $\tilde{n}$ ,  $\omega_0$ ,  $g$  and  $k_{ext}$  at 530 nm and correct  $\sigma_{scat}$  for the  
 6 angular truncature error (i.e. Figure 2). The parametrized size distributions were used as input  
 7 for the Mie scattering calculations (Bohren and Huffman, 1983), which were done by varying  
 8 stepwise the real part of the complex refractive index  $n_r$  from 1.33 to 1.60 and the imaginary  
 9 part of the complex refractive index  $n_i$  from 0.000 to 0.020.  $\tilde{n}$  was assumed to be constant with  
 10 particle size and have thus to be regarded as an effective value for the entire particle population.  
 11  $\sigma_{scat}$  was adjusted to the CAPS operation wavelength of 530 nm by using the following equation:

$$\mathring{A}(\lambda_1, \lambda_2) = - \frac{\ln(\sigma_{scat}(\lambda_1)/\sigma_{scat}(\lambda_2))}{\ln(\lambda_1/\lambda_2)} \quad (8)$$

12 where  $\mathring{A}$  represents the spectral dependence of the scattering coefficient and  $\lambda_1$  and  $\lambda_2$  are the  
 13 wavelength interval. The scattering Angstrom exponent  $\mathring{A}$  is often used as a qualitative indicator  
 14 of aerosol particle size or fine mode fraction (Seinfeld and Pandis, 1998). Typically, it is lower  
 15 than  $\sim 0.5$  for aerosols dominated by coarse particles, such as mineral dust or sea salt, but it is  
 16 higher than 1 for fine particles, such as pollution particles or biomass burning. The calculated  
 17 values of  $\sigma_{scat}(530\text{nm})$  and  $\sigma_{ext}(530\text{nm})$  were compared to that measured by the nephelometer  
 18 and the CAPS, and values having the closest agreement within the measurement error bars were  
 19 chosen as the best estimate.

20 The in-aircraft aerosol instruments sampled through isokinetic and isoaxial aerosol inlets. The  
 21 nephelometer and GRIMM were set up behind the AVIRAD inlet, while the CAPS, SMPS and  
 22 SP2 were set up behind the Community Aerosol Inlet (CAI). Particle loss can occur both as a  
 23 result of the inlet aspiration efficiency and the transport losses in the pipework between the inlet  
 24 and the instruments. The cut-off diameter, at which the passing efficiency of the inlet equals  
 25 50%, was determined by a set of wind-tunnel experiments (unpublished data). The passing  
 26 efficiency was determined as the ratio of the particle number concentration measured by  
 27 GRIMM optical counters behind the sampling lines of the AVIRAD and CAI inlets to the  
 28 particle number concentration measured in the main flow of the wing tunnel where the air speed  
 29 was 93 m s<sup>-1</sup> as the cruise speed of the ATR-42. Monodisperse polystyrene latex spheres of 0.6,

Code de champ modifié

1 1.2, 4.6, 7.9 and 11  $\mu\text{m}$  diameter (Duke Scientifics, Thermo Sci.) and polystyrene  
2 divinylbenzene spheres of diameter varying between 1 and 35  $\mu\text{m}$  in diameter (also purchased  
3 from Duke Scientifics) were first diluted and then put in a reservoir connected to a peristaltic  
4 pump. The pump tubing was connected to a pneumatic spinning disk (SPIDI) in order to spray  
5 a large amount of droplets from the solution, some droplets having a particle incorporated. An  
6 air mover was mounted beneath the SPIDI and thus the droplets were rapidly evaporated. The  
7 particle size-dependent passing efficiency of the AVIRAD and CAI sampling inlets shown in  
8 Figure S2 indicates that the cut-off diameter value, expressed as optical equivalent, is 12  $\mu\text{m}$   
9 for the AVIRAD inlet and 5  $\mu\text{m}$  for the CAI.

10 To assess the impact of the inlets sampling efficiency on the measured optical properties, Mie  
11 scattering calculations were performed to estimate  $n_r$ ,  $n_i$ ,  $\omega_0$ ,  $g$  and  $k_{ext}$  using either the full size  
12 distribution or the size distribution measured behind the aircraft inlets. For  $\omega_0$ ,  $g$  and  $k_{ext}$ , we  
13 considered a fixed refractive index of 1.52-0.003i, reflective of the values observed for Saharan  
14 dust in source region (Schladitz et al., 2009; Formenti et al., 2011a; Ryder et al., 2013a). The  
15 discrepancies between  $\omega_0$ ,  $g$  and  $k_{ext}$ , including or not larger particle sizes were used to estimate  
16 the errors associated to the inlets sampling efficiency. For  $n_r$  and  $n_i$ , we estimated the difference  
17 between  $\tilde{n}$  derived from the iterative procedure described above (i.e. Fig. 2) using the full size  
18 distribution as input parameter and that obtained from the size distribution measured behind the  
19 aircraft inlets. The absolute errors associated with  $\omega_0$ ,  $g$  and  $k_{ext}$  due to the passing efficiencies  
20 of the inlets were in the range covered by the measurements uncertainties of both optical  
21 parameters and size distributions, which were estimated to be 0.02, 0.002, 0.04, 0.05 and 0.08,  
22 respectively.

23 Particle loss can however occur both as a result of the inlet aspiration efficiency and the  
24 transport losses in the pipework between the inlet and the instruments. The cut off diameter,  
25 at which the passing efficiency of the inlet equals 50%, happened at around 12  $\mu\text{m}$  for the  
26 AVIRAD inlet and 5  $\mu\text{m}$  for the Community Aerosol Inlet in equivalent optical diameter. Mie  
27 scattering calculations were performed using either the size distribution measured behind the  
28 aircraft inlets or the full size distribution to assess the impact of the size selective aircraft  
29 inlets on optical parameters. The absolute errors associated with  $n_r$ ,  $n_i$ ,  $\omega_0$ ,  $g$  and  $k_{ext}$  due to the  
30 passing efficiencies of the inlets were in the range covered by the measurements uncertainties  
31 of both optical parameters and size distributions, which were estimated to be 0.02, 0.002,  
32 0.04, 0.05 and 0.08, respectively.

#### 34 **2.4. Ancillary products**

1 Weather Research and Forecasting (WRF; Skamarock et al. 2008) simulations were performed  
2 to investigate the meteorological conditions and the turbulence within the dust layers. The WRF  
3 model is operational at the Department of Physics of the University of Genoa, Italy, in a three-  
4 domain configuration. In particular, the simulations on the parent domain, covering the entire  
5 Mediterranean basin with a horizontal grid spacing of 10 km, have been considered for the  
6 present paper. Initial and boundary conditions were generated from the operational global  
7 model GFS (Environmental Modeling Center, 2003) outputs ( $0.5 \times 0.5$  degree resolution). More  
8 details about the modelling chain and the model setup are given in Bove et al. (2014), Cassola  
9 et al. (2015), and Mentaschi et al. (2015).

10 As a complement, synoptic conditions and sea level pressure composite anomalies over the  
11 Mediterranean basin during the campaign were analyzed using reanalysis data sets, such as the  
12 NCEP/NCAR Reanalysis (Kalnay et al. 1996) and the NCEP Climate Forecast System (CFS)  
13 reanalysis (Saha et al., 2010).

14 Source regions and atmospheric transport times of the dust plumes were determined through  
15 the combination of satellite products and backward trajectories analysis. The potential source  
16 regions active during the observational period were identified using the images from the  
17 Spinning Enhanced Visible and Infrared Imager (SEVIRI) onboard the Meteosat Second  
18 Generation (MSG) satellite. The NOAA HYbrid Single-Particle Lagrangian Integrated  
19 Trajectory Model (HYSPLIT, <http://www.arl.noaa.gov/HYSPLIT.php>) using the Global Data  
20 Assimilation System (GDAS) meteorological input was used to calculate whether an air mass  
21 sampled by the aircraft could have originated from one of the identified active dust sources.  
22 Backward trajectories were initialized using the time and the location when the aircraft  
23 intercepted the air mass and were extended for up to 5 days prior the measurement. Backward  
24 trajectory calculations were performed at the beginning, the middle and at the end of each SLR  
25 to check the origin and transport pathway of the air masses through the measurements. We then  
26 operationally define the dust age as the time elapsed since the calculated air mass trajectory  
27 leave the ground where an active source was detected and the time of sampling by the aircraft.  
28

### 29 **3. Results**

#### 30 **3.1. Identification of the dust source region and transport pathway**

31 During the ADRIMED campaign, the synoptic situation was characterized by a “dipolar” sea  
32 level pressure anomaly pattern, with positive anomalies in the western Mediterranean and  
33 negative ones in the eastern part of the basin, as illustrated in Figure 4 (left panel). While this  
34 situation induced stronger and more frequent than normal northwesterly winds over the Sardinia

1 and Sicily channels, the average conditions ~~at mid-atmospheric levels at upper atmospheric~~  
2 ~~levels~~ during the campaign were closer to climatological ones (Figure 4, right panel). Moulin  
3 et al. (1998) have documented the frequency of dust episodes across the Mediterranean Sea.  
4 summer occurrences are quite frequent.~~Relatively frequent dust episodes could be observed as~~  
5 ~~it is typical for the season (Moulin et al., 1998).~~

Mis en forme : Police :Non Italique

6 The synoptic conditions during each of the 9 flights described in Figure 1 and Table 1 are  
7 summarized in Figure ~~S2-S3~~ and ~~S3-S4~~ in the Supplementary Material, where sea level pressure  
8 and 500-hPa geopotential height are shown. A low-pressure system can be found over the  
9 Atlantic on June 16, moving towards the Iberian Peninsula, while a subtropical ridge extends  
10 from North Africa to Central Mediterranean. This situation induced a strong south-  
11 southwesterly flow, firstly towards Southern Iberia and western Mediterranean (16-17 June),  
12 then extending eastwards and reaching Corsica on the subsequent days, favouring dust transport  
13 from the Saharan region. This is quite evident from Figure ~~S5.4~~, showing 700-hPa wind and  
14 relative humidity maps from the WRF model. Figure 1 shows the likely sources regions for dust  
15 sampled during the flights, identified from HYSPLIT simulation and MSG-SEVIRI satellite  
16 products. Mineral dust were most likely uplifted from southern Morocco and Southern Algeria  
17 and were sampled during flights F29, F30, F31 and F32 after 3.5-4.5 days of transport.

18 On 19-20 June the remnants of the aforementioned low are still visible as an upper level trough  
19 over the western Mediterranean (Figure ~~S5.4~~), triggering meridional transport at higher levels  
20 from North Algeria/Tunisia region towards the Sardinia and Sicily Channels. This is confirmed  
21 by backward trajectory and satellite product analyses showing that the dust sampled during the  
22 flight F33-34 travelled 1 to 5 days from North Algeria/Tunisia before their sampling (not  
23 shown). On 28 June during flight F38, an upper level low is found over the Alps and Central  
24 Europe, inducing a westerly flow from Tunisia where mineral dust were most likely uplifted  
25 towards Sicily at 700 hPa (Figure ~~S6.5~~), while the surface high pressure over East Atlantic and  
26 Iberia is associated to northwesterly winds at lower levels throughout most of Central  
27 Mediterranean. Finally, the situation during the last flight F42 (3 July) was characterized by a  
28 modest depression over Iberia, while the Azores anticyclone extended towards the  
29 Mediterranean. As a consequence, upper level winds were mainly southwesterly over North  
30 Africa, veering to westerly or northwesterly over the Sardinia and Sicily Channel, thus  
31 contributing to dust transport in the area. We estimate that mineral dust originating from South  
32 Morocco and Tunisia was transported for 3.5 days before sampling.

33 The identification of the dust source regions was confirmed by the measurements of the  
34 elemental composition. Overall, Si/Al ranged between 2.4-2.7 and Fe/Ca between 0.3-0.7 in

1 the samples collected during ADRIMED. This is consistent with values previously reported for  
2 mineral dust originating from Algeria, Tunisia and Morocco (Scheuven et al., 2013; Formenti  
3 et al., 2014). The identified emission areas also correspond to known source regions such as the  
4 Grand Erg occidental at the border between Algeria and Morocco, the Mekkeranne in Algeria  
5 and the Chott El Jerid in Tunisia (Ginoux et al., 2012).

### 6 7 **3.2. Vertical distribution of mineral dust**

8 Figure 5 shows the vertical profiles of the aerosol scattering coefficient  $\sigma_{scat}$  at  $\lambda = 450, 550$  and  
9  $700$  nm, the total particle number concentration in the submicron ( $N_{fine}; 5\text{nm} < D_p < 1 \mu\text{m}$ ) and  
10 the supermicron ( $N_{coarse}; D_p > 1 \mu\text{m}$ ) size ranges, and the vertical distribution of the scattering  
11 Angstrom exponent  $\text{\AA}$  calculated between 450 and 770 nm. The top height of the boundary  
12 layer ( $Z_b$ ) and the wind shear level ( $Z_s$ ) are also indicated in Figure 5 by a solid and a dashed  
13 line, respectively. All the vertical profiles were characterized by a weak and positive gradient  
14 of the potential temperature, characteristic of a stratified atmosphere (Figure S7)(Figure S6).  
15 The top height of the boundary layer was identified as the height at which the temperature  
16 profile showed the highest discontinuity and the water vapor mixing ratio decreased the most  
17 rapidly. The shear level was determined from the sudden increase in wind speed and change in  
18 wind direction (Figure S7)(Figure S6).

19 Mineral dust was observed above the boundary layer in layers extending from 1 km to more  
20 than 6 km above sea level (asl) (Figure 5). The presence of mineral dust within the boundary  
21 layer was not attested neither by chemical analyses nor with the back-trajectories analyses,  
22 which revealed that in the 5 days prior sampling, low-level air masses originated from the  
23 European continent or recirculated within Mediterranean basin. The transport of mineral dust  
24 in the free troposphere up to 9 km in altitude is a common observation in the Mediterranean  
25 region, as previously reported by lidar measurements (Dulac and Chazette, 2003; Gobbi et al.,  
26 2000; Mona et al., 2006; Di Iorio et al., 2009; Gómez-Amo et al., 2011). Such high altitudes  
27 may be linked to the strong vertical convective processes over the dust source regions, which  
28 lift dust particles at high atmospheric levels (Flamant et al., 2007, Papayannis et al., 2008;  
29 Cuesta et al., 2009).

30 The dust vertical structures showed an important variability. Complex and stratified structures  
31 were observed depending on the position of  $Z_b$  and  $Z_s$ . During the campaign, the wind shear  
32 level was equal to or higher than the top of the boundary layer.

33 When  $Z_s$  and  $Z_b$  coincided (F30, F31, F32, F38), the dust vertical structure was characterized  
34 by a single and rather homogeneous layer. It is noteworthy that apparently similar thermo-

Code de champ modifié

Code de champ modifié

Code de champ modifié



1 dynamical situations displayed a different spectral dependence of the scattering coefficient, as  
2 for example is the case above the boundary layer for flights F32 ( $\text{\AA} \sim 0.3$ ) and F38 ( $\text{\AA} \sim 0.9$ ),  
3 pointing out differences in the particle type. The values of  $\text{\AA}$  observed during the flight F38  
4 were higher than the values of  $\sim 0.5$  reported for Saharan dust in source region (McConnell et  
5 al., 2008a; Muller et al., 2011), but lower than values of  $\text{\AA} > 1$  reported for air masses dominated  
6 by pollution aerosols in the western Mediterranean basin (Di Biagio et al., 2015). It is  
7 reasonable to suppose that the profile F38 reflects a situation where desert dust was mixed with  
8 pollution particles. This is confirmed by the five-day backward trajectories (Figure 6a), which  
9 indicates air parcel coming from Europe and traveling at least three days above the  
10 Mediterranean Sea within the boundary level before its uplift over Tunisia.

11 When  $Z_s$  was higher than  $Z_b$  (F33, F34, F35), mineral dust was found in two distinct layers at  
12 ~~below and above 3 km asl. intermediate (between 1-3 km asl.) and elevated altitude (above 3~~  
13 ~~km asl.)~~. The five-day backward trajectories suggest that these dust layers originated from  
14 different dust source regions (Figure 1 and Table 1). An example is given by the flight F35  
15 (Figure 6b) for which ~~the above-3km the elevated~~ dust layer originated from central Algeria  
16 and was carried by northern flow to Lampedusa in 3.5 days, whereas ~~the below-3km the dust~~  
17 ~~layer at intermediate altitude~~ was transported from the southeastern Morocco-southwestern  
18 Algeria border region by a westerly flow within 3 days. Similar structure with multilayering of  
19 the Saharan dust corresponding to air masses from different dust source regions was previously  
20 observed by lidar measurements in the Mediterranean region (Hamonou et al., 1999; Guerrero-  
21 Rascado et al. 2008).

22 Regardless of the thermo-dynamical structure of the atmosphere, the aerosol vertical profiles  
23 revealed a clear vertical variability of the contribution of fine mode particles in the dust layers.  
24 The values of  $N_{fine}$  and  $\text{\AA}$  were generally below  $1000 \text{ \# cm}^{-3}$  and 0.5, respectively, ~~in dust layers~~  
25 ~~above 3 km asl. in elevated dust layers~~. In contrast,  $N_{fine}$  and  $\text{\AA}$  were up to  $4000 \text{ \# cm}^{-3}$  and 2.2,  
26 respectively, in the intermediate dust altitude (Figure 5). These observations suggest that ~~either~~  
27 ~~the dust plumes carried more fine particles during transport below 3 km altitude either the~~  
28 ~~intermediate dust plumes carried more fine particles during transport at intermediate altitude~~ or  
29 dust particles in the fine mode exhibited a vertical gradient.

30

### 31 3.3. Size distribution of the dust plumes

32 Particle number size distributions classified as a function of altitude are shown in Figure 7.  
33 Table 3 presents the average characteristics of the parameterized four-modal number size  
34 distributions.

Code de champ modifié

1 In the fine mode, the size distributions showed three modes around 80, 120 and 320 nm (Figure  
2 7a). For particles smaller than 300 nm, the shapes of the size distributions in the dust layer and  
3 in the boundary layer were quite similar. As particles in this size range mostly reflect  
4 anthropogenic influences from near or distant sources (Birmili et al., 2010), this indicates that  
5 the pollution plumes from the surface were exported above the boundary layer and mixed with  
6 the dust layers. The particle size distributions in the elevated dust layers followed a similar  
7 pattern as in the intermediate dust layers but number concentrations 2 times smaller were  
8 observed for the modes at 80 and 120 nm, suggesting that the concentration of pollution  
9 particles varied with the altitude. For particles between 300 nm and 1  $\mu\text{m}$ , the particle size  
10 distributions were reasonably constant for dust layers at various altitudes. Kaaden et al. (2008)  
11 found dust particles as small as 300 nm diameter in Morocco, which was also confirmed by  
12 Kandler et al. (2009). The decrease of  $N_{\text{fine}}$  with altitude (i.e. Figure 5) was therefore most likely  
13 due to the larger concentration of sub-300 nm pollution particles transported in the intermediate  
14 dust plumes. The fact that an identical median diameter  $D_{p,g}$  was used to parameterize the  
15 number size distributions in the fine ~~for below- and above-3km layers mode at intermediate and~~  
16 ~~elevated layers~~-(Table 3) and the prevalence of a sub-300 nm particles ~~in the below-3 km dust~~  
17 ~~layer in the intermediate dust layer~~ (Figure 7a) might also reflect that the mixing between the  
18 pollution and the dust plumes was mostly external in the fine mode.

19 In the coarse mode, a modal diameter of the number size distribution between 1.3 and 2.0  $\mu\text{m}$   
20 was observed indiscriminately to dust altitude. This indicates that the dust layers transported  
21 over the Mediterranean basin were well-mixed vertically in terms of coarse particle population,  
22 as previously observed by Weinzierl et al. (2011) for mineral dust after short-range transport  
23 over the eastern Atlantic Ocean. Conversely, the number concentration of large dust particles  
24 decreased with increasing altitude for freshly uplifted Saharan dust (Weinzierl et al., 2009;  
25 Ryder et al., 2013a). There are some evidences suggesting that the well-vertical mixing of the  
26 dust plumes occurs during the first day following the dust uplifted (Ryder et al, 2013b).  
27 Turbulent fluxes within the dust layer might be responsible for the vertical distribution of the  
28 dust aerosols becoming more homogeneous in terms of coarse mode particles as the dust ages  
29 (Rosenberg et al., 2014). Particles in the coarse mode showed a large flight-to-flight variability  
30 with number concentrations varying by more than one order of magnitude. This is quite evident  
31 in Figure 7b showing the conversion of number size distributions into volume size distributions.  
32 This variation in concentration might reflect the wide range of dust event encountered during  
33 the campaign in terms of source regions, time of transport and meteorological conditions.

1 The spread of volume size distributions obtained during ADRIMED overlaps with those  
2 measured during other airborne campaigns close to dust source regions (AMMA, FENNEC and  
3 SAMUM-1) in the coarse mode size range~~The comparison of volume size distributions~~  
4 ~~obtained during ADRIMED with those measured during other airborne campaigns close to dust~~  
5 ~~source regions (AMMA, FENNEC and SAMUM-1) showed a good overlapping in the peak of~~  
6 ~~the coarse mode~~ (Figure 7c). Effective diameters of the coarse mode  $D_{eff,c}$  (i.e. estimated in the  
7 size 1-32  $\mu\text{m}$  as defined in eq. 7) ranged from 3.8 to 14.2  $\mu\text{m}$  during ADRIMED, which is in  
8 the range of magnitude of the mean values of 3.8, 8.8 and 7.4  $\mu\text{m}$  obtained during AMMA,  
9 FENNEC and SAMUM-1, respectively (Formenti et al., 2011b; Ryder et al. 2013a; Weinzierl  
10 et al., 2011). Contrastingly, fewer particles larger than 10  $\mu\text{m}$  were uncounted after short-range  
11 transport over the eastern Atlantic Ocean in the Cape-Verde region during SAMUM-2 with  
12 respect to the other campaigns.  $D_{eff,c}$  around 3.2  $\mu\text{m}$  was found in the dust layers during  
13 SAMUM-2 (Weinzierl et al., 2011).

#### 15 3.4. Optical properties of the dust plumes

16 Figure 8a-b shows the vertical distribution of the real and imaginary parts of the refractive index  
17  $\tilde{n}$ . Within the dust plumes,  $\tilde{n}$  ranged from 1.50 to 1.55 for the real part and remained below  
18 0.005 for the imaginary part. Since  $\tilde{n}$  is related to the aerosol chemical composition (Liu and  
19 Daum, 2008), it is expected to be influenced by the mixing rate of the dust plume with pollution  
20 particles. We thus plotted the values of  $\tilde{n}$  as a function of the Angstrom exponent  $\text{\AA}$ . Besides  
21 not displaying significant variation with the altitude, the values of  $\tilde{n}$  did not show any  
22 dependence on  $\text{\AA}$ . The results obtained during ADRIMED have been compared with data in the  
23 literature for Saharan dust in or near-sources in Figure 8. For both the real and imaginary parts,  
24 our estimates of  $\tilde{n}$  fall within the range of variability (1.51 - 1.57 and 0.0001 - 0.0046 for the  
25 real and the imaginary parts, respectively) documented in source regions (Schladitz et al., 2009;  
26 Formenti et al., 2011a; Ryder et al., 2013b). This variability was attributed to the variability of  
27 the mineralogical composition of dust originating from diverse source regions (Kandler et al.,  
28 2009; Petzold et al., 2009). Our data do not show any clear dependence of  $\tilde{n}$  on dust source  
29 region either (not shown), which is consistent with the limited regional variability of the dust  
30 optical properties found 1-2 days after emissions in Africa by Formenti et al. (2014) from  
31 aircraft measurements. This is probably a consequence of the mixing of dust from various active  
32 sources occurring with each other during transport shortly after emission. A number of  
33 uncertainties in our identification of dust source region is associated with the employed  
34 methodology. The trajectory error associated with calculation of back trajectories from

Mis en forme : Police :Non Gras, Couleur de police :  
Automatique

Code de champ modifié

Code de champ modifié

Code de champ modifié

1 HYSPLIT reaches 15–30 % of the travel distance (Draxler and Rolph, 2013). Another potential  
2 source of uncertainty is the difficulty to discriminate the satellite aerosol signals from the  
3 surface reflectance using MSG-SEVIRI observations, especially over bright surfaces (Kutuzov  
4 et al., 2013). Moreover, even if the origin of the air masses was checked at the beginning, the  
5 middle and at the end of each straight-levelled runs, larger number of sources could potentially  
6 contribute to the aircraft samples because of aircraft's movements during sampling.

7 The vertical distribution of intensive optical properties relevant to radiative transfer (i.e. single  
8 scattering albedo  $\omega_0$ , asymmetry parameter  $g$  and extinction mass efficiency  $k_{ext}$ ) are shown in  
9 Figure 8c-e and Table 4. Estimates of  $\omega_0$ ,  $g$  and  $k_{ext}$  fall within the range 0.90 - 1.00, 0.6 - 0.8  
10 and 0.2 - 0.7  $\text{m}^2 \text{g}^{-1}$ , respectively. Overall, there is not clear dependence on the altitude. Only  
11 slightly low values of  $g$  (from  $\sim 0.7$  to  $\sim 0.8$ ) and  $k_{ext}$  (from  $\sim 0.2$  to  $\sim 0.7 \text{m}^2 \text{g}^{-1}$ ) were observed  
12 for some dust layers below 3 km asl. As  $\bar{n}$  was found to be constant with the altitude (i.e. Figure  
13 8a-b), these variations in  $g$  and  $k_{ext}$  were probably due to the variability in particles size  
14 distributions, which is consistent with the larger fraction of fine particles found in the higher  
15 altitude dust layers~~in these dust layers~~ (i.e. Figure 7a). Values of  $\omega_0$ ,  $g$  and  $k_{ext}$  remained,  
16 however, within the range of values reported in source regions by Schladitz et al. (2009),  
17 Formenti et al., (2011a) and Ryder et al., (2013b). Despite the fact that dust plumes carried  
18 pollution particles during their long-range transport in the Mediterranean region, the dust  
19 optical properties appeared to be unaffected by this mixing.

20 In the Mediterranean region, previous estimates of  $\omega_0$  for dust particles were obtained from  
21 remote-sensing techniques. Mallet et al. (2013) reported from multi-year ground-based  
22 AERONET observations a column-averaged  $\omega_0$  of 0.92-0.95 between 440-880 nm for various  
23 sites over the Mediterranean under the influence of dust aerosols. Using a similar approach, Di  
24 Biagio et al. (2009) reported lower column-averaged  $\omega_0$  values during dust transport events  
25 when boundary-layer air masses are transported from central Europe, probably rich in absorbing  
26 particles from urban-industrial European areas. Values as low as 0.88 at 530 nm were also  
27 determined by Sicard et al. (2012) during a case study of a dust plume transported over  
28 Barcelona and accompanied by a biomass-burning outbreak. Recently, Valenzuela et al. (2014)  
29 presented eight months of dust optical properties over the Alborán Island from Sun photometer  
30 measurements for dust plumes originating from northwestern Africa and passing over several  
31 urban-industrial areas along the coast of Morocco and from eastern Africa and traveling over  
32 the Mediterranean Sea. No significant changes in column-averaged  $\omega_0$  were reported for the  
33 different air masses, which indicates that the influence of anthropogenic fine particles  
34 originating from the urban-industrial areas in the north of Africa during desert dust outbreaks

Code de champ modifié

Code de champ modifié

Code de champ modifié

1 was negligible. Overall, these contrasting results highlight the major role of the transport  
2 conditions (height, air mass encountered) of the dust plumes rather in governing the mixing  
3 processes of mineral dust with other aerosol species. ~~than the dust source region in governing~~  
4 ~~the dust layer optical properties in the Mediterranean.~~

## 6 **4. Discussion**

### 7 **4.1. On the role of transport conditions in the mixing of pollution particles with** 8 **mineral dust**

9 In this section, we investigate the transport conditions of the dust layers expected to influence  
10 the mixing of mineral dust with pollution particles. As previously mentioned, the highest  
11 concentrations of pollution particles were detected in the intermediate dust layers. We further  
12 investigate this result by examining the variations of  $D_{eff,f}$  and  $D_{eff,c}$  with the altitude of the dust  
13 plumes. We assume that changes in  $D_{eff,f}$  reflected different fractions of externally mixed  
14 pollution particles smaller than 300 nm in the dust plumes, as discussed in section 3.3. In Figure  
15 9a, a sharp transition in the proportion of fine particles can be seen in  $D_{eff,f}$  at 3 km asl. with  
16 greater proportion of pollution particles found in the lower 3 km of the atmosphere. The  
17 observation of pollution particles at altitudes up to 3 km during ADRIMED is comparable with  
18 the average height of pollution layers observed in the western Mediterranean basin (Meloni et  
19 al., 2003; Mallet et al., 2005; Junkermann et al., 2009; Di Biagio et al., 2015). Hence, the  
20 vertical extent of pollution particles might explain the fact that the intermediate dust plumes  
21 were more affected by fine particles than the elevated dust layer. The coarse mode of the dust  
22 plume is also expected to be impacted by the presence of pollution particles. In case of an  
23 internal mixing between pollution particles and mineral dust, the mean particles size should  
24 increase. During ADRIMED,  $D_{eff,c}$  of the dust plume did not show any systematic dependence  
25 on altitude (Figure 9b). This finding must however be interpreted with some caution since  $D_{eff,c}$   
26 was affected by the large uncertainties in FSSP-300 and GRIMM sizing (i.e. section 2.2.1.) that  
27 might hide the detection of small aggregates on dust.

28 The mixing extent of pollution particles in dust layers is also expected to depend on the transport  
29 time of the plumes. Figure 10 shows  $D_{eff,f}$  against the estimated age of the dust air mass and  
30 divided according to the height of transport of the dust plumes. From these measurements, we  
31 do not find significant trend in the dust mixing rate with transport time in both elevated and  
32 intermediate layers. This result is not surprising for the elevated dust layers since we found that  
33 the interaction of dust plumes with pollution particles was limited when they were transported  
34 above 3 km asl. For dust plumes below 3 km asl., their transport time was at least 3 days before

1 sampling during ADRIMED. Afterwards the dust spent time over pollution regions appeared  
2 to have no more effect on the mixing extent of pollution particles. The constant  $D_{eff}$  values  
3 observed within the intermediate dust plumes and the boundary layer (Figure 9a) suggests also  
4 that the vertical transport and mixing of pollution particles with dust plumes were already  
5 completed at the time of sampling. Note that the intermediate dust layers reached the  
6 Mediterranean coasts affected by urban/industrial emissions after having undergone around 2  
7 days of transport. Hence, the pollution mixing rate appears to be a relatively rapid process more  
8 likely driven by the height of transport of the dust layers.

9

#### 10 **4.2. Contribution of pollution particles to the absorption properties of the dust** 11 **plumes**

12 We evaluated the effect of the contribution of pollution particles to the absorption properties of  
13 the dust layers by calculating  $\omega_0$  from the mass concentration of the main anthropogenic  
14 compounds. Table 5 shows the mass concentration of major elements, ionic species and rBC  
15 measured in the dust plumes. The dust mass concentration estimated from the measured Al  
16 using the mean Al mass fraction in the crustal composition of 7.09% (Guieu et al., 2002) is  
17 also shown. In all samples, silicates were the most abundant type of dust particles, as expected  
18 from previous chemical analysis of dust in North Africa (Scheuven et al., 2013; Formenti et  
19 al., 2014). The presence of pollution particles within the dust plumes is confirmed by the  
20 detection of  $\text{SO}_4^{2-}$  and rBC as well as typical anthropogenic trace elements such as V, Pb and  
21 Zn.

22  $\text{SO}_4^{2-}$  reached concentrations typical of the Mediterranean region in summertime (Ripoll et al.,  
23 2015) with the largest concentration of  $2.5 \mu\text{g m}^{-3}$  found over Corsica during the flight F34. The  
24 positive correlation between the concentration of  $\text{SO}_4^{2-}$  and  $N_{fine}$  indicates the presence of  
25 externally mixed sulfate-containing particles in the fine mode particles, such as ammonium  
26 sulfate particles.  $\text{SO}_4^{2-}/\text{NH}_4^+$  ratios being higher than unity, the presence of  $\text{SO}_4^{2-}$  in the dust  
27 layers can also either be due to nucleation of sulfuric acid in polluted plumes, or to sulphate  
28 formation at the surface of preexistent particles by uptake of gaseous sulfur dioxide or by  
29 coagulation of sulphate particles (Ullerstam et al., 2002; Korhonen et al., 2003; Sullivan et al.,  
30 2009).

31 Concentrations of rBC ranged from 0.04 to  $0.13 \mu\text{g m}^{-3}$ . Although these values are much lower  
32 than concentrations measured in areas of high industrial or traffic density (Liu et al., 2014;  
33 Mantas et al., 2014), they are in agreement with concentrations found in continental and  
34 background area of the western Mediterranean (Ripoll et al., 2015). Except in the case of large

1 forest fires, rBC concentrations are generally low on average in summertime due to the absence  
2 of the major sources of emission, such as domestic wood burning (Tsyro et al., 2007).

3 Calculations of  $\omega_0$  from the aerosol chemical composition were performed assuming that dust  
4 was externally mixed with rBC and sulfate. Indeed, prevalence of an external mixing between  
5 dust particles and rBC has been observed from long-term measurements in the western  
6 Mediterranean basin (Ripoll et al., 2015). Moreover, coating of sulfate on mineral dust has been  
7 shown to have no significant effect on dust optical properties (Bauer et al., 2007). ]

8 Calculations of  $\omega_0$  were performed as follows:

$$\omega_0 = \frac{\sum_i (k_{ext,i} - k_{abs,i}) \cdot C_{m,i}}{\sum_i k_{ext,i} \cdot C_{m,i}} \quad (9)$$

9 We used mean mass absorption and extinction efficiencies (i.e. the total light absorption or  
10 extinction per unit mass of aerosol, referred as  $k_{abs}$  and  $k_{ext}$ ) of  $0.02 \text{ m}^2 \text{ g}^{-1}$  and  $0.64 \text{ m}^2 \text{ g}^{-1}$  for  
11 dust (Hess et al., 1998),  $7.5 \text{ m}^2 \text{ g}^{-1}$  and  $9.4 \text{ m}^2 \text{ g}^{-1}$  for rBC (Bond and Bergstrom, 2006) and  $0 \text{ m}^2$   
12  $\text{g}^{-1}$  and  $5.0 \text{ m}^2 \text{ g}^{-1}$  for sulfate (Charlson et al., 1992). As shown in Table 5,  $\omega_0$  obtained from this  
13 calculation ranged from 0.93-0.97, which falls within the range of values obtained from  
14 measurements ( $0.92-0.99 \pm 0.04$ ). For comparison, we estimate that  $\omega_0$  for pure mineral dust  
15 was 0.97. This simple approach confirms the small influence of pollution particles on the optical  
16 properties of the dust plumes over the Mediterranean region.

17 The ADRIMED field campaign was characterized by moderate AOD with averaged values  
18 ranging between 0.1 – 0.6 at 440 nm as observed by AERONET/PHOTONS sun-photometers  
19 (see Figure 19 of Mallet et al., 2015). Outside of dust events, the AOD displayed values from  
20 0.1 to 0.2 (440 nm), while it reached values up to 0.8 under dusty conditions. Although higher  
21 AOD values have already been observed in the Mediterranean region during intense pollution  
22 or biomass burning events (Pace et al., 2005; Alados-Arbodas et al., 2008; Péré et al., 2011),  
23 values obtained during ADRIMED are typical of those observed in summertime (Nabat et al.,  
24 2015). This observation is also supported by the mass concentration of the main anthropogenic  
25 compounds that reached typical values for the region, as discussed previously. Our result on the  
26 moderate absorption properties of the dust plumes is thus likely relevant to dust events in the  
27 western Mediterranean in the absence of intense pollution or biomass burning emissions and  
28 can be used for constraining modeling studies and satellite retrievals that make assumption on  
29 dust optical properties.

30 We compared our measurements on dust absorption properties with values published in the  
31 OPAC aerosol database that is widely used by modelling and remote sensing communities. The  
32 result of this comparison indicates an overestimation of dust absorption properties in the OPAC

Mis en forme : Standard



1 database. The  $n_i$  value achieved in the OPAC database ( $n_i=0.006$ ) are high compared to values  
2 observed for Saharan mineral dust in source region and over the Mediterranean during  
3 ADRIMED ( $n_i$  between 0.000–0.005). This finding is in line with previous studies showing  
4 disagreements in dust absorption between satellite retrievals and modelling studies that has been  
5 solved by decreasing the imaginary part of the dust refractive index (Kaufman et al, 2001;  
6 Moulin et al, 2001; Balkanski et al., 2007; Mian Chin et al., 2009). ▲

Mis en forme : Police :Non Gras

### 8 **4.3. Retention of coarse mode particles in the dust plumes**

9 Figure 11 shows  $D_{eff,c}$  against the estimated age of the dust air mass. Observations from aircraft  
10 during previous campaigns are shown for comparison. The  $D_{eff,c}$  values did not change with  
11 time, suggesting that the dust layers transported over the Mediterranean region tend to conserve  
12 their coarse mode with time. During ADRIMED,  $D_{eff,c}$  values obtained in dust layers having  
13 spent less than 1.5 days in the atmosphere are consistent with those obtained near dust source  
14 regions (Formenti et al, 2011b; Weinzierl et al., 2011). Conversely, dust layers having spent  
15 more than 1.5 days in the atmosphere present higher  $D_{eff,c}$  than previously observed over the  
16 Atlantic ocean (Maring et al., 2003; Weinzierl et al., 2011). Values obtained during ADRIMED  
17 are consistent with those obtained near dust source regions within 1.5 days after emission  
18 (Formenti et al., 2011b; Weinzierl et al., 2011; Ryder et al., 2013b), but, for a comparable  
19 transport time, higher than after long range transport over the Atlantic ocean (Maring et al.,  
20 2003; Weinzierl et al., 2011).

21 The loss of large dust particles after transport as observed over the Atlantic Ocean is most likely  
22 associated to the removal processes occurring as the dust travels downwind (Mahowald et al.,  
23 2014). As smaller particles fall downward much slower than larger particles, coarse particles  
24 are expected to be more prevalent close to the sources regions. To date only few studies have  
25 focused on understanding the evolution of dust size distribution, especially during transport  
26 over the Atlantic Ocean (Maring et al., 2003; Reid et al., 2003; Kalashnikova and Kahn, 2008).  
27 These measurements pointed out large differences between the observed and modeled evolution  
28 of dust size, with a lifetime of coarse particles longer than expected from deposition theories.  
29 This suggests that other processes counterbalanced the loss of large particles by dry deposition  
30 along transport. These processes seem to be particularly important in the Mediterranean region,  
31 since the proportional volume of coarse particles in the size distribution did not vary  
32 substantially even after 5 days of transport.

33 The persistence of coarse particles over the Mediterranean basin during transport could be  
34 explained by the presence of temperature inversions in the middle troposphere keeping the dust

1 layers confined due to the stable stratification. This was revealed by most of the aircraft  
2 temperature profiles (Figure S7). Furthermore, the WRF model simulations of the  
3 vertical velocity and vertical cross-section indicate the existence of updraft/downdraft due to  
4 the thermal turbulence within the dust layers circulating over the Mediterranean basin in  
5 summertime, due to elevated temperatures within the dust layers and large insolation. An  
6 example for flight F33 in the Corsica region is shown in Figure 12, where the vertical velocity  
7 showed updrafts and downdrafts up to  $0.5 \text{ Pa s}^{-1}$ , corresponding to about  $5 \text{ cm s}^{-1}$ . This value is  
8 at least one order of magnitude greater than the gravitational settling velocity ( $0.25 \text{ cm s}^{-1}$ )  
9 expected for particles of  $8 \mu\text{m}$  diameter, value indicated by Maring et al. (2003) as the threshold  
10 above which sensible changes in dust size distribution during atmospheric transport across the  
11 Atlantic could be observed. The occurrence of turbulent updraft and downdraft motion could  
12 therefore result in an enhancement of the particle lifetime in the atmosphere over the  
13 Mediterranean basin.

14

## 15 5. Conclusions

16 We presented the first *in situ* aircraft measurements of the size distribution and optical  
17 properties of Saharan dust transported over the western Mediterranean basin within the  
18 framework of the ADRIMED airborne campaign in June-July 2013. Dust particles originating  
19 from Algeria, Tunisia and Morocco were sampled in the western Mediterranean basin after 1-  
20 5 days of transport.

21 Measurements of aerosol vertical profiles revealed that dust particles were transported inside  
22 well-defined layers above the boundary layer ( $>1 \text{ km asl.}$ ) dominated by pollution and marine  
23 particles. The dust vertical structure was extremely variable and characterized either by a single  
24 layer or a more complex and stratified structure. Backward trajectories indicated that the  
25 multilayering of the Saharan dust corresponded to air masses originating from different dust  
26 source regions. Abundance of sub-300 nm particles in the Saharan dust layers suggested a  
27 strong mixing of dust with pollution particles. The height of transport of the dust layers  
28 appeared to be the main factor affecting the mixing extent of pollution particles with mineral  
29 dust. Measurements showed higher concentration of pollution particles in dust layers below 3  
30 km asl. than at higher altitude, resulting in scattering Angstrom exponent up to 2.2 below 3 km  
31 asl. Mineral dust carried higher concentration of pollution particles at intermediate altitude (1-  
32 3 km asl.) than at elevated altitude ( $>3 \text{ km asl.}$ ), resulting in scattering Angstrom exponent up  
33 to 2.2 within the intermediate layer. This coincides with the typical height of pollution layers  
34 ( $\sim 3 \text{ km asl.}$ ) observed in the western Mediterranean basin.

1 The optical properties of the dust layers were not significantly affected by this mixing with  
2 respect to values reported for native dust. Mineral dust aerosols were found to be moderately  
3 absorbing with values of  $\omega_0$  between 0.90 and 1.00 at 530 nm. Concurrent optical calculations  
4 from the aerosol chemical composition revealed that the contribution of pollution particles to  
5 absorption properties of the dust plumes was negligible. This was most likely due to the low  
6 contribution of rBC (~2% in mass) in regards to the fraction of dust (~84%) and sulfate (~14%)  
7 in the dust plumes. The concentrations of anthropogenic particles being typical of those  
8 observed in the Mediterranean region in summertime, these results demonstrate that outside  
9 severe episode of pollution or biomass burning, mineral dust dominate the optical properties of  
10 the dust plumes in the Mediterranean even if source of pollution particles are present.

11 An important question for the dust direct, semi-direct and indirect radiative effects is how long  
12 the coarse mode of dust particles is conserved during transport. We showed that the coarse  
13 mode was conserved even after 5 days of transport in the Mediterranean, which contrasts with  
14 the gravitational depletion of large dust particles observed during the transport of dust over the  
15 Atlantic Ocean. The global importance of this result is however still linked to whether these  
16 observations are ubiquitous or occur only for specific dust transport events. Dust events  
17 differing in terms of source region, time and height for transport were reported in this study.  
18 For all these case studies, the coarse mode of dust particles was conserved during transport,  
19 which might reflect the representativeness of the situation mostly occurring in summertime in  
20 the western Mediterranean basin.

21 Most climate models simulate currently the dry deposition as a positive relationship of the  
22 particles size, leading in an underestimation of the fraction of coarse particles being transported  
23 long distances (Mahowald et al., 2014). Given the scarcity of field studies investigating the  
24 evolution of the dust size distribution during transport, our results point out key processes  
25 controlling the retention of large dust aerosols. In particular, WRF model simulations  
26 highlighted a strong turbulence within the dust layer with vertical velocity at least one order of  
27 magnitude greater than the particle gravitational settling velocity. Particles could therefore  
28 remain trapped in the atmosphere by this strong turbulence. Further studies involving a deep  
29 analysis of aircraft measurements of turbulence parameters both in the Mediterranean and in  
30 other geographical areas such as the Atlantic region are required in order to quantitatively  
31 characterize this process and improve the representativeness of the temporal evolution of dust  
32 size distribution in climate models useful for radiative impact or marine biogeochemical  
33 applications.

1 The dataset obtained during the ADRIMED airborne campaign can also be used for  
2 constraining satellite retrievals that make assumptions on dust properties in order to derive  
3 water vapor profiles, surface temperatures and greenhouse gases concentrations. The results  
4 presented here suggest that the size and optical properties of the dust plumes could be  
5 assimilated to those of native dust in satellite retrievals in the western Mediterranean. [A](#)  
6 [straightforward comparison of our results with values published in the OPAC aerosol database,](#)  
7 [which is widely used by the remote sensing communities, suggests that the OPAC database](#)  
8 [overestimate dust absorption.](#) Moreover, this important dataset provides opportunities for  
9 evaluating satellite aerosol products (size, absorption properties, vertical profiles) over the  
10 Mediterranean through comparison with our in-situ airborne measurements.

11 In terms of significance for direct and semi-direct radiative effects, the presence of moderately  
12 absorbing particles within the dust layers can induce important modifications in the  
13 tropospheric heating and surface cooling by perturbing the incoming and outgoing radiations.  
14 Evidence for retention of coarse mode particles in the dust layers indicates also that mineral  
15 dust may still be a significant source of cloud condensation nuclei and ice nuclei despite having  
16 undergone long-range transport. Hence, mineral dust may have potentially important  
17 implications for the regional climate and the rainfall patterns in the west Mediterranean that  
18 should be quantitatively addressed in future modelling studies.

19

## 20 **Acknowledgements**

21 This research work has been supported by the French National Research Agency (ANR)  
22 through the ADRIMED program (contract ANR-11-BS56-0006). This work is part of the  
23 ChArMEx project supported by CNRS-INSU, ADEME, Météo-France and CEA in the  
24 framework of the multidisciplinary program MISTRALS (Mediterranean Integrated Studies at  
25 Regional And Local Scales; <http://mistrals-home.org/>). The aircraft deployment was also  
26 supported by CNES. We thank the instrument scientists, pilots and ground crew of SAFIRE for  
27 facilitating the instrument integration and conducting flying operations. We acknowledge Pierre  
28 Nabat and the ENM students, especially Damien Serça, Jonathan Guth and Valentin Seigner  
29 for their meteorological forecasts during the campaign. We thank the NOAA Air Resources  
30 Laboratory (ARL) for the provision of the HYSPLIT transport and dispersion model used in  
31 this study. [We gratefully acknowledge the two anonymous reviewers whose suggestions helped](#)  
32 [improve and clarify this manuscript.](#)

33

1 Table 1: Detailed information about the flights (number (ID), date, take-off time (TO), landing  
 2 time (L) and route), the vertical profiles (latitude (Lat), longitude (Lon) and start time) and the  
 3 dust layers sampled (height in meter, origin, age in day) during the ADRIMED airborne  
 4 campaign. Times are expressed in Coordinated Universal Time (UTC), ~~Greenwich Mean Time~~  
 5 ~~(GMT)~~.  
 6

Flight information					Vertical profile			Dust layer		
ID	Date	TO	L	Flight route	Lat	Lon	Start time	Height	Origin	Age
F29	16 June 2013	08:18	10:20	Cagliari - Minorca	40N	5E	09:50	2200-4500	southwestern Algeria	4.5
F30	16 June 2013	11:58	14:40	Minorca - Granada	37N	4W	14:20	2400-4800	southwestern Algeria	4
F31	17 June 2013	07:15	09:54	Granada - Minorca	37N	4W	07:15	2800-5400	southern Algeria	3.5
F32	17 June 2013	11:45	13:43	Minorca - Cagliari	40N	5E	11:45	1000-4600	southwestern Algeria	4.5
F33	19 June 2013	11:35	15:00	Cagliari - East Corsica	43N	9E	12:50	3000-4000	northeastern Algeria	2
								1500-3000	northeastern Algeria	3
F34	20 June 2013	11:00	14:15	Cagliari - West Corsica	43N	7E	12:20	>2800	Tunisia	1
								1600-2800	Tunisia	5
F35	22 June 2013	08:47	11:26	Cagliari - Lampedusa	36N	13E	10:25	>3500	southern Algeria	2
								1500-3500	southern Morocco	4
F38	28 June 2013	10:59	13:29	Cagliari - Lampedusa	36N	13E	12:30	1200-4500	Tunisia	3
F42	03 July 2013	08:29	11:55	Cagliari - Lampedusa	36N	13E	09:50	>3000	Tunisia	3.5
								<3000	southern Morocco	3.5

7  
8

1 Table 2: Instruments detailed in this article operating onboard the ATR-42 aircraft during the  
 2 ADRIMED campaign.  
 3

Parameter measured	Instrument	Abbreviation	Location in the aircraft	Wavelength (nm)	Nominal size range ( $\mu\text{m}$ )	Temporal resolution
Size distribution	Forward Scattering Spectrometer Probe, Model 300, Particle Measuring Systems	FSSP-300	wing-mounted	632.8	0.28 - 20	1 s
	Ultra High Sensitivity Aerosol Spectrometer, Droplet Measurement Technologies	UHSAS	wing-mounted	1054	0.04 - 1	1 s
	Sky-Optical Particle Counter, Model 1.129, Grimm Technik	GRIMM	AVIRAD inlet	655	0.25 - 32	6 s
	Scanning mobility particle sizer, custom-built (Villani et al., 2007)	SMPS	community aerosol inlet	n/a	0.03 - 0.4	2 min
Integrated number concentration	Condensation Particle Counters, Model 3075, TSI	CPC	AVIRAD inlet	n/a	> 0.005	1 s
Chemical composition	Filter sampling	n/a	AVIRAD inlet	n/a	n/a	20-40 min
	Single particle soot photometer, Droplet Measurement Technologies	SP2	community aerosol inlet	1064	0.08 - 0.5	1 s
Scattering coefficient	3 $\lambda$ Integrated Nephelometer, Model 3563, TSI	Nephelometer	AVIRAD inlet	450, 550, 700	n/a	1 s
Extinction coefficient	Cavity Attenuated Phase Shift, Aerodyne Research Inc.	CAPS	community aerosol inlet	530	n/a	1 s

4  
 5  
 6

1 Table 3: Parameters (geometric median diameter  $D_{p,g,i}$  in  $\mu\text{m}$ , standard deviation  $\sigma_i$ , and  
2 integrated number concentration  $N_{tot,i}$  in  $\# \text{cm}^{-3}$ ) of the four log-normal distributions used to  
3 parameterize the number size distributions obtained at the different altitudes. The mean,  
4 minimum and maximum of all parameters are listed.  
5

		$D_{p,g,1}$	$\sigma_1$	$N_{tot,1}$	$D_{p,g,2}$	$\sigma_2$	$N_{tot,2}$	$D_{p,g,3}$	$\sigma_3$	$N_{tot,3}$	$D_{p,g,4}$	$\sigma_4$	$N_{tot,4}$
<u>Above- 3kmElevated dust layerDust layer</u>	mean	0.08	1.25	170	0.12	1.60	300	0.32	1.70	15	1.3	2.2	3.0
	min	0.09	1.20	80.0	0.13	1.30	80.0	0.18	1.65	40	2.5	1.8	0.1
	max	0.08	1.25	320	0.12	1.56	600	0.32	1.70	45	1.3	2.2	12
<u>Below- 3kmIntermediate dust layerdust layer</u>	mean	0.08	1.25	300	0.12	1.60	700	0.32	1.70	15	2.0	2.4	1.0
	min	0.08	1.25	250	0.11	1.50	400	0.20	1.70	35	1.7	2.1	0.7
	max	0.08	1.25	600	0.13	1.50	1100	0.18	1.90	80	1.7	2.0	2.5
Boundary layer	mean	0.08	1.25	450	0.12	1.60	650	0.32	1.70	5.0	1.3	2.1	1.0
	min	0.08	1.25	150	0.12	1.60	200	0.30	1.70	1.8	1.0	2.1	0.1
	max	0.08	1.25	600	0.12	1.60	1400	0.32	1.70	15	1.3	2.1	3.0

6  
7  
8  
9



1 Table 4: Optical parameters (real part of the complex refractive index  $n_r$ , imaginary part of the  
 2 complex refractive index  $n_i$ , single scattering albedo  $\omega_0$ , asymmetry parameter  $g$  and mass  
 3 extinction efficiency  $k_{ext}$ ) all at  $\lambda=530$  nm as a function of the altitude. The mean, minimum and  
 4 maximum of all parameters are listed.  
 5

		$n_r$	$n_i$	$\omega_0$	$g$	$k_{ext}$
<u>Above-3km dust layer</u> <del>Elevated dust layer</del>	mean	1.53	0.003	0.95	0.8	0.4
	min	1.50	0.000	0.90	0.7	0.3
	max	1.55	0.005	1.00	0.8	0.5
<u>Below-3km dust layer</u> <del>Intermediate dust layer</del>	mean	1.52	0.003	0.94	0.7	0.5
	min	1.50	0.000	0.90	0.6	0.4
	max	1.55	0.005	1.00	0.7	0.7

6

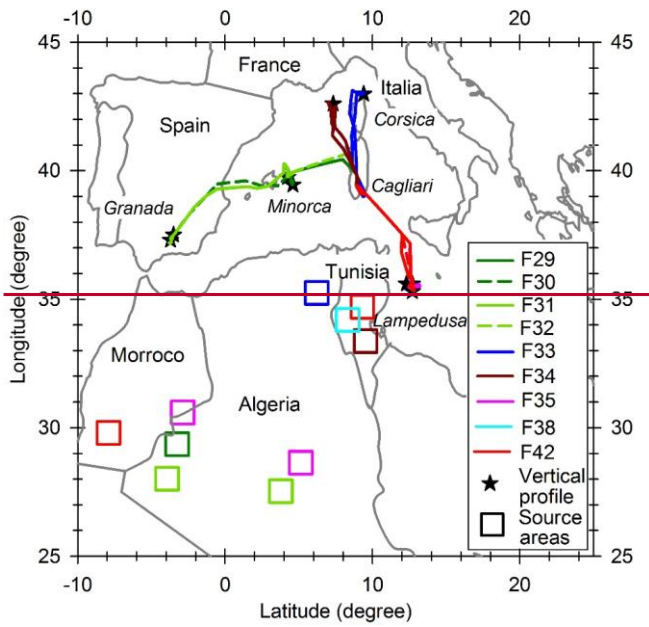
1 Table 5: Concentrations of major crustal (Si, Al, Fe and Ca, in  $\text{ng m}^{-3}$ ) and metallic tracers (Si,  
2 V, Pb and Zn, in  $\text{ng m}^{-3}$ ), ionic species ( $\text{SO}_4^{2-}$ ,  $\text{NO}_3^-$ ,  $\text{NH}_4^+$ , in  $\text{ng m}^{-3}$ ), black carbon (in  $\text{ng m}^{-3}$ )  
3  $^3$ ), mineral dust (in  $\mu\text{g m}^{-3}$ ) and integrated fine mode of particles (in  $\# \text{cm}^{-3}$ ) during the  
4 ADRIMED airborne campaign. Dash indicates that the specie concentration was lower than the  
5 detection limit. The dust mass concentration was estimated from the measured Al using the  
6 mean Al mass fraction in the crustal composition of 7.09 % (Guieu et al., 2002). A comparison  
7 of the single scattering albedos  $\omega_0$  measured by the nephelometer and CAPS with those  
8 estimated from chemical measurements is also shown. The absolute error associated with  $\omega_0$   
9 obtained from measurements is 0.04.

10

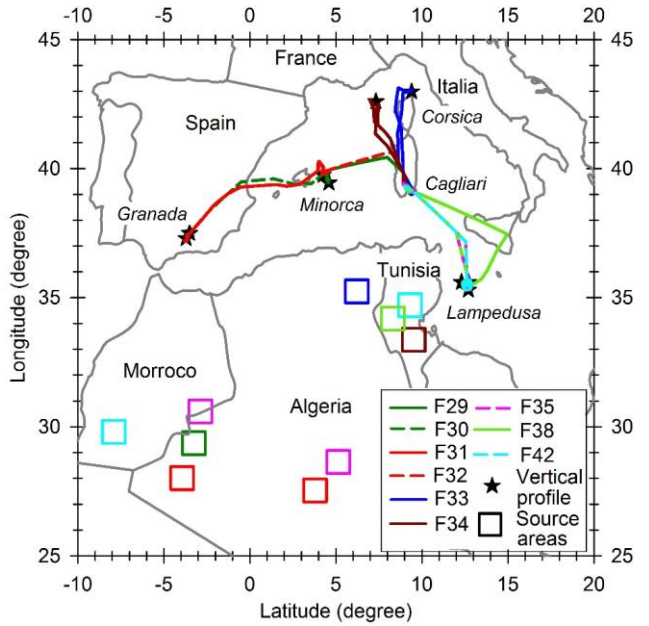
Flight number	F29	F30	F31	F32	F33	F34	F35	F38	F42
Si	3607	4955	4159	592	2426	9814	6430	2040	5366
Al	1404	2028	1719	225	975	3770	2519	746	2146
Fe	687	1085	845	146	536	1869	1239	416	1032
Ca	1099	1596	1547	-	1322	6404	2112	1374	1592
V	9	6	5	17	16	22	19	13	-
Pb	82	458	28	216	417	-	762	-	-
Zn	20	34	25	4	-	-	71	-	-
$\text{SO}_4^{2-}$	-	1740	-	2016	1574	2505	966	1764	2011
$\text{NO}_3^-$	-	-	-	206	-	285	309	-	467
$\text{NH}_4^+$	-	809	276	640	563	613	-	557	-
rBC	62	97	64	130	57	97	37	97	78
Dust	15.1	21.7	18.4	2.4	10.5	40.5	27.0	8.0	23.0
$N_{\text{fine}}$	316	416	457	881	515	988	229	485	714
$\omega_0$ (measured)	0.97	1.00	0.99	0.92	0.98	0.94	0.97	0.94	0.99
$\omega_0$ (chemistry)	0.93	0.96	0.95	0.94	0.96	0.96	0.97	0.94	0.96

11

1 Figure 1. Operating region of the ATR-42 aircraft during the ADRIMED flights that performed  
2 mineral dust measurements. Colors of the lines and squares correspond to the different flights.  
3 The positions of the middle of the profiles are shown in black stars. Squares indicate likely  
4 sources regions of the dust sampled during the flights. The aircraft was based at Cagliari in  
5 Sardinia.



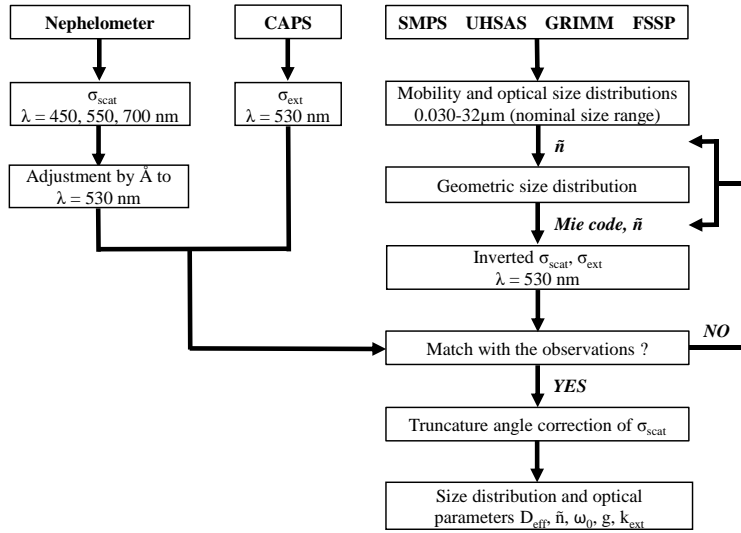
1



2

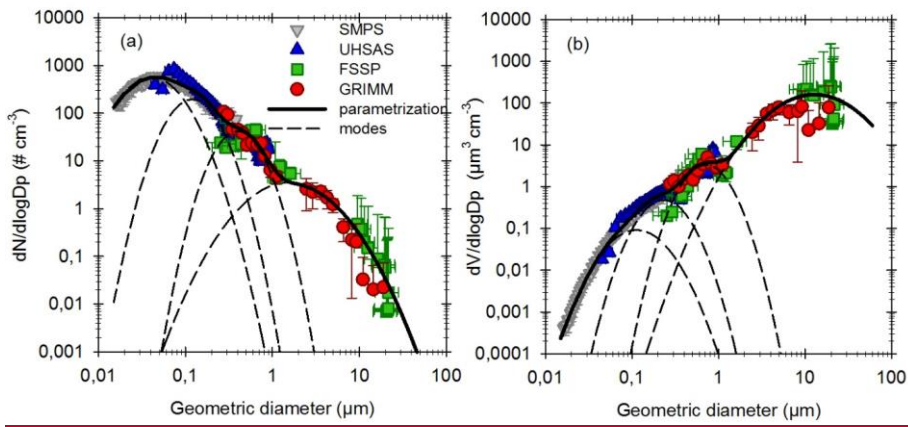
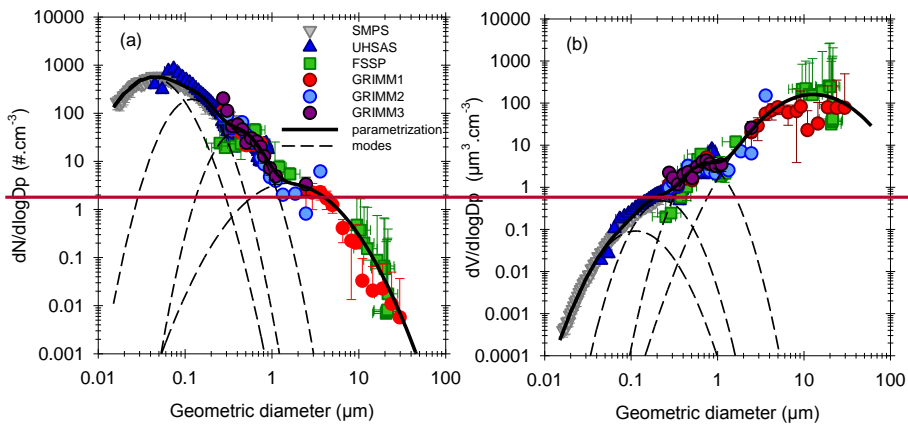
3

1 Figure 2: Data inversion procedure to retrieve the dust size distribution and optical parameters.  
 2



3

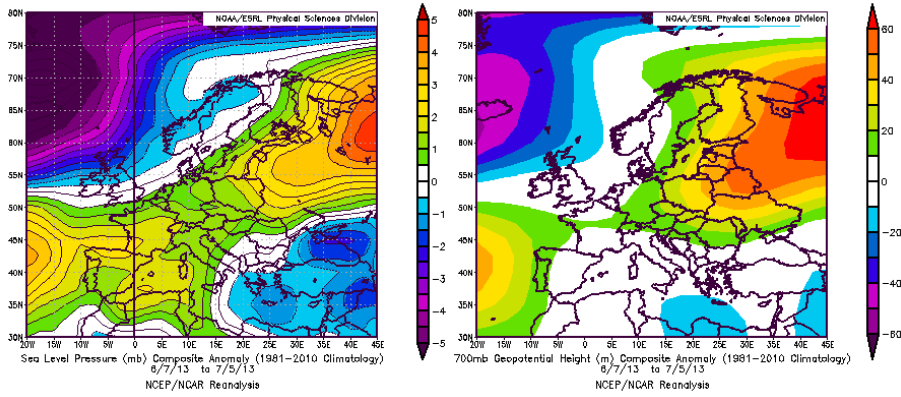
1 Figure 3. Number (a) and volume (b) size distributions obtained by the SMPS (gray), UHSAS  
 2 (blue), FSSP (green) and GRIMM (red) during the flight F35 including refractive index  
 3 corrections for  $\tilde{n} = 1.53 - 0.004i$ . Vertical errors bars indicate one standard deviation of the data  
 4 during the straight levelled run. Horizontal error bars display the bin sizing uncertainties of the  
 5 instruments. The dark line represents the parametrized fit with a sum of four log-normal modes  
 6 (shown in dashed lines).  
 7



8

9  
 10  
 11

1 Fig. 4. Sea level pressure in hPa (left) and 700 hPa geopotential height in m (right) composite  
2 anomalies with respect to the 1981-2010 climatology obtained from the NCEP/NCAR  
3 Reanalysis (images provided by the NOAA/ESRL Physical Sciences Division, Boulder  
4 Colorado, from their web site at <http://www.esrl.noaa.gov/psd/>).  
5

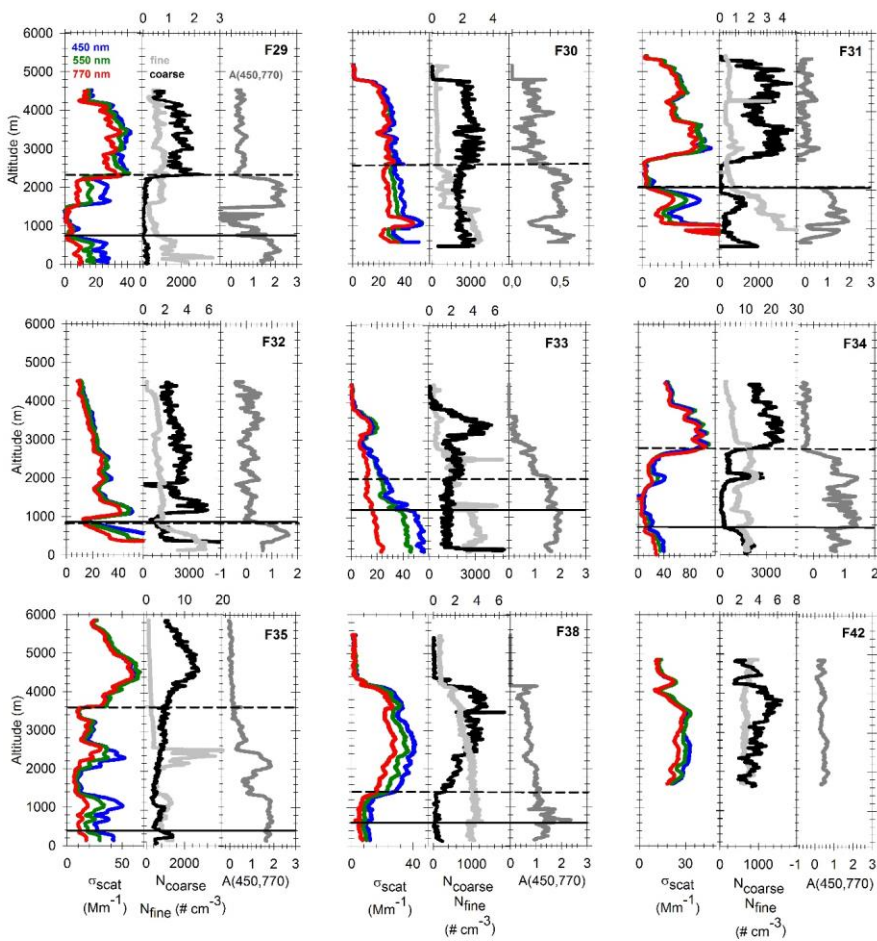


6  
7

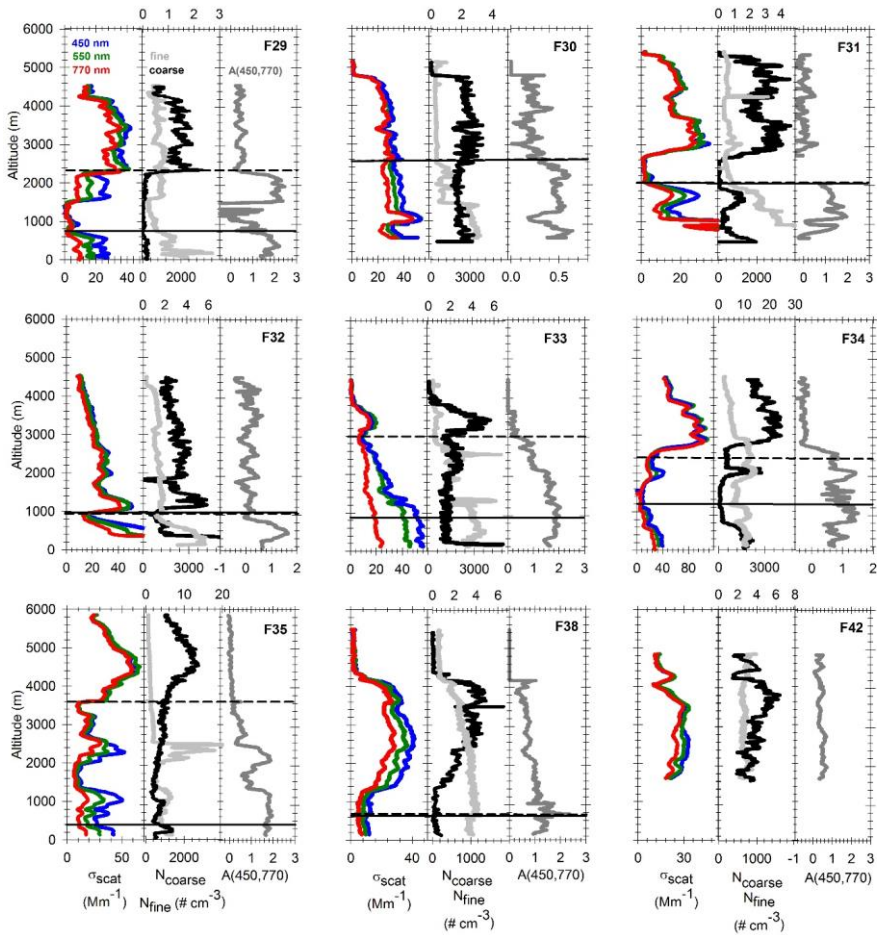


1 Figure 5. Vertical profiles of the spectral scattering coefficient  $\sigma_{scat}$  at  $\lambda=450, 550$  and  $770$  nm  
 2 (blue, green and red), the particle number concentration in the submicron  $N_{fine}$  (light grey) and  
 3 the supermicron  $N_{coarse}$  (dark) size ranges and the scattering Angstrom exponent  $\tilde{A}$  calculated  
 4 between 450 and 770 nm (dark grey).  $N_{coarse}$  is plotted using the upper horizontal axis. The top  
 5 of the boundary layer  $Z_b$  and the wind shear level  $Z_s$  are indicated in line and in dashed line  
 6 respectively. The height of  $Z_b$  was situated below the minimum flight level in F30 and F42.  
 7 The height of  $Z_s$  was situated below the minimum flight level in F42. ~~The heights of  $Z_b$  and  $Z_s$~~   
 8 ~~were situated below the minimum flight level in F42.~~ Data were corrected for Standard  
 9 Temperature and Pressure (STP) using  $T=20^\circ\text{C}$  and  $P=1013.25$  hPa.

10

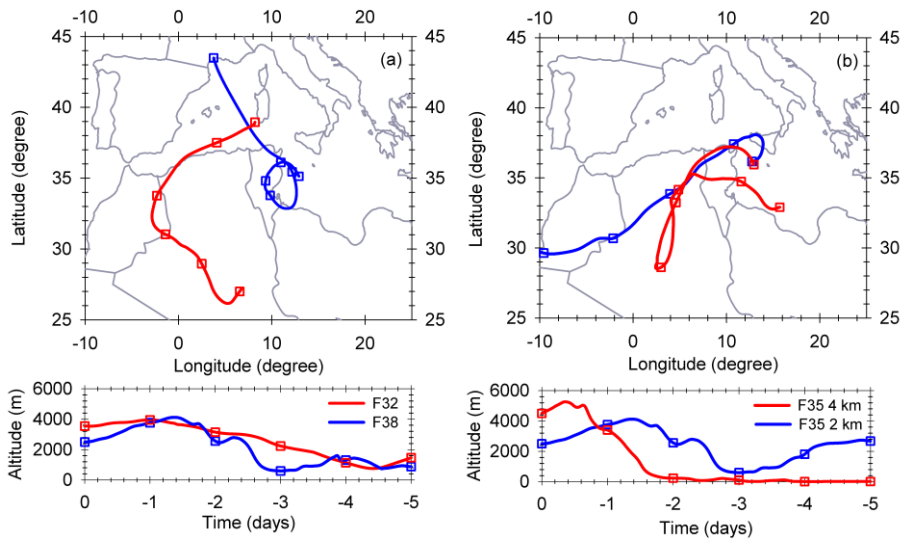


11



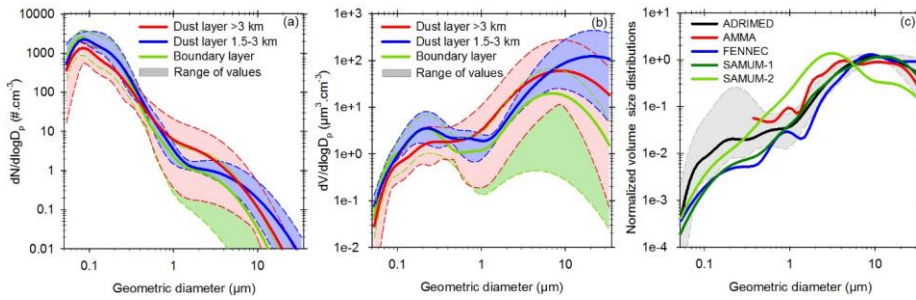
1  
2  
3

1 Figure 6. Five-day backward trajectories calculated for (a) flights F32 and F38 and (b) flight  
2 F35 arriving at intermediate (2 km asl.) and elevated (4 km asl.) altitudes in blue and red,  
3 respectively.  
4



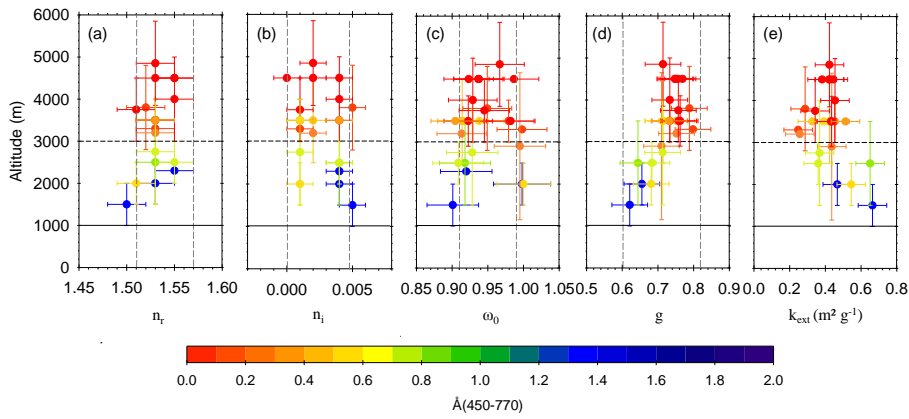
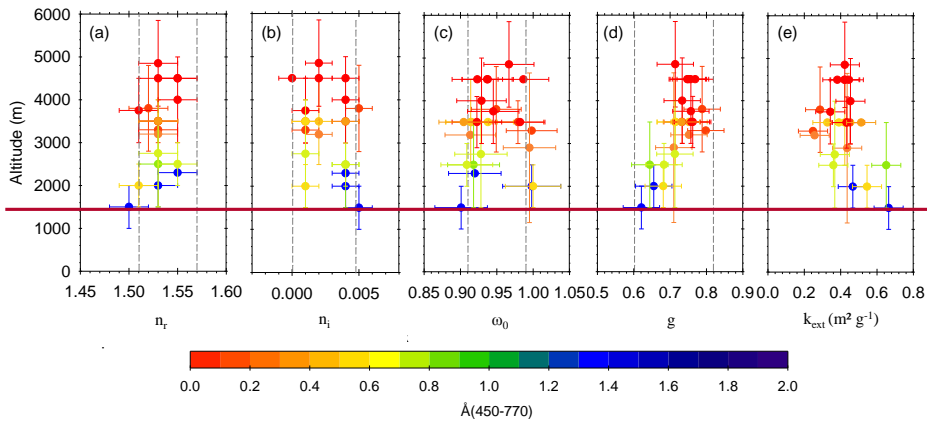
5

1 Figure 7. Particle size distributions obtained in the dust layers during ADRIMED for (a) number  
 2 distribution, (b) volume distribution and (c) volume distribution normalized by the total volume  
 3 concentration. In Figures (a) and (b), size distributions are classified as a function of the altitude  
 4 of the layer: elevated dust layer above 3 km asl (red), ~~intermediate~~ dust layer between 1.5-3 km  
 5 asl (blue) and the boundary layer below 1 km (green). The shading represents the minimum and  
 6 maximum throughout the campaign. In Figure (c), the mean (dark line), minimum and  
 7 maximum normalized size distributions (grey shading) observed above 1.5 km during the  
 8 ADRIMED campaign are compared with those observed in the source region during the  
 9 airborne campaigns AMMA (red line, Formenti et al., 2011a), FENNEC (blue line, Ryder et  
 10 al., 2013b) and SAMUM1 (dark green line, Weinzierl et al., 2009), as well as with  
 11 measurements at Cape-Verde region during SAMUM-2 campaign (light green line, Weinzierl  
 12 et al., 2011). The AMMA curve (Formenti et al., 2011) is curtailed to 0.3  $\mu\text{m}$  since there was  
 13 no measurement below this size during the campaign.



14  
 15

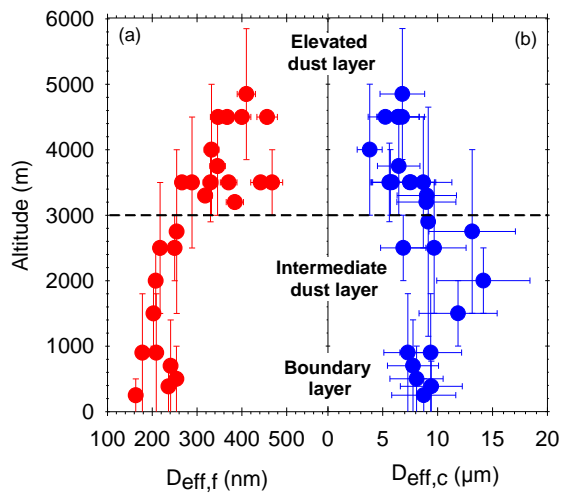
1 Figure 8. Scatter plots showing (a) the real part of the complex refractive index, (b) the  
 2 imaginary part of the complex refractive index, (c) the single scattering albedo, (d) the  
 3 asymmetry parameter and (e) the mass extinction efficiency all at  $\lambda=530$  nm as a function of  
 4 the altitude from all straight level runs and vertical profiles within the dust layers measured  
 5 during the campaign. The altitude indicated for vertical profiles refers to the middle of the layer.  
 6 Horizontal error bars display the uncertainties of the parameters. Vertical error bars indicate the  
 7 altitude range used to calculate each data point. Broad classifications of the above-3km dust  
 8 layer and the below-3km dust layer are shown in horizontal lines. Vertical dashed lines indicate  
 9 the range of values obtained in dust source regions. Dashed lines indicate the range of values  
 10 obtained in dust source regions. The maximum value of  $k_{ext}$  reported in the literature for dust in  
 11 source regions is above  $0.8 \text{ m}^2 \text{ g}^{-1}$ .  
 12



14  
 15  
 16

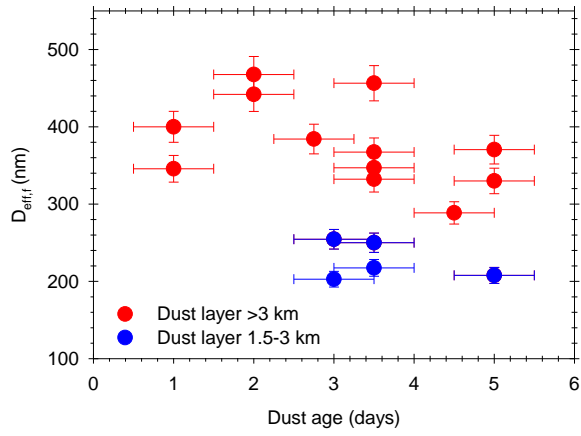
1 Figure 9. Altitude dependence of (a) the fine mode effective diameter  $D_{eff,f}$  (size range 0.053-1  
2  $\mu\text{m}$ ) and (b) the coarse mode effective diameter  $D_{eff,c}$  (size range 1-32  $\mu\text{m}$ ). The altitude reported  
3 for vertical profiles refers to the middle of the layer. Broad classifications of the elevated dust  
4 layer, the intermediate dust layer and the boundary layer have been added to the figure.

5



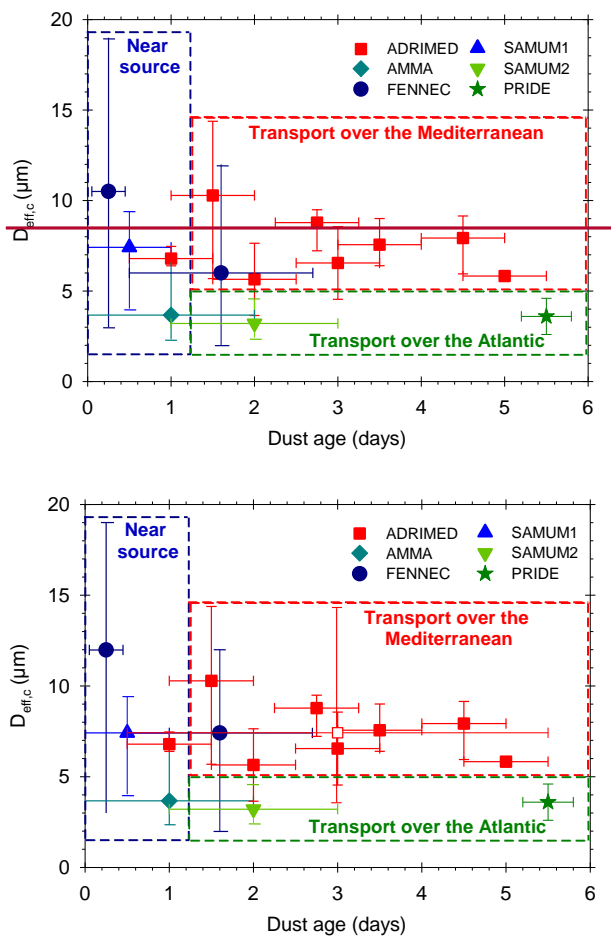
6

1 Figure 10. Effective diameter of the fine mode  $D_{eff}$  as a function of the dust age observed for  
2 elevated dust layers (red circles) and intermediate dust layers (blue circles).  
3



4

1 Figure 11. Effective diameter of the coarse mode  $D_{eff,c}$  as a function of the dust age observed  
 2 during ADRIMED (red squares). Filled red squares represent the average values observed for  
 3 each dust age and the empty red square represents the campaign average value. Values are  
 4 compared to those observed in dust source region (in blue) during FENNEC (circles),  
 5 SAMUM1 (triangle) and AMMA (diamond), as well as measurements in the Atlantic Ocean  
 6 (in green) at Cape-Verde region during SAMUM-2 (triangle) and at Puerto-Rico during PRIDE  
 7 (stars). The horizontal error bars represent uncertainties on the dust age estimated using  
 8 HYSPLIT and Sevir RGB images. The vertical error bars represent the range of values  
 9 obtained for each dust age.

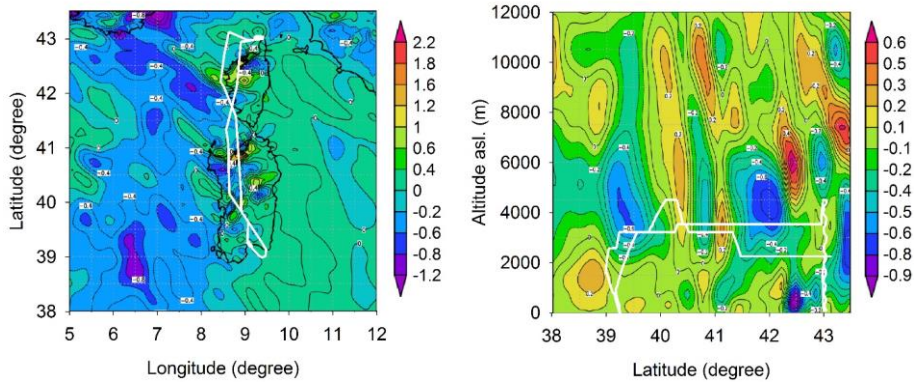


11  
12

13  
14  
15



1 Figure 12. 700-hPa vertical velocity field (a) and vertical cross section (b), taken along the F33  
2 flight track (white line), from the 10-km resolution WRF model simulations. Values are  
3 expressed in  $\text{Pa s}^{-1}$ .



4

## 1 References

- 2 [Alados-Arboledas, L., Müller, D., Guerrero-Rascado, J. L., Navas-Guzman, D. Pérez-](#)  
3 [Ramirez, D., and Olmo, F. J. : Optical and microphysical properties of fresh biomass burning](#)  
4 [aerosol retrieved by Raman lidar, and star-and sun-photometry, \*Geophys. Res. Lett.\*, 38,](#)  
5 [L01807, doi:10.1029/2010GL45999.](#)
- 6 Andreae, M. O., and Merlet, P.: Emission of trace gases and aerosols from biomass burning,  
7 *Global Biogeochem. Cy.*, 15, 955-966, 10.1029/2000GB001382, 2001.
- 8 Andreae, M. O., and Rosenfeld, D.: Aerosol-cloud-precipitation interactions. Part 1. The  
9 nature and sources of cloud-active aerosols, *Earth-Sci. Rev.*, 89, 13-41, 2008.
- 10 Ansmann, A., Baars, H., Tesche, M., Müller, D., Althausen, D., Engelmann, R.,  
11 Pauliquevis, T., and Artaxo, P.: Dust and smoke transport from Africa to South America: Lidar  
12 profiling over Cape Verde and the Amazon rainforest, *Geophys. Res. Lett.*, 36, L11802,  
13 10.1029/2009GL037923, 2009.
- 14 [Balkanski, Y., Schulz, M., Claquin, T., and Guibert, S.: Reevaluation of Mineral aerosol](#)  
15 [radiative forcings suggests a better agreement with satellite and AERONET data, \*Atmos. Chem.\*](#)  
16 [Phys., 7, 81-95, doi:10.5194/acp-7-81-2007, 2007](#)
- 17 Basart, S., Pérez, C., Cuevas, E., Baldasano, J. M., and Gobbi, G. P.: Aerosol  
18 characterization in Northern Africa, Northeastern Atlantic, Mediterranean Basin and Middle  
19 East from direct-sun AERONET observations, *Atmos. Chem. Phys.*, 9, 8265-8282,  
20 10.5194/acp-9-8265-2009, 2009.
- 21 [Bauer, S.E., Balkanski, Y., Shulz, M., Hauglustaine, D. A., and Dentener F., Global](#)  
22 [modelling of heterogeneous chemistry on mineral aerosol surfaces: The influence of ozone](#)  
23 [chemistry and comparison to observations, \*L. J. Geophys. Res.\*, 109, D02304,](#)  
24 [doi:10.1029/2003JD003868, 2004.](#)
- 25 Bauer, S. E., Mishchenko, M. I., Laci, A. A., Zhang, S., Perlwitz, J., and Metzger, S. M.:  
26 Do sulphate and nitrate coatings on mineral dust have important effects on radiative properties  
27 and climate modeling?, *J. Geophys. Res.-Atmos.*, 112, D06307, 10.1029/2005JD006977, 2007.
- 28 Baumgardner, D., Dye, J. E., Gandrud, B. W., and Knollenberg, R. G.: Interpretation of  
29 measurements made by forward scattering probe (FSSP-300) during the airborne arctic  
30 stratospheric expedition, *J. Geophys. Res.-Atmos.*, 97, 8035-8046, 1992.
- 31 Baumgardner, D., Popovicheva, O., Allan, J., Bernardoni, V., Cao, J., Cavalli, F., Cozic,  
32 J., Diapouli, E., Eleftheriadis, K., Genberg, P. J., Gonzalez, C., Gysel, M., John, A.,  
33 Kirchstetter, T. W., Kuhlbusch, T. A. J., Laborde, M., Lack, D., Müller, T., Niessner, R.,  
34 Petzold, A., Piazzalunga, A., Putaud, J. P., Schwarz, J., Sheridan, P., Subramanian, R.,  
35 Swietlicki, E., Valli, G., Vecchi, R., and Viana, M.: Soot reference materials for instrument  
36 calibration and intercomparisons: a workshop summary with recommendations, *Atmos. Meas.*  
37 *Tech.*, 5, 1869-1887, 10.5194/amt-5-1869-2012, 2012.
- 38 Bègue, N., Tulet, P., Chaboureau, J. P., Roberts, G., Gomes, L., and Mallet, M.: Long-range  
39 transport of Saharan dust over northwestern Europe during EUCAARI 2008 campaign:  
40 Evolution of dust optical properties by scavenging, *J. Geophys. Res.-Atmos.*, 117, D17201,  
41 10.1029/2012jd017611, 2012.
- 42 Birmili, W., Heinke, K., Pitz, M., Matuschulat, J., Wiedensohler, A., Cyrys, J., Wichmann,  
43 H. E., and Peters, A.: Particle number size distributions in urban air before and after  
44 volatilisation, *Atmos. Chem. Phys.*, 10, 4643-4660, 10.5194/acp-10-4643-2010, 2010.
- 45 Bohren, C. F., and Huffman, D. R.: Absorption and scattering of light by small particles,  
46 Wiley, New York, 1983.
- 47 Bove, M. C., Brotto, P., Cassola, F., Cuccia, E., Massabò, D., Mazzino, A., Piazzalunga,  
48 A., and Prati, P.: An integrated PM<sub>2.5</sub> source apportionment study: Positive Matrix  
49 Factorization vs. the Chemical Transport Model CAMx, *Atmos. Environ.*, 94, 274-286, 2014.

1 Cai, Y., Montague, D. C., Mooiweer-Bryan, W., and Deshler, T.: Performance  
2 characteristics of the ultra high sensitivity aerosol spectrometer for particles between 55 and  
3 800 nm: Laboratory and field studies, *J. Aerosol Sci.*, 39, 759-769,  
4 10.1016/j.jaerosci.2008.04.007, 2008.

5 Cassola, F., Ferrari, F., Mazzino, and Mazzino, A.: Numerical simulations of  
6 Mediterranean heavy precipitation events with the WRF model: A verification exercise using  
7 different approaches, *Atmos. Res.*, 164-165, 210-225, 10.1016/j.atmosres.2015.05.010, 2015.

8 Charlson, R. J., Schwartz, S. E., Hales, J. M., Cess, R. D., Coakley, J. A., Hansen, J. E.,  
9 and Hofmann, D. J.: Climate forcing by anthropogenic aerosols, *Science*, 255, 423-430,  
10 10.1126/science.255.5043.423, 1992.

11 Choobari, O. A., Zawar-Reza, P., and Sturman, A.: The global distribution of mineral dust  
12 and its impacts on the climate system: A review, *Atmos. Res.*, 138, 152-165,  
13 10.1016/j.atmosres.2013.11.007, 2014.

14 Chou, C., Formenti, P., Maille, M., Ausset, P., Helas, G., Harrison, M., and Osborne, S.:  
15 Size distribution, shape, and composition of mineral dust aerosols collected during the African  
16 Monsoon Multidisciplinary Analysis Special Observation Period 0: Dust and Biomass-Burning  
17 Experiment field campaign in Niger, January 2006, *J. Geophys. Res.-Atmos.*, 113, D00C10,  
18 10.1029/2008JD009897, 2008.

19 Clarke, A. D., Shinzuka, Y., Kapustin, V. N., Howell, S., Huebert, B., Doherty, S.,  
20 Anderson, T., Covert, D., Anderson, J., Hua, X., Moore, K. G., McNaughton, C., Carmichael,  
21 G., and Weber, R.: Size distributions and mixtures of dust and black carbon aerosol in Asian  
22 outflow: Physiochemistry and optical properties, *J. Geophys. Res.-Atmos.*, 109, D15S09,  
23 10.1029/2003JD004378, 2004.

24 Collaud Coen, M., Weingartner, E., Schaub, D., Hueglin, C., Corrigan, C., Henning, S.,  
25 Schwikowski, M., and Baltensperger, U.: Saharan dust events at the Jungfraujoch: detection by  
26 wavelength dependence of the single scattering albedo and first climatology analysis, *Atmos.*  
27 *Chem. Phys.*, 4, 2465-2480, 10.5194/acp-4-2465-2004, 2004.

28 Crumeyrolle, S., Gomes, L., Tulet, P., Matsuki, A., Schwarzenboeck, A., and Crahan, K.:  
29 Increase of the aerosol hygroscopicity by cloud processing in a mesoscale convective system:  
30 a case study from the AMMA campaign, *Atmos. Chem. Phys.*, 8, 6907-6924, 10.5194/acp-8-  
31 6907-2008, 2008.

32 Cuesta, J., Marsham, J. H., Parker, D. J., and Flamant, C.: Dynamical mechanisms  
33 controlling the vertical redistribution of dust and the thermodynamic structure of the West  
34 Saharan atmospheric boundary layer during summer, *Atmos. Sci. Lett.*, 10, 34-42,  
35 10.1002/asl.207, 2009.

36 d'Almeida, G. A.: A Model for Saharan Dust Transport, *Journal of Climate and Applied*  
37 *Meteorology*, 25, 903-916, 10.1175/1520-0450(1986)025<0903:AMFSDT>2.0.CO;2, 1986.

38 DeCarlo, P., Slowik, J., Worsnop, D., Davidovits, P., & Jimenez, J.: Particle Morphology  
39 and Density Characterization by Combined Mobility and Aerodynamic Diameter  
40 Measurements. Part I: Theory, *Aerosol Sci. Tech.*, 38, 1185-1205, 2004.

41 de Meij, A., and Lelieveld, J.: Evaluating aerosol optical properties observed by ground-  
42 based and satellite remote sensing over the Mediterranean and the Middle East in 2006, *Atmos.*  
43 *Res.*, 99, 415-433, 10.1016/j.atmosres.2010.11.005, 2011.

44 Di Biagio, C., di Sarra, A., Meloni, D., Monteleone, F., Piacentino, S., and Sferlazzo, D.:  
45 Measurements of Mediterranean aerosol radiative forcing and influence of the single scattering  
46 albedo, *J. Geophys. Res.-Atmos.*, 114, D06211, 10.1029/2008JD011037, 2009.

47 Di Biagio, C., Doppler, L., Gaimoz, C., Grand, N., Ancellet, G., Raut, J. C., Beekmann,  
48 M., Borbon, A., Sartelet, K., Attié, J. L., Ravetta, F., and Formenti, P.: Continental pollution in  
49 the Western Mediterranean Basin: vertical profiles of aerosol and trace gases measured over  
50 the sea during TRAQA 2012 and SAFMED 2013, *Atmos. Chem. Phys. Discuss.*, 15, 8283-  
51 8328, 10.5194/acpd-15-8283-2015, 2015.

1 Di Iorio, T., di Sarra, A., Sferlazzo, D. M., Cacciani, M., Meloni, D., Monteleone, F., Fuà,  
2 D., and Fiocco, G.: Seasonal evolution of the tropospheric aerosol vertical profile in the central  
3 Mediterranean and role of desert dust, *J. Geophys. Res.-Atmos.*, 114, D02201,  
4 10.1029/2008JD010593, 2009.

5 Draxler, R. R., and Rolph, G. D.: HYSPLIT (HYbrid Single-Particle Lagrangian Integrated  
6 Trajectory) Model access via NOAA ARL READY Website  
7 (<http://ready.arl.noaa.gov/HYSPLIT.php>). , NOAA Air Resources Laboratory, Silver Spring,  
8 MD, 2015.

9 Doherty, O. M., Riemer, N., and Hameed, S.: Saharan mineral dust transport into the  
10 Caribbean: Observed atmospheric controls and trends, *J. Geophys. Res.-Atmos.*, 113,  
11 10.1029/2007jd009171, 2008.

12 Dulac, F., and Chazette, P.: Airborne study of a multi-layer aerosol structure in the eastern  
13 Mediterranean observed with the airborne polarized lidar ALEX during a STAAARTE  
14 campaign (7 June 1997), *Atmos. Chem. Phys.*, 3, 1817-1831, 10.5194/acp-3-1817-2003, 2003.

15 Engelstaedter, S., Tegen, I., and Washington, R.: North African dust emissions and  
16 transport, *Earth-Sci. Rev.*, 79, 73-100, <http://dx.doi.org/10.1016/j.earscirev.2006.06.004>, 2006.

17 Environmental Modeling Center: The GFS Atmospheric Model. NCEP Office Note 442.  
18 National Oceanic and Atmospheric Administration, 2003.

19 Fan, X.-B., Okada, K., Niimura, N., Kai, K., Arao, K., Shi, G.-Y., Qin, Y., and Mitsuta, Y.:  
20 Mineral particles collected in china and japan during the same Asian dust-storm event, *Atmos.*  
21 *Environ.*, 30, 347-351, [http://dx.doi.org/10.1016/1352-2310\(95\)00271-Y](http://dx.doi.org/10.1016/1352-2310(95)00271-Y), 1996.

22 Flamant, C., Chaboureaud, J. P., Parker, D. J., Taylor, C. M., Cammas, J. P., Bock, O.,  
23 Timouk, F., and Pelon, J.: Airborne observations of the impact of a convective system on the  
24 planetary boundary layer thermodynamics and aerosol distribution in the inter-tropical  
25 discontinuity region of the West African Monsoon, *Q. J. Roy. Meteor. Soc.*, 133, 1175-1189,  
26 10.1002/qj.97, 2007.

27 Formenti, P., Andreae, M. O., Lange, L., Roberts, G., Cafmeyer, J., Rajta, I., Maenhaut,  
28 W., Holben, B. N., Artaxo, P., and Lelieveld, J.: Saharan dust in Brazil and Suriname during  
29 the Large-Scale Biosphere-Atmosphere Experiment in Amazonia (LBA) - Cooperative LBA  
30 Regional Experiment (CLAIRE) in March 1998, *J. Geophys. Res.-Atmos.*, 106, 14919-14934,  
31 10.1029/2000JD900827, 2001.

32 Formenti, P., Elbert, W., Maenhaut, W., Haywood, J., and Andreae, M. O.: Chemical  
33 composition of mineral dust aerosol during the Saharan Dust Experiment (SHADE) airborne  
34 campaign in the Cape Verde region, September 2000, *J. Geophys. Res.-Atmos.*, 108, 8576,  
35 10.1029/2002JD002648, 2003.

36 Formenti, P., Rajot, J. L., Desboeufs, K., Caquineau, S., Chevaillier, S., Nava, S.,  
37 Gaudichet, A., Journet, E., Triquet, S., Alfaro, S., Chiari, M., Haywood, J., Coe, H., and  
38 Highwood, E.: Regional variability of the composition of mineral dust from western Africa:  
39 Results from the AMMA SOP0/DABEX and DODO field campaigns, *J. Geophys. Res.-*  
40 *Atmos.*, 113, n/a-n/a, 10.1029/2008JD009903, 2008.

41 Formenti, P., Rajot, J. L., Desboeufs, K., Saïd, F., Grand, N., Chevaillier, S., and  
42 Schmechtig, C.: Airborne observations of mineral dust over western Africa in the summer  
43 Monsoon season: spatial and vertical variability of physico-chemical and optical properties,  
44 *Atmos. Chem. Phys.*, 11, 6387-6410, 10.5194/acp-11-6387-2011, 2011a.

45 Formenti, P., Schütz, L., Balkanski, Y., Desboeufs, K., Ebert, M., Kandler, K., Petzold, A.,  
46 Scheuvsens, D., Weinbruch, S., and Zhang, D.: Recent progress in understanding physical and  
47 chemical properties of African and Asian mineral dust, *Atmos. Chem. Phys.*, 11, 8231-8256,  
48 10.5194/acp-11-8231-2011, 2011b.

49 Formenti, P., Caquineau, S., Desboeufs, K., Klaver, A., Chevaillier, S., Journet, E., and  
50 Rajot, J. L.: Mapping the physico-chemical properties of mineral dust in western Africa:

1 mineralogical composition, *Atmos. Chem. Phys.*, 14, 10663-10686, 10.5194/acp-14-10663-  
2 2014, 2014.

3 Garrett, T. J., Russell, L. M., Ramaswamy, V., Maria, S. F., and Huebert, B. J.:  
4 Microphysical and radiative evolution of aerosol plumes over the tropical North Atlantic Ocean,  
5 *J. Geophys. Res.-Atmos.*, 108, 4022, 10.1029/2002JD002228, 2003.

6 Gkikas, A., Housos, E. E., Hatzianastassiou, N., Papadimas, C. D., and Bartzokas, A.:  
7 Synoptic conditions favouring the occurrence of aerosol episodes over the broader  
8 Mediterranean basin, *Q. J. Roy. Meteor. Soc.*, 138, 932-949, 10.1002/qj.978, 2012.

9 Ginoux, P., J. M. Prospero, T. E. Gill, N. C. Hsu, and M. Zhao (2012), Global-scale  
10 attribution of anthropogenic and natural dust sources and their emission rates based on MODIS  
11 Deep Blue aerosol products, *Rev. Geophys.*, 50, RG3005, doi:10.1029/2012RG000388, 2012.

12 ~~Gómez-Amo, J. L., Pinti, V., Di Iorio, T., di Sarra, A., Meloni, D., Becagli, S., Bellantone,  
13 V., Cacciani, M., Fuà, D., and Perrone, M. R.: The June 2007 Saharan dust event in the central  
14 Mediterranean: Observations and radiative effects in marine, urban, and sub urban  
15 environments, *Atmos. Environ.*, 45, 5385-5393,  
16 <http://dx.doi.org/10.1016/j.atmosenv.2011.06.045>, 2011.~~

17 Goudie, A. S., and Middleton, N. J.: Saharan dust storms: nature and consequences, *Earth-  
18 Sci. Rev.*, 56, 179-204, [http://dx.doi.org/10.1016/S0012-8252\(01\)00067-8](http://dx.doi.org/10.1016/S0012-8252(01)00067-8), 2001.

19 Guerrero-Rascado, J. L., Ruiz, B., and Alados-Arboledas, L.: Multi-spectral Lidar  
20 characterization of the vertical structure of Saharan dust aerosol over southern Spain, *Atmos.  
21 Environ.*, 42, 2668-2681, <http://dx.doi.org/10.1016/j.atmosenv.2007.12.062>, 2008.

22 Guieu, C., Loÿe-Pilot, M. D., Ridame, C., and Thomas, C.: Chemical characterization of  
23 the Saharan dust end-member: Some biogeochemical implications for the western  
24 Mediterranean Sea, *J. Geophys. Res.-Atmos.*, 107, ACH 5-1-ACH 5-11,  
25 10.1029/2001JD000582, 2002.

26 Hamonou, E., Chazette, P., Balis, D., Dulac, F., Schneider, X., Galani, E., Ancellet, G., and  
27 Papayannis, A.: Characterization of the vertical structure of Saharan dust export to the  
28 Mediterranean basin, *J. Geophys. Res.-Atmos.*, 104, 22257-22270, 10.1029/1999JD900257,  
29 1999.

30 Haywood, J. M., Johnson, B. T., Osborne, S. R., Baran, A. J., Brooks, M., Milton, S. F.,  
31 Mulcahy, J., Walters, D., Allan, R. P., Klaver, A., Formenti, P., Brindley, H. E., Christopher,  
32 S., and Gupta, P.: Motivation, rationale and key results from the GERBILS Saharan dust  
33 measurement campaign, *Q. J. Roy. Meteor. Soc.*, 137, 1106-1116, 10.1002/qj.797, 2011.

34 Heintzenberg, J.: The SAMUM-1 experiment over Southern Morocco: overview and  
35 introduction, *Tellus B*, 61, 2-11, 10.1111/j.1600-0889.2008.00403.x, 2009.

36 Hess, M., Koepke, P., and Schult, I.: Optical Properties of Aerosols and Clouds: The  
37 Software Package OPAC, *B. Am. Meteorol. Soc.*, 79, 831-844, 10.1175/1520-  
38 0477(1998)079<0831:OPOAAC>2.0.CO;2, 1998.

39 Hinds, W. C.: *Aerosol Technology: Properties, Behavior, and Measurement of Airborne  
40 Particles*, 2<sup>nd</sup> Edition. Wiley, New York, 1999.

41 Huneus, N., Chevallier, F., and Boucher, O.: Estimating aerosol emissions by assimilating  
42 observed aerosol optical depth in a global aerosol model, *Atmos. Chem. Phys.*, 12, 4585-4606,  
43 10.5194/acp-12-4585-2012, 2012.

44 IPCC, fifth assessment report - the physical science basis, <http://www.ipcc.ch>, 2013.

45 Jing, S., Jianping, H., Qiang, F., Minnis, P., Jinming, G., and Jianrong, B.: Estimation of  
46 Asian dust aerosol effect on cloud radiation forcing using Fu-Liou radiative model and CERES  
47 measurements, *Atmos. Chem. Phys.*, 8, 2763-2771, 10.5194/acp-8-2763-2008, 2008.

48 Junkermann, W.: On the distribution of formaldehyde in the western Po-Valley, Italy,  
49 during FORMAT 2002/2003, *Atmos. Chem. Phys.*, 9, 9187-9196, 10.5194/acp-9-9187-2009,  
50 2009.

1 Kaaden, N., Massling, A., Schladitz, A., Müller, T., Kandler, K., Schutz, L., Weinzierl, B.,  
2 Petzold, A., Tesche, M., Leinert, S., Deutscher, C., Ebert, M., Weinbruch, S., and  
3 Wiedensohler, A.: State of mixing, shape factor, number size distribution, and hygroscopic  
4 growth of the Saharan anthropogenic and mineral dust aerosol at Tinfou, Morocco, *Tellus B*,  
5 61, 51-63, 10.1111/j.1600-0889.2008.00388.x, 2009.

6 Kalashnikova, O. V., and Kahn, R. A.: Mineral dust plume evolution over the Atlantic from  
7 MISR and MODIS aerosol retrievals, *J. Geophys. Res.-Atmos.*, 113, n/a-n/a,  
8 10.1029/2008JD010083, 2008.

9 Kalnay, E., Kanamitsu, M., Kistler, R., Collins, W., Deaven, D., Gandin, L., Iredell, M.,  
10 Saha, S., White, G., Woollen, J., Zhu, Y., Leetmaa, A., Reynolds, R., Chelliah, M., Ebisuzaki,  
11 W., Higgins, W., Janowiak, J., Mo, K. C., Ropelewski, C., Wang, J., Jenne, R., and Joseph, D.:  
12 The NCEP/NCAR 40-Year Reanalysis Project, *B. Am. Meteorol. Soc.*, 77, 437-471,  
13 10.1175/1520-0477(1996)077<0437:TNYP>2.0.CO;2, 1996.

14 Kandler, K., SchÜtz, L., Deutscher, C., Ebert, M., Hofmann, H., JÄckel, S., Jaenicke, R.,  
15 Knippertz, P., Lieke, K., Massling, A., Petzold, A., Schladitz, A., Weinzierl, B., Wiedensohler,  
16 A., Zorn, S., and Weinbruch, S.: Size distribution, mass concentration, chemical and  
17 mineralogical composition and derived optical parameters of the boundary layer aerosol at  
18 Tinfou, Morocco, during SAMUM 2006, *Tellus B*, 61, 32-50, 10.1111/j.1600-  
19 0889.2008.00385.x, 2009.

20 Kanitz, T., Engelmann, R., Heinold, B., Baars, H., Skupin, A., and Ansmann, A.: Tracking  
21 the Saharan Air Layer with shipborne lidar across the tropical Atlantic, *Geophys. Res. Lett.*, 41,  
22 1044-1050, 10.1002/2013GL058780, 2014.

23 ~~Koçak, M., Theodosi, C., Zarrmpas, P., Séguret, M. J. M., Herut, B., Kallos, G.,~~  
24 ~~Mihalopoulos, N., Kubilay, N., and Nimmo, M.: Influence of mineral dust transport on the~~  
25 ~~chemical composition and physical properties of the Eastern Mediterranean aerosol, *Atmos-*~~  
26 ~~*Environ.*, 57, 266-277, <http://dx.doi.org/10.1016/j.atmosenv.2012.04.006>, 2012.~~

27 Koehler, K. A., Kreidenweis, S. M., DeMott, P. J., Petters, M. D., Prenni, A. J., and Carrico,  
28 C. M.: Hygroscopicity and cloud droplet activation of mineral dust aerosol, *Geophys. Res. Lett.*,  
29 36, L08805, 10.1029/2009GL037348, 2009.

30 Korhonen, H., Napari, I., Timmreck, C., Vehkamäki, H., Pirjola, L., Lehtinen, K. E. J.,  
31 Lauri, A., and Kulmala, M.: Heterogeneous nucleation as a potential sulphate-coating  
32 mechanism of atmospheric mineral dust particles and implications of coated dust on new  
33 particle formation, *J. Geophys. Res.-Atmos.*, 108, 4546, 10.1029/2003JD003553, 2003.

34 Koren, I., Joseph, J. H., and Israelevich, P.: Detection of dust plumes and their sources in  
35 northeastern Libya, *Can. J. Remote Sens.*, 29, 792-796, 10.5589/m03-036, 2003.

36 Kutuzov, S., Shahgedanova, M., Mikhaleenko, V., Ginot, P., Lavrentiev, I., and Kemp, S.:  
37 High-resolution provenance of desert dust deposited on Mt. Elbrus, Caucasus in 2009-2012  
38 using snow pit and firn core records, *The Cryosphere*, 7, 1481-1498, 10.5194/tc-7-1481-2013,  
39 2013.

40 Laborde, M., Mertes, P., Zieger, P., Dommen, J., Baltensperger, U., and Gysel, M.:  
41 Sensitivity of the Single Particle Soot Photometer to different black carbon types, *Atmos. Meas.*  
42 *Tech.*, 5, 1031-1043, 10.5194/amt-5-1031-2012, 2012.

43 Lack, D. A., and Cappa, C. D.: Impact of brown and clear carbon on light absorption  
44 enhancement, single scatter albedo and absorption wavelength dependence of black carbon,  
45 *Atmos. Chem. Phys.*, 10, 4207-4220, 10.5194/acp-10-4207-2010, 2010.

46 Levin, Z., Ganor, E., and Gladstein, V.: The Effects of Desert Particles Coated with Sulfate  
47 on Rain Formation in the Eastern Mediterranean, *J. Appl. Meteorol.*, 35, 1511-1523,  
48 10.1175/1520-0450(1996)035<1511:TEODPC>2.0.CO;2, 1996.

49 Levin, Z., Teller, A., Ganor, E., and Yin, Y.: On the interactions of mineral dust, sea-salt  
50 particles, and clouds: A measurement and modeling study from the Mediterranean Israeli Dust  
51 Experiment campaign, *J. Geophys. Res.-Atmos.*, 110, n/a-n/a, 10.1029/2005JD005810, 2005.

1 Liu, Y. G., and Daum, P. H.: Relationship of refractive index to mass density and self-  
2 consistency of mixing rules for multicomponent mixtures like ambient aerosols, *J. Aerosol Sci.*,  
3 39, 974-986, 10.1016/j.jaerosci.2008.06.006, 2008.

4 Liu, D., Allan, J. D., Young, D. E., Coe, H., Beddows, D., Fleming, Z. L., Flynn, M. J.,  
5 Gallagher, M. W., Harrison, R. M., Lee, J., Prevot, A. S. H., Taylor, J. W., Yin, J., Williams,  
6 P. I., and Zotter, P.: Size distribution, mixing state and source apportionment of black carbon  
7 aerosol in London during wintertime, *Atmos. Chem. Phys.*, 14, 10061-10084, 10.5194/acp-14-  
8 10061-2014, 2014.

9 Ma, Q. X., Liu, Y. C., Liu, C., and He, H.: Heterogeneous reaction of acetic acid on MgO,  
10 alpha-Al<sub>2</sub>O<sub>3</sub>, and CaCO<sub>3</sub> and the effect on the hygroscopic behaviour of these particles, *Phys.*  
11 *Chem. Chem. Phys.*, 14, 8403-8409, 10.1039/c2cp40510e, 2012.

12 Mahowald, N., Albani, S., Kok, J. F., Engelstaeder, S., Scanza, R., Ward, D. S., and  
13 Flanner, M. G.: The size distribution of desert dust aerosols and its impact on the Earth system,  
14 *Aeolian Research*, 15, 53-71, <http://dx.doi.org/10.1016/j.aeolia.2013.09.002>, 2014.

15 Mallet, M., Van Dingenen, R., Roger, J. C., Despiou, S., and Cachier, H.: In situ airborne  
16 measurements of aerosol optical properties during photochemical pollution events, *J. Geophys.*  
17 *Res.-Atmos.*, 110, 10.1029/2004jd005139, 2005.

18 Mallet, M., Dubovik, O., Nabat, P., Dulac, F., Kahn, R., Sciare, J., Paronis, D., and Léon,  
19 J. F.: Absorption properties of Mediterranean aerosols obtained from multi-year ground-based  
20 remote sensing observations, *Atmos. Chem. Phys.*, 13, 9195-9210, 10.5194/acp-13-9195-2013,  
21 2013.

22 Mallet, M., Dulac, F., Formenti, P., Nabat, P., Sciare, J., Roberts, G., Pelon, J., Ancellet,  
23 G., Tanré, D., Parol, F., di Sarra, A., Alados, L., Arndt, J., Auriol, F., Blarel, L., Bourriane,  
24 T., Brogniez, G., Chazette, P., Chevaillier, S., Claeys, M., D'Anna, B., Denjean, C., Derimian,  
25 Y., Desboeufs, K., Di Iorio, T., Doussin, J. F., Durand, P., Féron, A., Freney, E., Gaimoz, C.,  
26 Goloub, P., Gómez-Amo, J. L., Granados-Muñoz, M. J., Grand, N., Hamonou, E., Jankowiak,  
27 I., Jeannot, M., Léon, J. F., Maillé, M., Mailler, S., Meloni, D., Menut, L., Momboisse, G.,  
28 Nicolas, J., Podvin, J., Pont, V., Rea, G., Renard, J. B., Roblou, L., Schepanski, K.,  
29 Schwarzenboeck, A., Sellegri, K., Sicard, M., Solmon, F., Somot, S., Torres, B., Totems, J.,  
30 Triquet, S., Verdier, N., Verwaerde, C., Wenger, J., and Zapf, P.: Overview of the Chemistry-  
31 Aerosol Mediterranean Experiment/Aerosol Direct Radiative Forcing on the Mediterranean  
32 Climate (ChArMEx/ADRMED) summer 2013 campaign, *Atmos. Chem. Phys. Discuss.*, 15,  
33 19615-19727, 10.5194/acpd-15-19615-2015, 2015.

34 Mantas, E., Remoundaki, E., Halari, I., Kassomenos, P., Theodosi, C., Hatzikioseyan, A.,  
35 and Mihalopoulos, N.: Mass closure and source apportionment of PM<sub>2.5</sub> by Positive Matrix  
36 Factorization analysis in urban Mediterranean environment, *Atmos. Environ.*, 94, 154-163,  
37 <http://dx.doi.org/10.1016/j.atmosenv.2014.05.002>, 2014.

38 Marconi, M., Sferlazzo, D. M., Becagli, S., Bommarito, C., Calzolari, G., Chiari, M., di  
39 Sarra, A., Ghedini, C., Gómez-Amo, J. L., Lucarelli, F., Meloni, D., Monteleone, F., Nava, S.,  
40 Pace, G., Piacentino, S., Rugi, F., Severi, M., Traversi, R., and Udisti, R.: Saharan dust aerosol  
41 over the central Mediterranean Sea: PM<sub>10</sub> chemical composition and concentration versus  
42 optical columnar measurements, *Atmos. Chem. Phys.*, 14, 2039-2054, 10.5194/acp-14-2039-  
43 2014, 2014.

44 Maring, H., Savoie, D. L., Izaguirre, M. A., Custals, L., and Reid, J. S.: Mineral dust aerosol  
45 size distribution change during atmospheric transport, *J. Geophys. Res.-Atmos.*, 108,  
46 10.1029/2002jd002536, 2003.

47 [Massoli, P., Kebabian, P. L., Onasch, T. B., Hills, F. B., and Freedman, A., Aerosol light](#)  
48 [extinction measurements by Cavity Attenuated Phase Shift \(CAPS\) Spectroscopy: Laboratory](#)  
49 [validation and field deployment of a compact aerosol particle extinction monitor, \*Aerosol Sci.\*](#)  
50 [Tech., 44:6, 428-435, DOI:10.1080/02786821003716599, 2010.](#)



1 McConnell, C. L., Highwood, E. J., Coe, H., Formenti, P., Anderson, B., Osborne, S., Nava,  
2 S., Desboeufs, K., Chen, G., and Harrison, M. A. J.: Seasonal variations of the physical and  
3 optical characteristics of Saharan dust: Results from the Dust Outflow and Deposition to the  
4 Ocean (DODO) experiment, *J. Geophys. Res.-Atmos.*, 113, 10.1029/2007jd009606, 2008.

5 Meloni, D., di Sarra, A., DeLuisi, J., Di Iorio, T., Fiocco, G., Junkermann, W., and Pace,  
6 G.: Tropospheric aerosols in the Mediterranean: 2. Radiative effects through model simulations  
7 and measurements, *J. Geophys. Res.-Atmos.*, 108, n/a-n/a, 10.1029/2002JD002807, 2003.

8 Meloni, D., di Sarra, A., Pace, G., and Monteleone, F.: Aerosol optical properties at  
9 Lampedusa (Central Mediterranean). 2. Determination of single scattering albedo at two  
10 wavelengths for different aerosol types, *Atmos. Chem. Phys.*, 6, 715-727, 10.5194/acp-6-715-  
11 2006, 2006.

12 Mentaschi, L., Besio, G., Cassola, F., and Mazzino, A.: Performance evaluation of  
13 WavewatchIII in the Mediterranean Sea, *Ocean Model.*, 90, 82-94,  
14 10.1016/j.ocemod.2015.04.003, 2015.

15 [Mian Chin, Diehl, T., Dubovick, O., Eck, T. F., Holben, B. N., Sinyuk, A., and Streets, D.  
16 G.: Light absorption by pollution, dust, and biomass burning aerosols: a global model study and  
17 evaluation with AERONET measurements, \*Ann. Geophys.\*, 27, 3439-3464, doi:10.5194/angeo-  
18 27-3439-2009, 2009.](#)

19 [Mishchenko, M. I., Lacis, A. A., Carlson, B. E., and Travis, L. D. : Nonsphericity of dust-  
20 like tropospheric aerosols : implications for aerosol remote sensing and climate modelling,  
21 \*Geophys. Res. Lett.\*, 22\(9\), 1077-1080, 1995.](#)

22 Mona, L., Amodeo, A., Pandolfi, M., and Pappalardo, G.: Saharan dust intrusions in the  
23 Mediterranean area: Three years of Raman lidar measurements, *J. Geophys. Res.-Atmos.*, 111,  
24 D16203, 10.1029/2005JD006569, 2006.

25 Moteki, N., and Kondo, Y.: Dependence of Laser-Induced Incandescence on Physical  
26 Properties of Black Carbon Aerosols: Measurements and Theoretical Interpretation, *Aerosol  
27 Sci.Tech.*, 44, 663-675, 10.1080/02786826.2010.484450, 2010.

28 Moulin, C., Lambert, C. E., Dulac, F., and Dayan, U.: Control of atmospheric export of  
29 dust from North Africa by the North Atlantic Oscillation, *Nature*, 387, 691-694, 1997.

30 Moulin, C., Lambert, C. E., Dayan, U., Masson, V., Ramonet, M., Bousquet, P., Legrand,  
31 M., Balkanski, Y. J., Guelle, W., Marticorena, B., Bergametti, G., and Dulac, F.: Satellite  
32 climatology of African dust transport in the Mediterranean atmosphere, *J. Geophys. Res.-  
33 Atmos.*, 103, 13137-13144, 10.1029/98JD00171, 1998.

34 Muller, T., Schladitz, A., Kandler, K., and Wiedensohler, A.: Spectral particle absorption  
35 coefficients, single scattering albedos and imaginary parts of refractive indices from ground  
36 based in situ measurements at Cape Verde Island during SAMUM-2, *Tellus B*, 63, 573-588,  
37 10.1111/j.1600-0889.2011.00572.x, 2011a.

38 [Muller, T., Schladitz, A., Kandler, K., and Wiedensohler, A.: Spectral particle absorption  
39 coefficients, single scattering albedos and imaginary parts of refractive indices from ground  
40 based in situ measurements at Cape Verde Island during SAMUM-2, \*Tellus B\*, 63, 573-588,  
41 10.1111/j.1600-0889.2011.00572.x, 2011b.](#)

42 [Nabat, P., Solmon, F., Mallet, M., Michou, M., Sevault, F., Driouech, F., Meloni, D., di  
43 Sarra, A., Di Biagio, C., Formenti, P., Sicard, M., Léon, J.-F., and Bouin, M. -N.: Dust aerosol  
44 radiative effects during summer 2012 simulated with a coupled regional aerosol-atmosphere-  
45 ocean model over the Mediterranean, \*Atmos. Chem. Phys.\*, 15, 3303-3326, doi:10.5194/acp-  
46 15-3303-2015, 2015.](#)

47 Osborne, S. R., Johnson, B. T., Haywood, J. M., Baran, A. J., Harrison, M. A. J., and  
48 McConnell, C. L.: Physical and optical properties of mineral dust aerosol during the Dust and  
49 Biomass-burning Experiment, *J. Geophys. Res.-Atmos.*, 113, 10.1029/2007jd009551, 2008.

50 Otto, S., Bierwirth, E., Weinzierl, B., Kandler, K., Esselborn, M., Tesche, M., Schladitz,  
51 A., Wendisch, M., and Trautmann, T.: Solar radiative effects of a Saharan dust plume observed



1 during SAMUM assuming spheroidal model particles, *Tellus B*, 61, 270-296, 10.1111/j.1600-  
2 0889.2008.00389.x, 2009.

3 [Pace, G., Meloni, D., and di Sarra, A.: Forest fire aerosol over the Mediterranean basin](#)  
4 [during summer 2003, \*J. Geophys. Res.\*, 110, D21202, doi:10.1029/2005JD005986, 2005.](#)

5 Papayannis, A., Amiridis, V., Mona, L., Tsaknakis, G., Balis, D., Bosenberg, J.,  
6 Chaikovski, A., De Tomasi, F., Grigorov, I., Mattis, I., Mitev, V., Muller, D., Nickovic, S.,  
7 Perez, C., Pietruczuk, A., Pisani, G., Ravetta, F., Rizi, V., Sicard, M., Trickl, T., Wiegner, M.,  
8 Gerding, M., Mamouri, R. E., D'Amico, G., and Pappalardo, G.: Systematic lidar observations  
9 of Saharan dust over Europe in the frame of EARLINET (2000-2002), *J. Geophys. Res.-*  
10 *Atmos.*, 113, 10.1029/2007jd009028, 2008.

11 Perrone, M. R., and Bergamo, A.: Direct radiative forcing during Sahara dust intrusions at  
12 a site in the Central Mediterranean: Anthropogenic particle contribution, *Atmos. Res.*, 101, 783-  
13 798, 10.1016/j.atmosres.2011.05.011, 2011.

14 Perry, K. D., Cahill, T. A., Eldred, R. A., Dutcher, D. D., and Gill, T. E.: Long-range  
15 transport of North African dust to the eastern United States, *J. Geophys. Res.-Atmos.*, 102,  
16 11225-11238, 10.1029/97JD00260, 1997.

17 Petzold, A., Rasp, K., Weinzierl, B., Esselborn, M., Hamburger, T., DÖrnbrack, A.,  
18 Kandler, K., SchÜTz, L., Knippertz, P., Fiebig, M., and Virkkula, A. K. I.: Saharan dust  
19 absorption and refractive index from aircraft-based observations during SAMUM 2006, *Tellus*  
20 *B*, 61, 118-130, 10.1111/j.1600-0889.2008.00383.x, 2009.

21 Pey, J., Querol, X., Alastuey, A., Forastiere, F., and Stafoggia, M.: African dust outbreaks  
22 over the Mediterranean Basin during 2001&ndash;2011: PM10 concentrations,  
23 phenomenology and trends, and its relation with synoptic and mesoscale meteorology, *Atmos.*  
24 *Chem. Phys.*, 13, 1395-1410, 10.5194/acp-13-1395-2013, 2013.

25 Prospero, J. M., Ginoux, P., Torres, O., Nicholson, S. E., and Gill, T. E.: Environmental  
26 characterization of global sources of atmospheric soil dust identified with the nimbus 7 total  
27 ozone mapping spectrometer (TOMS) absorbing aerosol product, *Rev. Geophys.*, 40, 1002,  
28 10.1029/2000RG000095, 2002.

29 Querol, X., Alastuey, A., Pey, J., Cusack, M., Pérez, N., Mihalopoulos, N., Theodosi, C.,  
30 Gerasopoulos, E., Kubilay, N., and Koçak, M.: Variability in regional background aerosols  
31 within the Mediterranean, *Atmos. Chem. Phys.*, 9, 4575-4591, 10.5194/acp-9-4575-2009, 2009.

32 Reid, J. S., Kinney, J. E., Westphal, D. L., Holben, B. N., Welton, E. J., Tsay, S.-C.,  
33 Eleuterio, D. P., Campbell, J. R., Christopher, S. A., Colarco, P. R., Jonsson, H. H., Livingston,  
34 J. M., Maring, H. B., Meier, M. L., Pilewskie, P., Prospero, J. M., Reid, E. A., Remer, L. A.,  
35 Russell, P. B., Savoie, D. L., Smirnov, A., and Tanré, D.: Analysis of measurements of Saharan  
36 dust by airborne and ground-based remote sensing methods during the Puerto Rico Dust  
37 Experiment (PRIDE), *J. Geophys. Res.-Atmos.*, 108, 8586, 10.1029/2002JD002493, 2003.

38 Ripoll, A., Minguillón, M. C., Pey, J., Pérez, N., Querol, X., and Alastuey, A.: Joint analysis  
39 of continental and regional background environments in the western Mediterranean: PM1 and  
40 PM10 concentrations and composition, *Atmos. Chem. Phys.*, 15, 1129-1145, 10.5194/acp-15-  
41 1129-2015, 2015.

42 Rosenberg, P. D., Parker, D. J., Ryder, C. L., Marsham, J. H., Garcia-Carreras, L., Dorsey,  
43 J. R., Brooks, I. M., Dean, A. R., Crosier, J., McQuaid, J. B., and Washington, R.: Quantifying  
44 particle size and turbulent scale dependence of dust flux in the Sahara using aircraft  
45 measurements, *J. Geophys. Res.-Atmos.*, 119, 7577-7598, 10.1002/2013JD021255, 2014.

46 Rosenfeld, D., Rudich, Y., and Lahav, R.: Desert dust suppressing precipitation: A possible  
47 desertification feedback loop, *P. Natl. Ac. Sci.*, 98, 5975-5980, 10.1073/pnas.101122798, 2001.

48 Ryder, C. L., Highwood, E. J., Lai, T. M., Sodemann, H., and Marsham, J. H.: Impact of  
49 atmospheric transport on the evolution of microphysical and optical properties of Saharan dust,  
50 *Geophys. Res. Lett.*, 40, 2433-2438, 10.1002/grl.50482, 2013a.

1 Ryder, C. L., Highwood, E. J., Rosenberg, P. D., Trembath, J., Brooke, J. K., Bart, M.,  
2 Dean, A., Crosier, J., Dorsey, J., Brindley, H., Banks, J., Marsham, J. H., McQuaid, J. B.,  
3 Sodemann, H., and Washington, R.: Optical properties of Saharan dust aerosol and contribution  
4 from the coarse mode as measured during the Fennec 2011 aircraft campaign, *Atmos. Chem.*  
5 *Phys.*, 13, 303-325, 10.5194/acp-13-303-2013, 2013b.

6 Saha, A., Mallet, M., Roger, J. C., Dubuisson, P., Piazzola, J., and Despiou, S.: One year  
7 measurements of aerosol optical properties over an urban coastal site: Effect on local direct  
8 radiative forcing, *Atmos. Res.*, 90, 195-202, <http://dx.doi.org/10.1016/j.atmosres.2008.02.003>,  
9 2008.

10 Saha, S., Moorthi, S., Pan, H.-L., Wu, X., Wang, J., Nadiga, S., Tripp, P., Kistler, R.,  
11 Woollen, J., Behringer, D., Liu, H., Stokes, D., Grumbine, R., Gayno, G., Wang, J., Hou, Y.-  
12 T., Chuang, H.-Y., Juang, H.-M. H., Sela, J., Iredell, M., Treadon, R., Kleist, D., Van Delst, P.,  
13 Keyser, D., Derber, J., Ek, M., Meng, J., Wei, H., Yang, R., Lord, S., Van Den Dool, H., Kumar,  
14 A., Wang, W., Long, C., Chelliah, M., Xue, Y., Huang, B., Schemm, J.-K., Ebisuzaki, W., Lin,  
15 R., Xie, P., Chen, M., Zhou, S., Higgins, W., Zou, C.-Z., Liu, Q., Chen, Y., Han, Y., Cucurull,  
16 L., Reynolds, R. W., Rutledge, G., and Goldberg, M.: The NCEP Climate Forecast System  
17 Reanalysis, *B. Am. Meteorol. Soc.*, 91, 1015-1057, 10.1175/2010BAMS3001.1, 2010.

18 Said, F., Canut, G., Durand, P., Lohou, F., and Lathon, M.: Seasonal evolution of boundary-  
19 layer turbulence measured by aircraft during the AMMA 2006 Special Observation Period, *Q.*  
20 *J. Roy. Meteor. Soc.*, 136, 47-65, 10.1002/qj.475, 2010.

21 Salvador, P., Alonso-Pérez, S., Pey, J., Artfñano, B., de Bustos, J. J., Alastuey, A., and  
22 Querol, X.: African dust outbreaks over the western Mediterranean Basin: 11-year  
23 characterization of atmospheric circulation patterns and dust source areas, *Atmos. Chem. Phys.*,  
24 14, 6759-6775, 10.5194/acp-14-6759-2014, 2014.

25 Scheuven, D., Schütz, L., Kandler, K., Ebert, M., and Weinbruch, S.: Bulk composition of  
26 northern African dust and its source sediments — A compilation, *Earth-Sci. Rev.*, 116, 170-  
27 194, <http://dx.doi.org/10.1016/j.earscirev.2012.08.005>, 2013.

28 Schladitz, A., Müller, T., Kaaden, N., Massling, A., Kandler, K., Ebert, M., Weinbruch, S.,  
29 Deutscher, C., and Wiedensohler, A.: In situ measurements of optical properties at Tinfou  
30 (Morocco) during the Saharan Mineral Dust Experiment SAMUM 2006, *Tellus B*, 61, 64-78,  
31 10.1111/j.1600-0889.2008.00397.x, 2009.

32 Schladitz, A., Müller, T., Nordmann, S., Tesche, M., Groß, S., Freudenthaler, V.,  
33 Gasteiger, J., and Wiedensohler, A.: In situ aerosol characterization at Cape Verde, *Tellus B*,  
34 63, 549-572, 10.1111/j.1600-0889.2011.00568.x, 2011.

35 Seinfeld, J. H., and Pandis, S. N.: *Atmospheric chemistry and physics: From air pollution*  
36 *to climate change*, 714 pp., 1998.

37 Sicard, M., Mallet, M., García-Vizcaíno, D., Comerón, A., Rocadenbosch, F., Dubuisson,  
38 P., and Muñoz-Porcar, C.: Intense dust and extremely fresh biomass burning outbreak in  
39 Barcelona, Spain: characterization of their optical properties and estimation of their direct  
40 radiative forcing, *Environ. Res. Lett.*, 7, 034016, 2012.

41 Sicard, M., Bertolín, S., Mallet, M., Dubuisson, P., and Comerón, A.: Estimation of mineral  
42 dust long-wave radiative forcing: sensitivity study to particle properties and application to real  
43 cases in the region of Barcelona, *Atmos. Chem. Phys.*, 14, 9213-9231, 10.5194/acp-14-9213-  
44 2014, 2014.

45 Skamarock, W. C., Klemp, J. B., Dudhia, J., Gill, D. O., Barker, D. M., Huang, X. Z.,  
46 Wang, W., and Powers, J. G.: A Description of the Advanced Research WRF Version 3.  
47 Technical report. Mesoscale and Microscale Meteorology Division, NCAR, Boulder, Colorado,  
48 2008.

49 Sokolik, I. N., and Toon, O. B.: Direct radiative forcing by anthropogenic airborne mineral  
50 aerosols, *Nature*, 381, 681-683, 1996.

1 Sullivan, A. P., and Weber, R. J.: Chemical characterization of the ambient organic aerosol  
2 soluble in water: 2. Isolation of acid, neutral, and basic fractions by modified size-exclusion  
3 chromatography, *J. Geophys. Res.*, 111, D05315, 2006.

4 Sullivan, R. C., and Prather, K. A.: Investigations of the Diurnal Cycle and Mixing State of  
5 Oxalic Acid in Individual Particles in Asian Aerosol Outflow, *Environ. Sci. Technol.*, 41, 8062-  
6 8069, 10.1021/es071134g, 2007.

7 Sullivan, R. C., Moore, M. J. K., Petters, M. D., Kreidenweis, S. M., Roberts, G. C., and  
8 Prather, K. A.: Effect of chemical mixing state on the hygroscopicity and cloud nucleation  
9 properties of calcium mineral dust particles, *Atmos. Chem. Phys.*, 9, 3303-3316, 2009.

10 Swap, R., Garstang, M., Greco, S., Talbot, R., and KÄLLberg, P.: Saharan dust in the  
11 Amazon Basin, *Tellus B*, 44, 133-149, 10.1034/j.1600-0889.1992.t01-1-00005.x, 1992.

12 Tegen, I., and Lacis, A. A.: Modeling of particle size distribution and its influence on the  
13 radiative properties of mineral dust aerosol, *J. Geophys. Res.-Atmos.*, 101, 19237-19244,  
14 10.1029/95JD03610, 1996.

15 Trochline, D., Iwasaka, Y., Matsuki, A., Yamada, M., Kim, Y. S., Nagatani, T., Zhang, D.,  
16 Shi, G. Y., and Shen, Z.: Mineral aerosol particles collected in Dunhuang, China, and their  
17 comparison with chemically modified particles collected over Japan, *J. Geophys. Res.-Atmos.*,  
18 108, 8642, 10.1029/2002JD003268, 2003.

19 Tsyro, S., Simpson, D., Tarrasón, L., Klimont, Z., Kupiainen, K., Pio, C., and Yttri, K. E.:  
20 Modeling of elemental carbon over Europe, *J. Geophys. Res.-Atmos.*, 112, D23S19,  
21 10.1029/2006JD008164, 2007.

22 Ullerstam, M., Vogt, R., Langer, S., and Ljungstrom, E.: The kinetics and mechanism of  
23 SO<sub>2</sub> oxidation by O<sub>3</sub> on mineral dust, *Phys. Chem. Chem. Phys.*, 4, 4694-4699,  
24 10.1039/B203529B, 2002.

25 Valenzuela, A., Olmo, F. J., Lyamani, H., Granados-Muñoz, M. J., Antón, M., Guerrero-  
26 Rascado, J. L., Quirantes, A., Toledano, C., Perez-Ramírez, D., and Alados-Arboledas, L.:  
27 Aerosol transport over the Western Mediterranean basin: Evidence of fine particles to desert  
28 plumes over Alboran Island, *J. Geophys. Res.-Atmos.*, 2014JD022044,  
29 10.1002/2014JD022044, 2014.

30 [Van Dingenen, R., Putaud, J.-P., Martins-Dos Santos, S., and Raes, F., Physical aerosol  
31 properties and their relation to air mass origin at Monte Cimone \(Italy\) during the first  
32 MINATROC campaign, \*Atmos. Chem. Phys.\*, 5, 2203-2226, doi:10.5194/acp-5-2203-2005,  
33 2005.](#)

34 Villani, P., Picard, D., Marchand\*, N., and Laj, P.: Design and Validation of a 6-Volatility  
35 Tandem Differential Mobility Analyzer (VTDMA), *Aerosol Sci.Tech.*, 41, 898-906,  
36 10.1080/02786820701534593, 2007.

37 Weinzierl, B., Petzold, A., Esselborn, M., Wirth, M., Rasp, K., Kandler, K., SchÜTZ, L.,  
38 Koepke, P., and Fiebig, M.: Airborne measurements of dust layer properties, particle size  
39 distribution and mixing state of Saharan dust during SAMUM 2006, *Tellus B*, 61, 96-117,  
40 10.1111/j.1600-0889.2008.00392.x, 2009.

41 Weinzierl, B., Sauer, D., Esselborn, M., Petzold, A., Veira, A., Rose, M., Mund, S., Wirth,  
42 M., Ansmann, A., Tesche, M., Gross, S., and Freudenthaler, V.: Microphysical and optical  
43 properties of dust and tropical biomass burning aerosol layers in the Cape Verde region-an  
44 overview of the airborne in situ and lidar measurements during SAMUM-2, *Tellus B*, 63, 589-  
45 618, 10.1111/j.1600-0889.2011.00566.x, 2011.

46 Wiedensohler, A., Birmili, W., Nowak, A., Sonntag, A., Weinhold, K., Merkel, M.,  
47 Wehner, B., Tuch, T., Pfeifer, S., Fiebig, M., Fjåraa, A. M., Asmi, E., Sellegri, K., Depuy, R.,  
48 Venzac, H., Villani, P., Laj, P., Aalto, P., Ogren, J. A., Swietlicki, E., Williams, P., Roldin, P.,  
49 Quincey, P., Hüglin, C., Fierz-Schmidhauser, R., Gysel, M., Weingartner, E., Riccobono, F.,  
50 Santos, S., Gröning, C., Faloon, K., Beddows, D., Harrison, R., Monahan, C., Jennings, S. G.,  
51 O'Dowd, C. D., Marinoni, A., Horn, H. G., Keck, L., Jiang, J., Scheckman, J., McMurry, P. H.,

1 Deng, Z., Zhao, C. S., Moerman, M., Henzing, B., de Leeuw, G., Löschau, G., and Bastian, S.:  
2 Mobility particle size spectrometers: harmonization of technical standards and data structure to  
3 facilitate high quality long-term observations of atmospheric particle number size distributions,  
4 *Atmos. Meas. Tech.*, 5, 657-685, 10.5194/amt-5-657-2012, 2012.

5 Zhou, M., Okada, K., Qian, F., Wu, P. M., Su, L., Casareto, B. E., and Shimohara, T.:  
6 Characteristics of dust-storm particles and their long-range transport from China to Japan - case  
7 studies in April 1993, *Atmos. Res.*, 40, 19-31, [http://dx.doi.org/10.1016/0169-8095\(95\)00023-](http://dx.doi.org/10.1016/0169-8095(95)00023-2)  
8 2, 1996.  
9